6-22-2021 10:00 AM

Generation and Characterization of an In Vitro Organotypic Foreskin Model for Future Study of the Penile Microbiome

Geoffrey J. Rempel, *The University of Western Ontario*

Supervisor: Prodger, Jessica L., *The University of Western Ontario*

A thesis submitted in partial fulfillment of the requirements for the Master of Science degree in Microbiology and Immunology

Abstract

The foreskin is a site of HIV-1 acquisition in heterosexual males. The lack of relevant *in vitro* models that mimic the foreskin microenvironment, including innate immune and barrier functions, has limited our understanding of susceptibility at this site. We hypothesize that we can establish organotypic *in vitro* foreskin that mimics *in vivo* tissue. Organotypic foreskin models were generated and are composed of stratified cell layers that express E-cadherin suprabasally, filaggrin apically, and expressed TLR1, TLR2, and β-defensin-1 mRNA similar to *in vivo* foreskin. Preliminary results suggest organotypic foreskin tissues retain the ability to respond to LPS. Lastly, organotypic foreskin permeability appears high when subject to mechanical agitation. This work has established culture techniques to generate multi-layer epithelia and the methods necessary to characterize innate immune and barrier functions. This sets the foundation for future work to fully develop the model, including integrating immune cells, the microbiota, or HIV-1.

Keywords

HIV-1, HIV Susceptibility, Foreskin, Innate Immune Defense, Permeability, Skin Mimic, Artificial Foreskin, Anaerobic Bacteria

Summary for Lay Audience

The foreskin creates a fold of skin that provides an environment where bacteria intolerant to oxygen (known as anaerobes) can live. These anaerobes have been linked to the risk of acquiring human immunodeficiency virus (HIV) in heterosexual men. Our group has shown that anaerobes may increase HIV risk by causing local foreskin inflammation (an immune response) while disrupting foreskin permeability. This could allow HIV to penetrate the foreskin and infect immune cells (HIVs target cell type) that have gathered in the area due to this inflammation.

To discern how bacteria mechanistically alter susceptibility to HIV, we propose creation of an artificial foreskin that mimics natural foreskin in structure and function. Cells will be isolated from donor foreskins and grown on top of one another to generate layers of the skin. The artificial foreskin will be characterized next to the donor foreskin to see if it successfully mimics important aspects of the skin, such as the ability to detect and respond to bacteria on its surface and form a barrier to the outside environment.

In this study, artificial foreskins were generated that mimicked the structure of the natural foreskin, such as being composed of multiple cell layers stacked on top of one another. Tissues also expressed structural proteins commonly found in the natural foreskin such as E-cadherin (helps attach cells together) and filaggrin (helps in developing and maintaining the outer barrier of the skin). Similar to natural foreskin, artificial foreskins maintained gene expression of microbe sensors Toll-like Receptor 1 and 2, and antimicrobial protein β-defensin-1. Preliminary data suggests they may be able to respond to stimulation with a bacterial ligand. Lastly, data suggests that mechanical shaking during tissue development results in disorganized organotypic foreskin tissue structure with increased permeability.

This body of work has established culture conditions to isolate and propagate primary keratinocytes from adult foreskin tissue and use these to generate organotypic foreskin tissues. These tissues show multilayer stratification and differentiation, and expression of innate immune molecules and barrier proteins. These important developmental steps lay the groundwork for full model characterization, eventual incorporation of anaerobes, and challenge with HIV-1.

Acknowledgements

I would like to thank my fellow lab members for their aid in completing the work detailed herein. This includes Lane Buchanan for assistance in cryosectioning, immunostaining, and imaging foreskin tissues, as well as with troubleshooting the image analysis pipelines used throughout this work. As well, I would like to thank Zhongtian (Eric) Shao for his assistance in setting up the HPV16 E6E7 PCR used to assay transduced cells. A big thank you is also extended to Dr. David Zuanazzi for his valuable assistance on generating and troubleshooting the (*very tricky*) organotypic foreskin model. This thanks also extends to the many good times spent chatting about science, coffee (your favourite thing, David), and life over the course of these two years – I am very appreciative of this.

I would also like to thank Omar Almomani for cataloguing participant data for me, as well as Yuan Chun (Daniel) Jiang for teaching me how to use the immunoreactivity quantification pipeline described within. I would also like to extend thanks to Kathy Yu, who provided me long distance support and advice with planning statistical analyses. A very big thank you is extended to Abbie Lai (my amazing neighbour and lab mate) who very generously read and edited several portions of my thesis, helped me with immunostaining tissues, and supported me throughout (I most enjoyed our cooking/baking sessions and occasional strolls)! Another thank you is extended to Sarah Gowanlock, whose positive, friendly, and supportive attitude was very appreciated both in and outside of the lab space! I would also like to thank all the members of the shared laboratory space I worked in, as your kind interactions and comradery have helped make these years (including during the COVID-19 pandemic) highly enjoyable and memorable.

I am also very grateful for my advisory committee members Drs. Lina Dagnino, Lauren Flynn, and Martin McGavin who each provided valuable written and oral feedback at all stages of my degree. I would additionally like to thank Dr. Lina Dagnino for reading and editing my thesis: your keen attention to detail and deep knowledge base have continually helped improve my quality of work, which is extremely appreciated.

As well, I would like to extend thanks to Jake Davidson, Deborah Patrick, Dr. Peter Wang, Dr. Sumit Dave, and Dr. Magdy Hassouna who helped our laboratory enroll paediatric and adult participants for our study and secure tissue donations.

I would also like to acknowledge the Canadian Institutes of Health Research for supporting my work through a Canada Graduate Student – Master's Program scholarship.

Lastly, I want to thank my mentor and supervisor Dr. Jessica Prodger, whose continual uplifting spirit; dedication to her students; incredible intelligence; and personable, friendly nature have made this project so enjoyable. You are an inspiration and role model to us all, both in the lab space and Department of Microbiology and Immunology as a whole!

Table of Contents

List of Tables

List of Figures

List of Abbreviations and Symbols

ADLT – Adult

AF – Alexa Fluor

AMP – Antimicrobial Peptide

ART – Antiretroviral Therapy

ATCC – American Type Culture Collection

AIDS – Acquired Immunodeficiency Syndrome

Batf – Basic Leucine Zipper Transcription Factor ATF-Like

Bcl-2 – B-cell Lymphoma 2

bp – Base Pair

BPE – Bovine Pituitary Extract

BV – Bacterial Vaginosis

BXO – Balanitis Xerotica Obliterans

CCL5 – C-C Chemokine Ligand 5

CCR5 – C-C Chemokine Receptor type 5

CD – Cluster of Differentiation

cDC – Conventional Dendritic Cell

cDNA – Complementary Deoxyribonucleic Acid

Cldn – Claudin

COVID-19 – Coronavirus Disease 2019

CXCR4 – C-X-C Chemokine Receptor type 4

Da – Dalton

DMEM – Dulbecco's Modified Eagle Medium

DMSO – Dimethyl Sulfoxide

DNA – Dideoxyribonucleic acid

DPBS – Dulbecco's Phosphate Buffered Saline

EDTA – Ethylenediaminetetraacetic Acid

e.g. – *exempli gratia*

EGTA – Ethylene Glycol-bis(β-aminoethyl ether)-N,N,N′,N′-Tetraacetic Acid

ELISA – Enzyme-linked Immunosorbent Assay

Env – Envelope

ES – Epithelial Surface

E2F – E2 Transcription Factor

HI FBS – Heat-Inactivated Fetal Bovine Serum

FITC – Fluorescein Isothiocyanate

FOV – Field of View

GAPDH – Glyceraldehyde 3-Phosphate Dehydrogenase

gp – Glycoprotein

GUD – Genital Ulcer Disease

GUSB – β-Glucuronidase

HIV – Human Immunodeficiency Virus

HPV – Human Papilloma Virus

hTERT – Human Telomerase Reverse Transcriptase

HSV – Herpes Simplex Virus

H & E – Haematoxylin and Eosin

ICAM – Intercellular Adhesion Molecule

i.e. – *id est*

IF – Immunofluorescence

IL – Interleukin

IRB – Institutional Review Board

JAM – Junctional Adhesion Molecule

Kb – Kilobase

kDa – Kilodalton

kPa – Kilopascal

K-SFM – Keratinocyte Serum Free Media

LFA – Lymphocyte Function-Associated Antigen

LHSC – London Health Sciences Centre

LPS – Lipopolysaccharide

LTR – Long Terminal Repeat

MC – Male Circumcision

MHC – Major Histocompatibility Complex

MIG – Monokine Induced by Interferon Gamma

Min – Minute

MIP – Macrophage Inflammatory Protein

mL – Milliliter

mM – Millimolar

mm – Millimeter

mRNA – Messenger Ribonucleic Acid

MUPP – Multi-PDZ Domain Protein

NF-κB – Nuclear Factor-Kappa-Light-Chain-Enhancer of Activated B Cells

ng – Nanogram

NHEK – Normal Human Epidermal Keratinocyte

ns – Non-Significant

NQ – Not Quantifiable

Ocln – Occludin

OCT – Optimal Cutting Temperature

p – Protein

PA GFP – Photoactivatable Green Fluorescent Protein

PCR – Polymerase Chain Reaction

PDMS – Polydimethylsiloxane

PED – Paediatric

PIPES – Piperazine-N,N′-Bis(2-Ethanesulfonic Acid)

pRb – Retinoblastoma Protein

P/S – Penicillin and Streptomycin

qPCR – Quantitative Polymerase Chain Reaction

RCT – Randomized Control Trial

rEGF – Recombinant Epithelial Growth Factor

RNA – Ribonucleic Acid

ROUT – Robust Regression and Outlier Removal

RPM – Revolutions Per Minute

s – Second

SC – Stratum Corneum

SDM – Substitute Decision Maker

SIV – Simian Immunodeficiency Virus

SV40 – Simian Virus 40

TAE – Tris-acetate-EDTA

TEER – Transepithelial Electrical Resistance

Th – T Helper

TLR – Toll-like Receptor

TNF – Tumour Necrosis Factor

UTI – Urinary Tract Infection

UUA – University Urology Associates

Yrs – Years

ZO – Zonula Occludens

µg – Microgram

µL – Microliter

µM – Micromolar

µm – Micrometer

1° – Primary

2° – Secondary

3′ – Three Prime

5′ – Five Prime

Chapter 1

1 Introduction

Human immunodeficiency virus type 1 (HIV-1) is a lentiviral species identified as the causative agent of acquired immunodeficiency syndrome (AIDS)[1–5]. Approximately 38 million people across the world were living with HIV in 2019, with 1.9 million new infections that year alone[6]. Up to 33 million people have died since the start of the HIV epidemic, with 690,000 having died as a result of HIV/AIDS in 2019[6,7]. HIV most heavily impacts sub-Saharan Africa, where it is the leading cause of morbidity and mortality[8,9]. HIV acts to compromise the adaptive immune system by infecting and killing cluster of differentiation 4 positive (CD4+) T cells, leading to AIDS[10]. This condition is marked by (1) an inability to fight against and (2) heightened susceptibility towards otherwise rare opportunistic infections or cancers[5,11]. After HIV infection is established, AIDS will typically develop within one decade and after the onset of AIDS, one- and five-year survival rates are 76% and 46% respectively[12]. As of 2021, there is no cure for HIV: infected individuals must undertake lifelong antiretroviral therapy (ART) to prevent AIDS onset, virus transmission, and permit a relatively normal lifespan[4,13–16]. Regrettably, ART is prohibitively expensive ($15,552 Canadian Dollars per person per year) and adherence difficult, which puts a significant burden on poorer regions of the world where HIV is most prevalent[17–29]. Understanding this, it is imperative that novel and efficacious methods of preventing HIV transmission and acquisition are developed.

1.1 Study Overview

HIV can be transmitted in three ways. This includes through parenteral routes common with injection drug use-based needle sharing, sexual contact, and through maternal-infant exposure[30]. Most HIV infections are the result of sexual exposure, which accounts for approximately 80% of total infections[31]. This is in stark contrast with both parenteral and mother-to-child transmission, which account for the remaining 20%[31]. Transmission via sexual contact, despite being the root cause of most HIV infections, is extremely

inefficient. The probability of male-to-female HIV transmission between serodiscordant partners is estimated to be around 1:200 to 1:2,000 per sex act, while female-to-male transmission is estimated at 1:700 to 1:3,000[32]. The inefficiency of transmission through sexual contact can be attributed to two factors: variable infectiousness of the HIV-infected partner, and the variable susceptibility of the uninfected partner. The infectiousness of a partner is the result of the concentration of HIV in one's blood plasma and genital secretions (known as the "viral load"), as has been highlighted by research showing a complete lack of transmission when an infected individual is virally suppressed with ART[33]. The variable susceptibility of a non-HIV infected partner has correlated to a variety of factors, such as age, gender, race, and circumcision status[34–38].

Circumcision status has been shown to decrease a heterosexual man's risk of contracting HIV by up to 60% in three separate, randomized control studies in Kenya, South Africa, and Uganda[36–38]. This protective effect has been correlated with inflammatory markers and the prevalence of various anaerobic bacteria in the penile subpreputial (underneath the foreskin) space[39–42]. Further, strong correlations have been made between six penile anaerobic species, HIV seroconversion, subpreputial interleukin-8 (IL-8) levels, and foreskin CD4+ T cell densities in heterosexual men[43]. It is, however, unclear how anaerobic bacteria may mechanistically alter HIV susceptibility, as (1) these microbes frequently co-occur in the subpreputial space, and (2) the studies investigating this relationship have thus far been observational. Additionally, there exists no relevant *in vitro* method to empirically discern the mechanism behind altered HIV transmission at the level of the foreskin and beyond. This presents a significant barrier in understanding how HIV is successfully transmitted to heterosexual men and represents a substantial roadblock in the way of generating new, targeted HIV prevention modalities. This thesis is the result of work done to generate a relevant tissue model so as to, in the future, elucidate the how anaerobic subpreputial bacteria mechanistically influence heterosexual male HIV susceptibility. To do this, I first generated and optimized methods for the development of a full-depth foreskin equivalent, based on current literature. I then assessed the ability of this artificial tissue to mimic the innate immune defense parameters of *in vivo* foreskin tissues in terms of tissue permeability, pathogen sensors, and secretion of innate immune factors.

This introduction will first establish my rationale for examining heterosexual male HIV susceptibility in relation to the foreskin. Following this, I will examine literature regarding the penile microbiota in relation to HIV-1 susceptibility and discuss the defense capabilities of the skin. This will establish the reasons for our investigation into these specific skin parameters. Finally, I will discuss currently available tissue models (and their limitations), and the overall need for a full depth, three-dimensional *in vitro* organotypic foreskin model.

1.2 Human Immunodeficiency Virus Type 1 and the Foreskin

1.2.1 HIV Introduction and Virology

HIV belongs to the genus *Lentivirus*, family *Retroviridae*, subfamily *Orthoretrovirinae*, and is grouped into two types – HIV type 1 and 2 (HIV-1 and HIV-2)[1,2,44]. The HIV genome consists of two identical single-stranded RNA molecules which, upon infection, are reverse transcribed into double stranded DNA, which is in turn inserted into the genome of susceptible host cells[1,45]. The genome for all retroviruses consists of three structural genes known as *gag*, *pol*, and *env*, with the different HIV types varying in the organization of these genes. The *gag* gene encodes proteins comprising the capsid, nucleocapsid, and protective inner matrix that lines the host-derived membrane (p24, p7, and p17 respectively)[1,44]. The *pol* gene encodes protease, reverse transcriptase, either RNase H or reverse transcriptase complexed with RNase H, and integrase (p12, p51, p15, p66 (reverse transcriptase complex), and p32 respectively)[1,44]. Lastly, the *env* gene encodes both a surface and transmembrane glycoprotein (gp) which are known as gp120 and gp41, respectively[1,44]. Alongside *gag*, *pol*, and *env* exists a complex combination of regulatory and accessory genes that assist in viral replication and host immune evasion[1,44]. These include *tat* and *rev*, which are necessary for HIV replication initiation, as well as *nef*, *vif*, *vpr*, and *vpu* which are important for viral replication, virus budding, and viral pathogenesis[1,44]. A schematic overview of the HIV genome is provided in Figure 1.1. While HIV-1 and HIV-2 can both infect humans, HIV-1 is the most infectious

and most significant contributor to the global HIV pandemic[2,44]. For the remainder of this thesis, the acronym HIV will be referring to HIV-1.

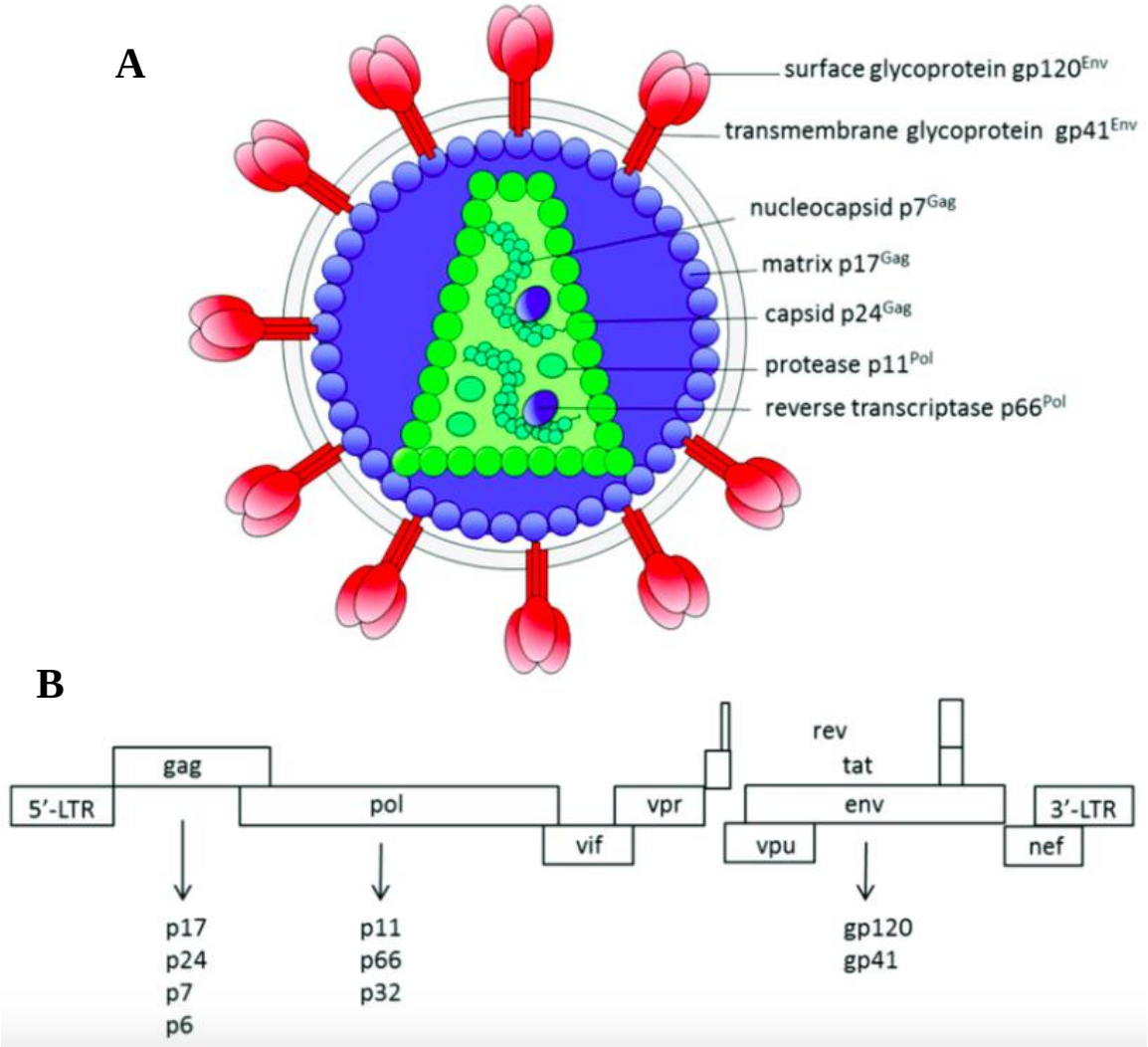

Figure 1.1: Structure of the HIV Virion and Genome. (**A**) shows the HIV virion while (**B**) shows the organization of the viral genome. From Trovato *et al*, International Journal of Molecular Sciences, 2018[46].

Each infectious particle (as shown in Figure 1.1) consists of a viral core and outer lipid envelope[1]. The viral core is conical in shape, consists of repeating units of capsid protein (p24), and contains two identical single-stranded RNA molecules alongside the enzymes integrase, reverse transcriptase, and protease[1,44]. In addition to these enzymes are the regulatory proteins Tat, Rev, Nef, Vpu, Vpr, and Vif[1,44]. The viral core is surrounded by a lipid envelope, a phospholipid bilayer that is acquired when mature viral particles bud from an infected host cell[1,44]. Just below the lipid envelope is a viral protein matrix composed of p17[1,44]. The surface of the lipid envelope comprises host proteins and most notably envelope (Env) glycoprotein complexes[45]. The Env glycoprotein complex is a highly glycosylated heterodimer consisting of a transmembrane gp41 trimer and surface gp120 trimer non-covalently linked to one another[1,44,45]. These complexes project from the surface of the lipid envelope, with the gp120 trimer forming the extracellular domain responsible for interacting with host target cell receptors[1,44,45].

1.2.2 Virus Entry into Host Cells

The Env glycoprotein complex on surface of the HIV lipid envelope acts to facilitate entry into susceptible host cells. The surface gp120 trimer binds with high affinity to CD4, the primary receptor used by primate lentiviruses for attachment to host cells[1,44,45,47]. CD4 binding causes a subsequent conformational change in gp120, and exposes a co-receptor binding site[1,44,45,47]. One co-receptor is required to facilitate entry into cells: these co-receptors include C-X-C chemokine receptor type 4 (CXCR4) and C-C chemokine receptor type 5 (CCR5)[1,44,45,47]. Following binding of a co-receptor, additional conformational changes in gp120 and subsequently gp41 trigger a membrane fusion event between the host cell and viral envelope, depositing the viral core into the host cell cytoplasm[1,44,45,47].

HIV strains that utilizes CCR5 as a co-receptor are known as R5 tropic, and infect primary CD4+ T cells, as well as macrophages and dendritic cells[1,44,47]. HIV transmitted through use of CXCR4 as a co-receptor is known as X4 tropic, and typically infects only CD4+ T cells[1,44,47]. Dual/mixed tropic viruses (known as X4R5 tropic) can infect all three

types of cells[1,44,47]. HIV also exhibits a very high mutation rate, which – in untreated individuals – can often lead to rapid evolution and development of diverse viral quasispecies[48–50]. While both R5 and X4 strains appear in bodily fluids, sexual/mucosal transmission of HIV occurs exclusively via R5 or dual tropic strains. Despite the diversity of viral strains present in an infected partner's genital secretion, the majority of the time only a single strain is transmitted from an infected to a non-infected individual[51–53]. Although R5 tropic virus dominates acute infection, late stage infection is often associated with the evolution of X4 and X4R5 tropic strains which coincides with rapid progression to AIDS[1,47].

Once successful infection of a host cell has occurred, HIV can be transferred to other immune cells in the body. This spread of HIV is believed to contribute to productive infection, and eventual depletion of immune cells that leads to AIDS[54,55]. This is a process that can occur in several ways: through (1) budding off and diffusing passively to other susceptible cells as described previously, and (2) direct cell-to-cell transfer as through use of either an infectious or virological synapse[51].

Direct cell-to-cell transfer through an infectious synapse is a unique process that occurs when dendritic cells are able to capture HIV-1 virions without becoming productively infected, and transfer them intact to susceptible CD4+ T cells[56,57]. This process is known as *trans*-infection, and occurs via formation of an adhesion molecule-based infectious synapse between a dendritic cell and an uninfected CD4 T cell (as reviewed by McDonald *et al*, 2010)[58]. Dendritic cells begin this process by engulfing pathogens at a site of infection, where they mature and then migrate to local lymph nodes[58]. This maturation itself is accompanied by increased antigen degradation and presentation, shutdown of phagocytosis and macropinocytosis, and stabilization of peptide-MHC-II (major histocompatibility complex class II) complex expression on the dendritic cell surface[58]. As endocytosis is shut down, newly acquired antigens are not trafficked into and degraded by the lyososomal degradation pathway[58]. Once a T cell has encountered a dendritic cell in the lymph node, adhesion molecules such as lymphocyte function-associated antigen-1 (LFA-1) and intercellular adhesion molecule-1 (ICAM-1) arrest cell movement and allow T cell screening of the dendritic cell surface[58]. If the dendritic cell

presents the correct peptide-MHC-II complexes, the T cell responds through concentrating T cell receptors, CD4, and other molecules to form an immunological synapse[58]. Intact pathogens such as HIV-1 can be transferred to T cells during this contact, as a portion of pathogens are sequestered in invaginated membrane fold-based structures that either traffic to the lysosome or are rerouted to the surface and excreted as exosomes[58]. Sequestered HIV-1 is rapidly recruited to sites of T cell contact, viral particles trafficked out of the HIV-1 containing cellular compartment, and into the infectious synapse where they fuse with the uninfected T cell[58].

The last HIV cell-cell transfer method occurs via formation of the virological synapse, an adhesive supramolecular structure that acts to pass virions from an HIV infected CD4+ T cell to an uninfected one[54,59,60]. When a virological synapse is being formed, Env glycoprotein complexes displayed on the surface of infected cells bind to CD4 receptors on uninfected cells via gp120, which forms adhesions between them (reviewed by Bracq *et al*, 2018 and Ménager, M. M. & Littman, D. R., 2016)[56,60]. The interaction between viral gp120 and cellular CD4 acts to recruit viral Gag protein precursors to the intercellular surface, while also recruiting coreceptors CCR5 or CXCR4 and the adhesion molecules LFA-1 and ICAM-1[56,60]. Additionally, the interaction between gp120 and CD4 will trigger actin cytoskeleton remodeling and microtubule polarization towards the developing virological synapse[56,60]. This allows for the formation of a stable, adhesive junction between the two cells where assembly and budding of immature HIV virions can occur[56]. These budded immature viral particles are internalized into the target cell via endocytosis, mature within the endocytic compartment, fuse with the endosomes luminal membrane, and are subsequently released into the cells cytoplasm[56].

1.2.3 Skin Biology and Tissue HIV Infection

A key area of investigation in HIV transmission is the skin. The skin is the largest organ of the body and acts as a complex physical barrier protecting the body from the external environment[61–63]. The skin provides many critical functions, such as protection against physical injury, ultraviolet radiation, and moisture loss, while also regulating

temperature, synthesizing vitamin D, and acting as a sensory organ[61,64,65]. Importantly, the skin acts in immunological defense of the body through providing a passive physical barrier to microbes, producing biomolecules, and hosting immune cell sentinels[63,65,66].

The skin is comprised of three major layers, the hypodermis, dermis, and the epidermis. For the purpose of this thesis, the dermis and epidermis will be discussed.

The dermis is the layer of tissue below the epidermis, is usually >2 mm thick in most areas of the body (extending to 4 mm thick in areas such as the back), and provides mechanical strength and resistance to shear forces[62,65,67]. The dermis contains fibroblasts, dendrocytes, macrophages, lymphocytes, mast cells, histiocytes, nerve fibres, and is traversed by blood and lymph vessels[62,65–67]. The extracellular matrix of the dermis is synthesized by fibroblasts and consists of collagen and elastic fibres, as well as proteoglycans[62,65,66]. The dermis itself consists of two layers with no clear boundary between them[62,66,67]. The uppermost layer is known as the papillary dermis, while the lower portion is called the reticular dermis[62,65–67]. Collagen type I and III fibres are oriented horizontally in the reticular dermal layer and provide mechanical toughness to skin, while elastic fibres permit elastic recoil and are loosely arranged in all directions[62,67]. Collagen type I comprises the bulk (80-90%) of dermal collagen, while collagen type III makes up the rest (10-20%); despite this, other collagens such as collagen type IV have been located here[67]. The papillary dermis consists of thin (mean = 38,000 nm) collagen fibres interspersed with elastic fibres, and interdigitates with the epidermal rete ridges while the reticular dermis is composed of thick fibres of collagen[62,67]. In humans, the reticular dermis is thicker than the papillary dermis as there are large concentrations of collagen and reticular fibres localized here[62,65,66].

The epidermis is the outermost layer of skin, and is a stratified squamous epithelium: most apical is the stratum corneum, followed with the stratum lucidum, stratum granulosum, stratum spinosum, and stratum basale[62,64,66]. The total thickness of the epidermis is approximately 50 to 150 μm, although this can extend to 600 μm in the thicker skin of the palms of the hands and soles of the feet[63,67]. The epidermis is composed of keratinocytes which can produce keratin proteins[62]. Keratins are a family of

30 proteins, each produced by a single gene[62]. These keratins form keratin intermediate filaments that make up the internal skeleton of the keratinocytes, and as these cells mature and differentiate, they express many different keratins dependent on the stage of differentiation[62]. At the final stage of differentiation, keratinocytes contain impermeable, tough, fibrous keratin[62].

Keratinocytes are arranged in layers due to their unique lifecycle of maturation and differentiation, as shown in Figure 1.2[62,68]. The stratum basale of the epidermis is composed of a single layer of continually renewing columnar basal keratinocytes, and as these cells mature they are pushed apically which results in the formation of the stratum spinosum[62,64]. Further, the keratinocytes of the stratum basale predominantly contain keratin tonofilaments[62,64]. The stratum basale is also populated with melanocytes that provide skin pigmentation, as well as immune cells like Langerhans cells and T cells[64,66,69,70]. The stratum spinosum is a layer of polyhedral cells approximately four to ten cells thick, and exists apically to the stratum basale[62,64]. The epithelial cells of this layer also contain keratin tonofilaments and form multiple intercellular junctions with one another called desmosomes, contributing to its "prickly" appearance[62,64]. As the cells of the stratum spinosum further differentiate and push further outward, they form the stratum granulosum[62,64]. This layer is granular in appearance, contains diamond-shaped cells, is three to four cell layers thick, and is marked by the generation and secretion of lipid-filled lamellar bodies and keratohyaline granules[62–64,67]. Lamellar bodies function to create the skins water-impermeable barrier function of the skin, whereas keratohyaline granules contain proteins like filaggrin which help aggregate keratin filaments in later stages of maturation[61–64]. These granules also contain proteins that bind the cells of the more apical stratum corneum together[62]. The stratum lucidum is the next layer of the epidermis, and it lies between the stratum granulosum and stratum corneum[62,64]. This layer is thin, comprised of very dense translucent cells, and is only present in very thick skin such as that of the palms of the hands and soles of the feet[62,66]. Lastly is the most apical layer, the stratum corneum[62,64]. The cells that comprise this layer are terminally differentiated and known as corneocytes; they are large, flattened, and polyhedral in shape, and contain cytokeratin filaments bound together by filaggrin, while the layer itself is just 15-20 cells or 10-15 μm thick[61–63,66]. These cells are also dead, anuclear, and

held together in an overlapping fashion within an organized lipid matrix[61–63,66,67]. These lipids (e.g., ceramides, fatty acids, and cholesterols) are derived from the stratum granulosum and give the stratum corneum the ability to flex and move in conjunction with the rest of the body, while also promoting the formation of a permeability barrier[61,63,66,67]. The overlapping arrangement of the cells in this layer also contributes to the barrier function of the skin[62]. Additionally, the uppermost portions of the stratum corneum are loosely organized and are shed from the skin as microscopic scales, a process known as desquamation[61–64]. The total transit time of cells from the basal layer to the stratum corneum in humans is approximately 52-75 days, with 26-42 days spent migrating to the top of the stratum granulosum and 13-14 required to migrate to the top of the stratum corneum[62]. The epidermis itself is connected to the basement membrane, an important part of the dermoepidermal junction that connects the dermis to the epidermis[67]. This basement membrane is mainly composed of laminin 332, collagen type IV, nidogen, perlecan, heparin sulphate proteoglycans, and junctional proteins[67]. The basement membrane acts as an additional mechanical barrier to the passage of pathogens, alongside the epidermis[67].

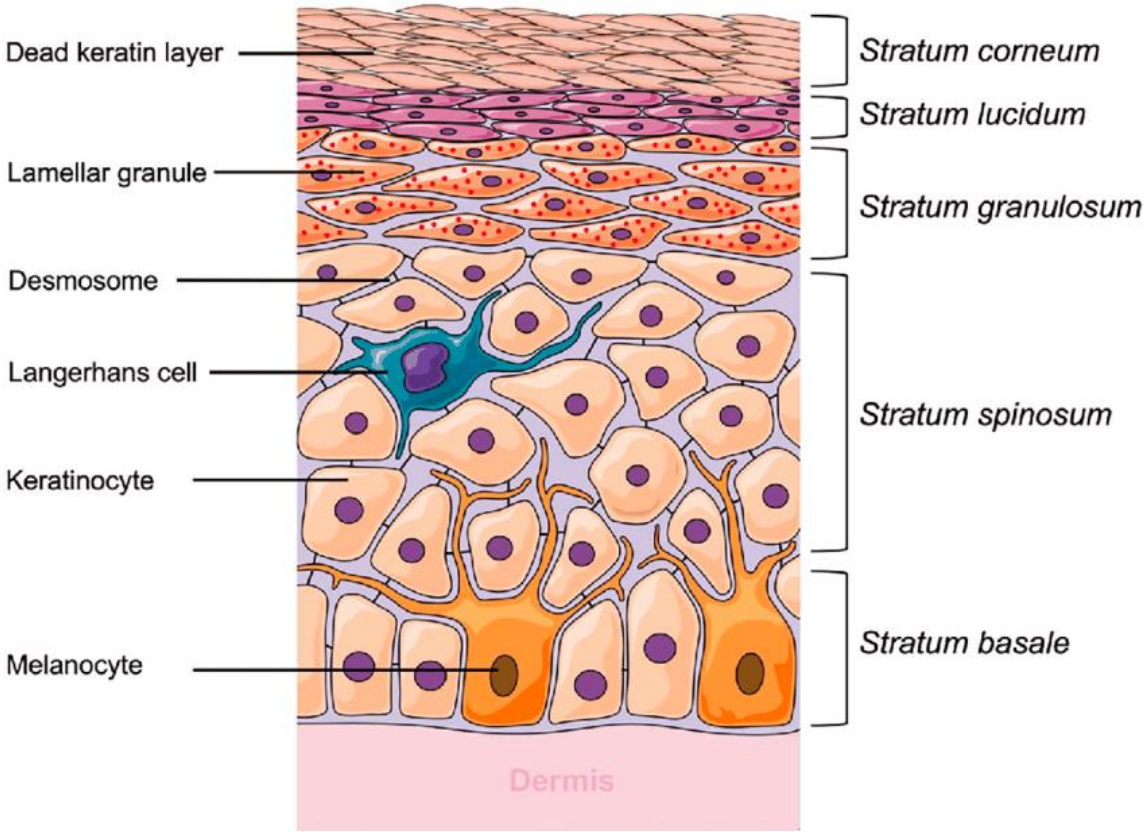

Figure 1.2: The Layers and Composition of Human Skin. From Ramadon *et al*, Drug Delivery and Translational Research, 2021[68].

When genital secretions containing HIV contact the foreskin, the first cells the virus will encounter are keratinocytes. These cells are not susceptible to direct infection as they do not express CD4, but the immune cells of the epidermis and underlying dermis are. The epidermis contains susceptible Langerhans cells, as well as CD4+ and CD8+ T cells[66,69,70]. The dermis also contains susceptible resident immune cell populations that are susceptible (e.g., dendritic, Langerhans, and CD4+ T cells), as well as blood vessels that enclose susceptible circulating immune cells. HIV needs to pass through the outer epithelial layer to gain access to deeper immune cells and blood vessels. *In vivo* studies utilizing rhesus macaques have revealed that HIV can cross the epithelial barrier through physical breaks in the epithelium, and simple diffusion between the epithelial cells themselves. Physical breaks may occur through ulceration (due to sexually transmitted

infections), or possibly coital injury[71]. As shown through *in vivo* and *ex vivo* studies using a macaque model, as well as *ex vivo* human studies of the female genital tract, simple diffusion of HIV virions can occur through squamous epithelia until encountering cellular tight junctions (Figure 1.3)[72]. Virions can continue to permeate the tissue via this mechanism in areas where cell-cell junctions are absent[72]. These mechanisms allow for HIV to access the deeper layers of the stratum corneum and dermal compartment, where it can then proceed to infect susceptible immune cells.

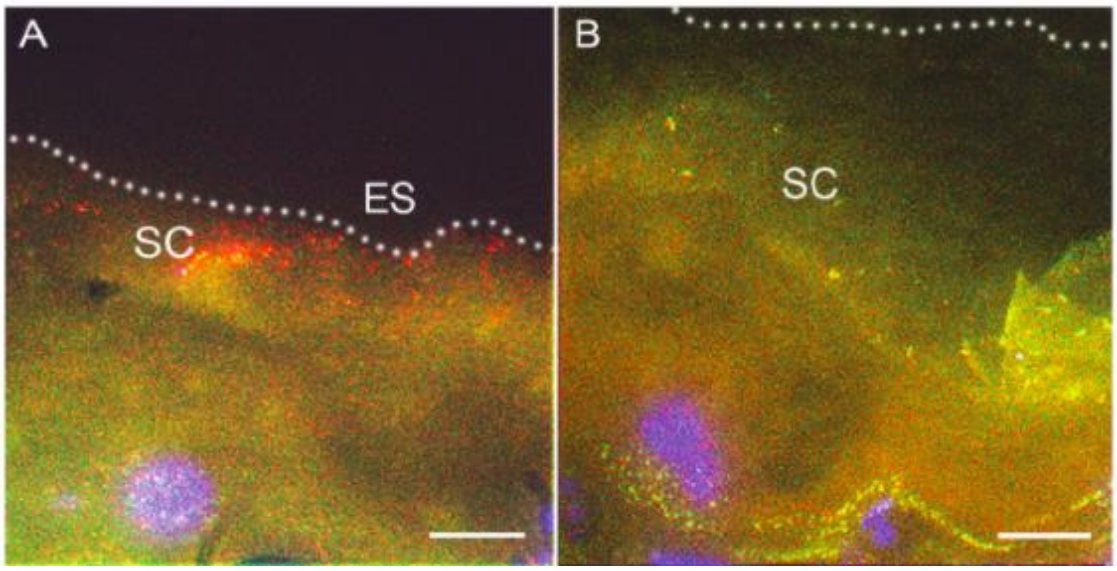

Figure 1.3: *Ex Vivo* Foreskin Tissue Penetration by Labelled HIV. Inner (**A**) and outer (**B**) foreskin tissues (foreskin anatomy found in **Section 1.2.4**) were immunofluorescently imaged after being exposed to photoactivatable green fluorescent protein Vpr-labelled HIV-1 (PA GFP-Vpr HIV-1; red) and stained for nuclei (blue). Virions are typically found on the surface of the tissue (ES, epithelial surface) or in the stratum corneum (SC, stratum corneum). White bar = 10 µm. From Dinh *et al*, PLOS Pathogens, 2015[73].

1.2.4 The Foreskin, Male Circumcision, and HIV Acquisition

The foreskin constitutes a fold of skin that covers the coronal sulcus, glans, and urethral meatus of the non-erect penis, and is stretched back on the erect penis. While the foreskin is one continuous sheet of skin, the portion of the foreskin that lies against the glans on the non-erect penis is referred to as the "inner" foreskin, while that which is exposed to air at all times is referred to as the "outer" foreskin. These two aspects are highly similar in appearance and may differ only slightly in pigmentation. Removal of the foreskin is termed male circumcision (MC) and removes both inner and outer aspects (Figure 1.4).

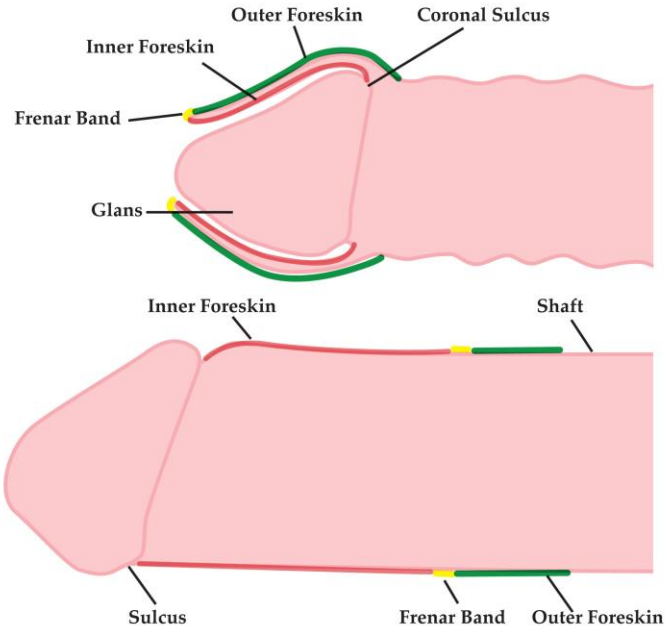

Figure 1.4: The Anatomy of the Foreskin. The non-erect penis (top) shows the inner foreskin (red) covering the glans and coronal sulcus. This is in contrast to the outer foreskin (green) that is always exposed. The erect penis (bottom) shows the foreskin pulled back, exposing the coronal sulcus and glans, with both the inner and outer foreskin aspects also exposed to external elements. Both the inner and outer aspects are removed during circumcision, leaving the glans and coronal sulcus exposed at all times. From Dinh *et al.*, PLOS One, 2012[74].

The foreskin is an important area known to be involved in HIV acquisition. More than 30 ecological and observational studies have suggested that HIV acquisition is reduced in circumcised men, relative to those who are uncircumcised[75,76]. A meta-analysis of 27 studies showed a 68% decrease in HIV acquisition in circumcised men[77]. These results and a need to discern whether they were confounded by participant behaviours (i.e., sexual behaviours) inspired the investigation of MC via randomized control trials (RCTs)[75]. Three randomized trials were conducted, in Kenya, South Africa, and Uganda[36–38]. These studies enrolled more than 10,000 heterosexual adult men overall, and each trial concluded that there was a significant decrease, of about 50-60%, in HIV acquisition among circumcised participants[36–38,75]. A further meta-analysis of these trials highlighted they were consistent and showed little heterogeneity, despite trial variability in terms of circumcision technique, urban vs. rural setting, age, and HIV incidence[78]. This same meta-analysis highlighted that 12 months after circumcision, the protective effect of MC was 50%, which increased to 54% at 24 months[78]. Additional intent-to-treat efficacy estimates found that the trials were consistent, showing 60%, 53%, and 57% decreases in HIV acquisition for the South African, Kenyan, and Ugandan trials respectively[37,75]. Furthermore, post-trial follow-ups highlighted that the efficacy of circumcision on hindering HIV acquisition increased over time. Three years after the Ugandan trial closed, it was noted that circumcision was associated with a 73% decrease in HIV acquisition[79]. The Kenyan trial also demonstrated increasing protective effects 42 months post circumcision[75].

This protective effect has not only been limited to HIV as these RCTs demonstrated that heterosexual male circumcision confers protection against numerous sexually transmitted infections. This includes human papillomavirus (HPV), herpes simplex virus type 2 (HSV-2), and genital ulcer disease (GUD)[37,75]. The South African trial showed urethral HPV prevalence was significantly lower 21 months after MC compared to control men (14.8% compared to 22.3%)[75,80]. This was consistent in the Ugandan trial (18.0% compared to 27.9%), which evaluated the prevalence of HPV at the glans and coronal sulcus at the two-year visit mark[81]. In the Ugandan trial, the probability of HSV-2 seroconversion over two years was 7.8% compared to 10.3% in the control arm[75,81,82].

There were, however, no differences in HSV-2 acquisition between the intervention and control arms for the Kenyan trial[83].

In addition to the protective benefits of circumcision for males, this procedure can also reduce female partner risk for developing GUD, bacterial vaginosis (BV), or being infected with either HPV or trichomonas infection. In the Uganda trial, female partner HPV prevalence at year two was decreased when their male partner was circumcised, compared to uncircumcised controls (27.8% and 38.7% respectively)[82]. This was suggested to be due to both decreased acquisition and increased viral clearance in the females[84]. There was also decreased GUD, trichomonas infection, and BV amongst the female partners of circumcised men[85]. This decrease in BV is most likely due to decreased total penile bacterial load and reduced pro-inflammatory anaerobic bacteria as found in circumcised men[39,86]. These results suggest circumcision provides a substantial protective benefit to both men and their female partners.

1.2.5 Hypotheses Regarding the Protective Effect of Male Circumcision

Many hypotheses have been postulated for why MC impacts HIV susceptibility in men. As of yet, four different mechanisms have been proposed: (1) the inner aspect of the foreskin has a thinner keratin layer (and thus decreased barrier function) compared to the remaining penile skin; (2) the foreskin harbours a greater density of susceptible immune cells; (3) the immune cell populations found in the foreskin are functionally different and more susceptible; and (4) decreased foreskin epithelial barrier integrity.

The earliest hypothesis as mentioned above was related to the thickness of the stratum corneum of the foreskin, whereby the inner foreskin was thought to be more thinly keratinized (cornified) compared to the skin on the shaft remaining after circumcision[74]. This could allow easier passage of HIV virions through the surface of the inner foreskin epithelium, and access to a pro-inflammatory immune milieu rich in susceptible CD4+ T cell subsets[74,87,88]. In contrast, the remaining penile skin was hypothesized to harbour a thicker cornified layer, providing a robust physical barrier to HIV virions[74,89]. Due to the

difficulty in examining penile shaft skin, several groups have explored this hypothesis by comparing the inner foreskin to the outer foreskin, taking the outer foreskin as representative of the shaft skin remaining after circumcision. Four studies have supported this hypothesis, with one examining cadaveric tissue, two observing but not quantifying a thinner inner foreskin cornified layer, and the last finding a very small increase in outer foreskin cornification[90–93]. However, additional quantitative studies noted either no difference or an increased inner foreskin cornified layer thickness[74,94,95]. One study in particular controlled for certain confounding variables found in other studies examining cornified layer thickness (such as clinical indication for circumcision, or ethnic differences in participants that can limit generalizability)[74]. In this study, cornified layer thickness was examined in a blinded fashion by two independent laboratories[74]. Of note, no significant differences were found in cornified layer thickness between the inner and outer foreskin aspects or the frenar band of the healthy Ugandan men who participated in the study[74].

Secondly, it has been suggested that foreskin tissue contains a greatly increased number of HIV susceptible immune cells relative other skin tissues. Studies of simian immunodeficiency virus (SIV) transmission in female macaques have shown SIV infects cells in areas of increased immune cell density below the stratum basale[96]. These dense foci of immune cells additionally occur early on in infection, indicating they may be the result of pre-existing inflammation[96]. Thus, it can be argued that similar increases in foreskin immune cell density could do the same. This has been examined in several studies looking at immune cell populations in the inner and outer aspects of the foreskin[90–92,94,97–99]. Despite this, results have been inconclusive as of yet, with some studies showing increased[91,92,97,98] and some decreased[90,94] inner foreskin immune cell densities, and others no difference at all in immune cell densities between the inner and outer foreskin[99].

Third, a recent hypothesis has also suggested that HIV susceptibility in relation to the foreskin may be due to functional differences in the immune cells residing in the tissue. One study examined differences in immune cells between the inner and outer aspects of the foreskin[99]. This study found similar densities in certain immune cells across the inner

and outer foreskin (i.e., Langerhans and T cells), but noted that the Langerhans cells of the inner foreskin sample their environment more frequently and are more responsive to cytokine stimulation[99]. Stimulation of the inner foreskin with tumour necrosis factor-alpha (TNF-α) or macrophage inflammatory protein-one alpha (MIP-1α) revealed increased CD4+ cell recruitment to the epidermis[99]. Two additional studies conducted by a different group exposed explanted foreskin tissues to HIV and found that more HIV virions entered the inner aspect compared to the outer aspect of the foreskin[91,98]. Additionally, more chemokine C-C motif ligand 5 (CCL5) was found to be released from the epithelial cells of the inner foreskin which resulted in a greater recruitment of CD4+ cells to the epidermis of the inner foreskin[91,98]. This is important as CCL5 is the ligand for the HIV-associated CCR5 receptor expressed on immune cells (e.g., monocytes, natural killer cells, memory T cells, dendritic cells, eosinophils), and acts as a chemoattractant for them (reviewed in Crawford *et al*, 2011)[100]. Further, this group also observed migration of Langerhans cells, uptake of HIV by them, and subsequent formation of contacts with CD4+ T cells in the inner aspects of the foreskin[91,98]. In sum, increased activity by Langerhans cells, formation of contacts with CD4+ T cells, and differences in epithelial cell cytokine secretion and response common in inflammation could render the inner foreskin more susceptible to HIV.

Lastly, decreases in epithelial barrier permeability could be altering male HIV susceptibility. In the same study mentioned as part of hypothesis three, inner foreskin tissue cultured *ex vivo* with TNF-α was found to contain greater quantities of activated Langerhans cells than that of outer foreskin tissues[99]. With cytokine stimulation, there was also an influx of CD4+ T cells into the tissue epithelium, as mentioned previously[99]. This could also indicate that there are differences in tissue permeability between the inner and outer foreskin. Additionally, studies with female macaques have highlighted that elevated inflammatory cytokine secretion in the female genital tract is associated with proteases and negatively associated with protease inhibitors, suggesting they act to decrease tissue barrier functionality[101]. Taken together, it is possible that similar cytokine and protease production common in inflammation may influence inner foreskin permeability and thus alter HIV susceptibility.

An overarching theme linking hypotheses two, three, and four together is that environmental factors may be inducing localized inflammation of the foreskin which result in the observed changes in immune cell density, function, cytokine secretion, and permeability. The foreskin may be influenced by the subpreputial microbiota, for example, as examination of similar inflammation, tissue immune cell densities, and cytokine secretion is common in vaginal microbiota-associated BV[102,103]. Understanding this, it has been suggested that MC may alter the local inflammatory environment of the foreskin by altering the composition of the penile microbiota, leading to reduced susceptibility to HIV.

Our group has previously shown that the abundance of anaerobic bacteria in the microbiota of uncircumcised men is correlated with HIV seroconversion; six species in particular are correlated with increased immune cell densities in the foreskin tissues, secretion of inflammatory cytokines, and HIV seroconversion[39,41–43]. Our group also found that circumcision decreases total penile bacterial load and decreases anaerobe prevalence[39]. Thus, current evidence suggests that the prevalence of certain anaerobic species as part of the penile microbiota could lead to increased foreskin immune activation and inflammatory responses. This in turn could be increasing the number of HIV target cells present in the tissue, Langerhans cell sampling, and cytokine responsiveness. As well, inflammatory cytokine-induced decreases in junction-mediated barrier function may permit HIV virions to pass through the outer epidermis to access tissue immune cells. This final hypothesis, however, has never been examined mechanistically and is only posited based on observational studies.

1.3 Immune Defenses of the Skin

The skin plays a major role in protecting an individual from the external environment, and one particular way it does so is in preventing invasion by pathogenic microbes[66,104–107]. The skin employs a variety of methods to do so, which includes physical and immunological barriers, the commensal microbiota, as well as biomolecules and pH[66,104–107]. Lastly, Toll-like receptors (TLRs) act to sense microbial components and can activate

different gene programs that initiate both innate and adaptive immune responses in the host[108–110].

1.3.1 Physical Barriers

The skin forms a physical barrier against the exterior environment and protects the host through the formation of two mechanical barriers[106,107,111]. These two mechanical barriers are the stratum corneum (an air-liquid interface barrier) and tight junctions of the stratum granulosum (a liquid-liquid interface barrier)[106,107,111]. The stratum corneum is the foremost physical barrier against pathogens and other external forces, and its barrier function is based on its biochemical composition and tissue structure[107,111,112], which is often likened to “bricks and mortar”. Flattened corneocytes are surrounded by insoluble cornified envelopes and crosslinked lipid envelopes, with lipid envelopes generated by a monolayer of ceramides that replace the plasma membranes of the cells[107]. Lipid envelopes of the cells also comprise the scaffold that extracellular lipids use to fill the intercellular space[107,111]. Corneocytes are also connected to one another through corneodesmosomes, which are modified desmosomes originating from the uppermost-nucleated layers of the epidermis[107,111]. Corneodesmosomes are molecularly the same compared to desmosomes in other differentiated keratinocytes but are different in that they are immobilized at the cell periphery through enzymatic cross-linking by transglutaminases 1, 3, and 5[107,113]. The layered lipid structure of the stratum corneum provides waterproofing to the skin, and the permeability barrier as well, with the barrier held together via corneodesmosomes[107,111,114]. Disruption of corneodesmosomes in particular can cause loss of barrier function and inflammatory diseases as observed in multiple studies involving humans and mice[107,111,115–118]. In one particular set of studies, this was evident in individuals with homozygous nonsense mutations in the gene encoding corneodesmosin, a corneodesmosome component involved in adhesive functions[107,111,118–121]. This mutation leads to the extracellular portions of corneodesmosomes being less resistant to stress, and thus are easily cleaved[107,111]. This is especially present in the bottom most portion of the stratum corneum, at the interface with the stratum granulosum[107]. The consequence is development of peeling skin disease,

where mechanical separation of the stratum granulosum leaves entire areas of the skin with no stratum corneum-based barrier function[107,111]. Thus, these components form an important portion of the skin's barrier defense, and as a whole constitute the first protective barrier of the skin.

The tight junctions of the stratum granulosum form a second mechanical barrier against host invasion[66,106,122]. Tight junctions are cell-cell junctions present in simple and multilayered epithelia and endothelia[106]. Tight junctions consist of transmembrane proteins (proteins of the claudin family, junctional adhesion molecules (JAMs), and tight junction-associated marvel proteins like occludin) and plaque proteins (zonula occludens (ZO) 1-3, multi-PDZ domain protein-1 (MUPP-1), cingulin)[66,106]. Tight junction proteins connect to the actin cytoskeleton of neighbouring cells and act to prevent paracellular transport of molecules in the space between cells [66,106]. Only a few tight junction proteins are unique to the stratum granulosum (i.e., occludin, cingulin)[106], while others are also present in the upper stratum spinosum (such as ZO-1, ZO-2; claudin-4, 6, 18) or all living layers of the epidermis (claudin-1, 7; JAM-A, MUPP-1)[106]. The distribution and composition of tight junction proteins is shown in Figure 1.5.

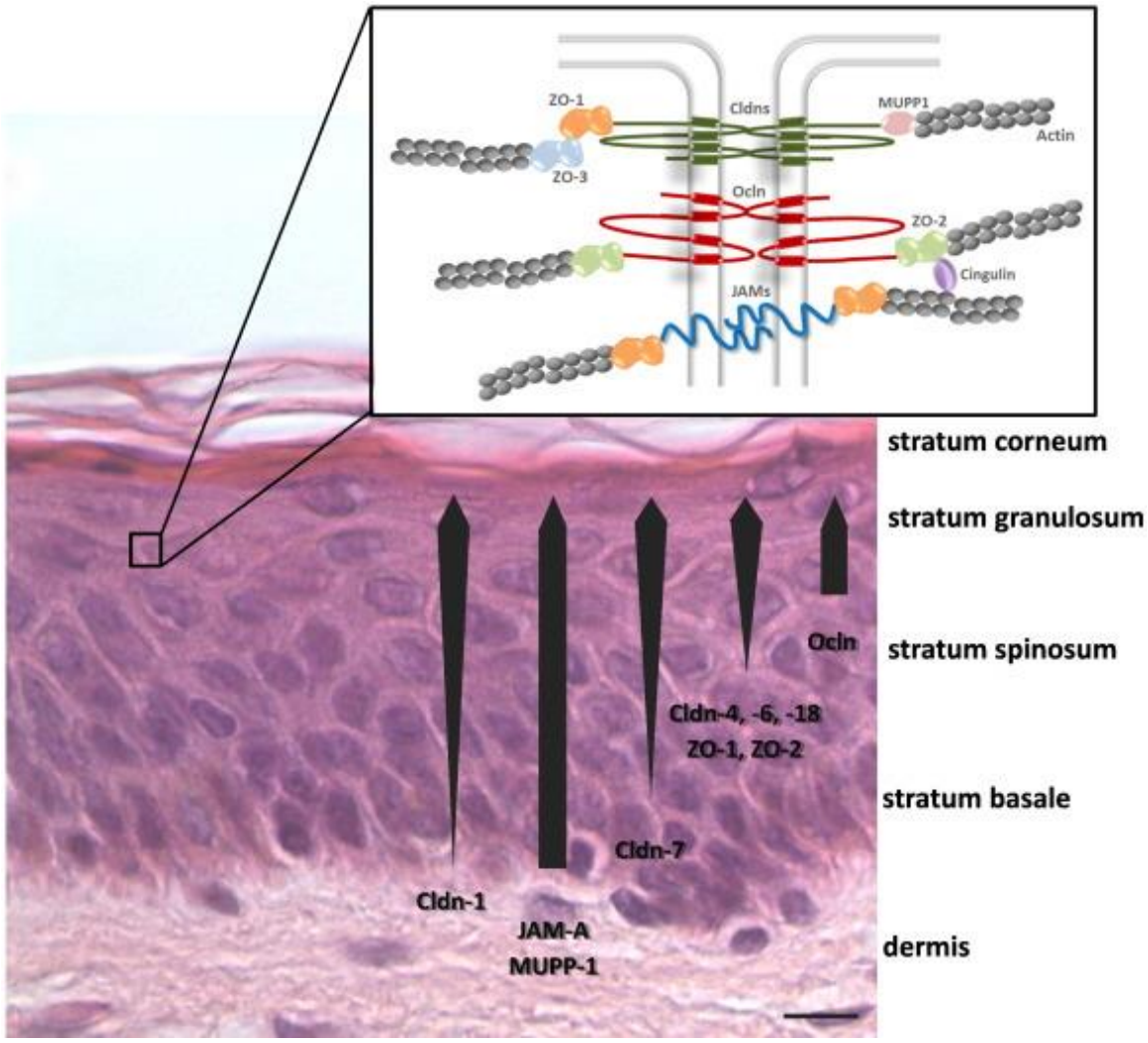

Figure 1.5: Distribution of Tight Junction Proteins Throughout the Epidermis and Tight Junction Composition. Cldn, Claudin; ZO, Zonula Occludens; Ocln, Occludin. From Bäsler *et al*, Journal of Controlled Release, 2016[106].

Experiments looking at the barrier function of tight junctions have shown they can form an effective inside-out barrier to molecules of various sizes. Tracer molecules weighing 557 Daltons (Da), 1500 Da, 5 kilodaltons (kDa), 31 kDa, and 32 kDa can accumulate at the tight junctions in the stratum granulosum after being injected intradermally, as well as lanthanum^{3+} cations[106,123–128]. This has also been demonstrated through *in vitro* experiments examining outside-in barrier function, where normal human epidermal

keratinocyte (NHEK) cultures have been shown to stop apically applied tracers[106,129,130]. NHEK cultures were shown to be able to exclude both ions and intermediate sized tracers like 4 kDa fluorescein isothiocyanate (FITC) labelled dextran through action of claudin-1, claudin-4, occludin, and ZO-1[106,129,131]. Claudin-1 and ZO-1 were also shown as contributing to the barrier function against large tracers like 40 kDa FITC labelled dextran[106,129]. Alterations in the expression or function of these components can result in various pathologies and ultimately disrupted barrier function[63,66,106,132]. Numerous studies using mice, cultured cells, and human participants have been conducted to investigate the interactions between tight junctions and varying components of the skin barrier (reviewed in Bäsler *et al*, 2016)[106]. A mouse study found that deletion of claudin-1 lead to death shortly after birth due to defects in the skin barrier leading to fluid loss[66,123]. In a study of patients with atopic dermatitis, it was found that at both the mRNA and protein level, patients with atopic dermatitis had reduced expression of both claudin-1 and claudin-23[132]. This is interesting in the sense that atopic dermatitis is a condition known for hyperactive immune responses and dry skin (hallmarks of tight junction impairment)[132]. Additional experiments in this study showed that silencing of claudin-1 expression in primary human keratinocytes resulted in diminished tight junction function and barrier dysfunction[132]. Additionally, another study showed tape stripping of mice skin (used to remove the stratum corneum) caused downregulation of claudin-1 and 4 protein levels (no change in mRNA expression), as well as disrupted barrier function to lanthanum^{3+} cations after 30 minutes[133]. Subsequently, an increase in claudin-4 protein expression restored barrier function one-hour post tape stripping[133]. From these investigatory studies and knockout experiments, it can be shown that tight junction proteins play an important role in the formation of an “inside-out” barrier preventing fluid loss, as well as an “outside-in” barrier preventing foreign substance entry.

1.3.2 The Immunological Barrier

There are several immune cells localized to the skin, and they all play an important role in promoting and maintaining tissue function[66]. Dendritic cells localized and specific to the epidermis, known as Langerhans cells, are thought to play a large role in inducing T

cell responses to specific antigens, while recruiting peripheral immune cells through cytokine secretion[66,111,128]. Langerhans cells anchor themselves to keratinocytes in the epidermis through interacting with epithelial cell adhesion molecules or E-cadherin[66]. In this, they can act to sample their environment through aiming the tips of their dendrites at the basal portion of tight junctions or below towards the stratum basale[66,111,128]. Upon Langerhans cell activation, these processes can extend upward through the tight junction to sample the region just below the stratum corneum, or extend downward towards the stratum basale[66,111,128]. Tight junctions are not broken in the former, and the epidermal barrier is maintained: this is through the formation of a new claudin-dependent tricellular tight junction between the dendrites of the Langerhans cell and surrounding keratinocytes[66,111,128,134]. These processes allow for sampling of the environment, uptake of external antigens by the tips of extended Langerhans cell dendrites, and immune activation[66,111]. This is, however, reliant on external antigens penetrating the layers of the stratum corneum in order to be taken up by the extended Langerhans cell dendrites[66,111,128]. Langerhans cells also move from the skin towards skin draining lymph nodes to promote tolerance in homeostasis[66].

Dendritic cells reside in the dermis, known as dermal dendritic cells[66]. These dermal cells can move to lymph nodes and act to promote the priming of adaptive immune responses similar to Langerhans cells[135,136]. These cells are involved in maintaining homeostasis between the host's commensal bacteria and body, as demonstrated through studying mice deficient in basic leucine zipper transcription factor ATF-like 3 (Batf3) necessary for conventional dendritic cell 1 (cDC1) activation[137]. These mice had lower levels of CD8+ T cells specific for *Staphylococcus epidermidis*, a common skin bacterium, highlighting the importance of dermal dendritic cells in maintaining control of T cells specific for commensal bacteria[137]. Additionally, found in the dermal layer are macrophages, mast cells, eosinophils, and lymphoid immune cells (reviewed in Nguyen, A.V. & Soulika, A.M., 2019)[66]. Skin resident macrophages develop an immunoregulatory role, and act to remove cellular debris; they are usually located at post capillary venules, and can act to recruit neutrophils in the event of skin wounding[66]. Mast cells are involved in allergic reactions, whereby they produce histamine[66]. Mast cells also produce leukotrienes that can act to attract neutrophils to sites of inflammation, while interestingly acting to prime

adaptive responses during cutaneous infection[66]. Eosinophils can produce extracellular DNA traps in their granules, which play a role in antibacterial defense, as well as toxic proteins and cytokines that can be used against parasitic infections[66]. Lastly, the dermis contains many different lymphocytes that are important in inflammatory and homeostatic mechanisms[66]. These include natural killer T cells, and most predominantly in human skin, αβT cells[66].

1.3.3 Biomolecule Defenses and pH

In defense against bacterial insult, skin cells produce antimicrobial peptides (AMPs) and lipids[138,139]. AMPs are amphipathic molecules that act synergistically to disrupt microbial membranes across a broad range of microbial species[66]. They can be expressed constitutively or induced through inflammation or homeostatic changes[66]. AMPs are produced as a pro-peptide and upon proteolytic cleavage, become active[66]. There are two well studied families of AMPs in humans, the defensins and cathelicidins[66,140,141]. Defensins are encoded by distinct genes, whereas cathelicidin is encoded by one gene[66]. β-defensins differ in expression between cells, and keratinocytes of the skin constitutively express β-defensin-1, while β-defensin-2 to 4 are expressed upon infection or injury[140,142]. Cathelicidin LL-37 is also expressed differentially and can be found constitutively expressed in neutrophils but induced by exposure to lipopolysaccharide (LPS) or vitamin D3 in keratinocytes[140,142]. The pro-peptide generated from the cathelicidin gene, known as cathelicidin antimicrobial peptide or CAMP, is proteolytically cleaved to result in a number of mature, biologically active peptides[66,140,141]. The most well studied mature peptide of this grouping is known as cathelicidin LL-37[66,140,141]. β-defensins and cathelicidins then act to supplement the stratum corneum mechanical barrier by providing an additional layer of antimicrobial defense[143,144]. Upon generation, they are then placed into lamellar bodies, then localized to the stratum corneum to do so[143,144]. Aside from contributing to host innate immunity, AMPs are involved in modulating host immune responses to selectively control pathogen-induced inflammatory responses (reviewed in Niyonsaba *et al*, 2006 and Pfalzgraff *et al*, 2018)[66,139,140]. Cathelicidin LL-37 in humans has been shown to induce monocyte derived dendritic cell differentiation, cytokine

secretion, and expression of CD86[66]. α- and β-defensins also act as chemoattractants for immature dendritic cells, activated neutrophils, memory T cells, and Naïve T cells[66]. β-defensins 3 and 4 have also been shown to recruit monocytes and macrophages[66].

Aside from AMPs, antimicrobial lipids have also been shown to exert antimicrobial activity against specific bacterial species[63,66]. Molecules such as sphingomyelin and glucosylceramides are converted into sphingosine and dihydrosphingosine that exact antimicrobial activity against bacteria like *Streptococcus pyogenes* or *Staphylococcus aureus*[63,66].

1.3.4 The Skin Microbiota

The human skin microbiota is an incredibly important defense mechanism, acting as an additional physical and biochemical barrier to the external environment[104–106]. This barrier is established on the microbial level through (1) competitive exclusion of other microbes, and (2) production of various antimicrobial compounds[104–106]. This acts to limit the colonization of the skin by limiting the growth of possibly pathogenic microorganisms[104–106]. This is best observed through studies on microbial dysbiosis and disease development. Disturbing the skin microbiota and its homeostatic balance with the host often leads to the development of inflammatory skin diseases, such as atopic dermatitis or psoriasis[104,106]. Studies of atopic dermatitis have shown that the disease arises due to a compromised stratum corneum [104]. Additionally, copy number differences for AMP genes like β-defensins could lead to psoriasis[104]. When these two important barrier functions are reduced in the skin, it might lead to altered skin-microbiota homeostasis through penetration of and sensitization to microbes or their components[104]. Additionally, the microbiota in atopic dermatitis patients is altered in most cases of the disease. In healthy individuals, the commensal skin microbiota is composed of bacteria belonging to the genus *Firmicutes* (such as *Staphylococcus epidermidis*) and *Actinobacteria* (such as *Propionibacterium* and *Corynebacterium*)[104]. In the case of atopic dermatitis, *Staphylococcus aureus* colonization disrupts the microbiota and decreases overall bacterial abundance[104]. Additionally, *in vitro* experiments examining

the effect of commensal bacteria on the skin barrier have shown they are important for epithelial barrier function[106,145–147]. Application of probiotic bacterial cell lysates to NHEK cell monolayers can increase both tight junction protein expression and transepithelial electrical resistance (TEER; a measure of permeability), which may improve barrier function[147]. Despite this evidence, it is still unclear whether microbial dysbiosis is causally linked to disease development, or is simply the result of abnormal skin biology[104]. Thus, together with the evidence presented in Section 1.2, it is possible that certain perturbations in the microbiota could be implicated in the development of disease, and that this should be investigated further to establish a causal link.

1.3.5 Toll-like Receptors

Toll-like receptors (TLRs) are a class of pattern recognition receptors that sense a wide range of microbial components and serve to protect the host by initiating innate and adaptive immune responses (reviewed in Miller, L. S., 2008; Fore *et al*, 2020; Takeda, K. and Akira, S., 2005)[108–110]. These microbial components are known as pathogen associated molecular patterns (PAMPs), which are highly conserved molecular patterns found in microorganisms[108–110]. TLRs exist as transmembrane glycoproteins that can initiate intracellular signaling cascades that activate nuclear factor-kappa-light-chain-enhancer of activated B cells (NF-κB) and end in the expression of immunomodulatory genes encoding many different proteins[96,133]. Cytokines, chemokines, interferons, AMPs, co-stimulatory molecules, and adhesion molecules can all be expressed upon activation of TLRs[108,110]. In humans, there are 10 TLRs that differ in sub-cellular expression, as shown in Figure 1.6. TLRs 1, 2, 4, 5, 6, and 10 are all found on the cell surface, while TLRs 3, 7, 8, and 9 are found intracellularly on the surface of endosomes[108,109]. TLRs located on the external surface of cells can detect various distinct external PAMPs[108–110]. TLR2 can form heterodimers with either TLR1 or TLR6 to detect triacyl and diacyl lipopeptides, which originate from *Mycoplasma* and various bacteria, respectively[108,110]. TLR2 can also recognize peptidoglycan common to Gram-positive and -negative bacteria, and the TLR2/6 heterodimer can recognize lipoteichoic acid found in Gram-positive bacteria[108,110]. TLR4 can recognize lipopolysaccharide from Gram-negative bacteria,

while TLR5 can detect flagellin from flagellated bacteria[108–110]. Intracellular TLRs detect components of microbes that can be found within the cell itself[108–110]. TLR7 and 8 can detect uridine- or guanosine-rich single-stranded viral RNA (such as that of HIV or influenza), while TLR9 detects hypomethylated CpG motifs in bacterial double-stranded DNA[108,110]. TLR10, often found expressed on the surface of B cells, monocytes, dendritic cells, and neutrophils, has no known PAMP that it responds to[108–110]. TLRs are expressed by many cells of the skin, including keratinocytes, fibroblasts, adipocytes, Langerhans cells, monocytes, dendritic cells, B-cells, mast cells, and monocytes[105,108,109,141]. Keratinocytes are known to express TLRs 1-6, and 9 in particular[96,133]. By stimulating the secretion of immune factors such as cytokines, and recruiting immune cells like phagocytes to a site of possible infection, TLRs help in establishing and maintaining another layer of immune defense atop of the already established barriers in this section (reviewed in Takeda, K. & Akira, S., 2005)[108–110]

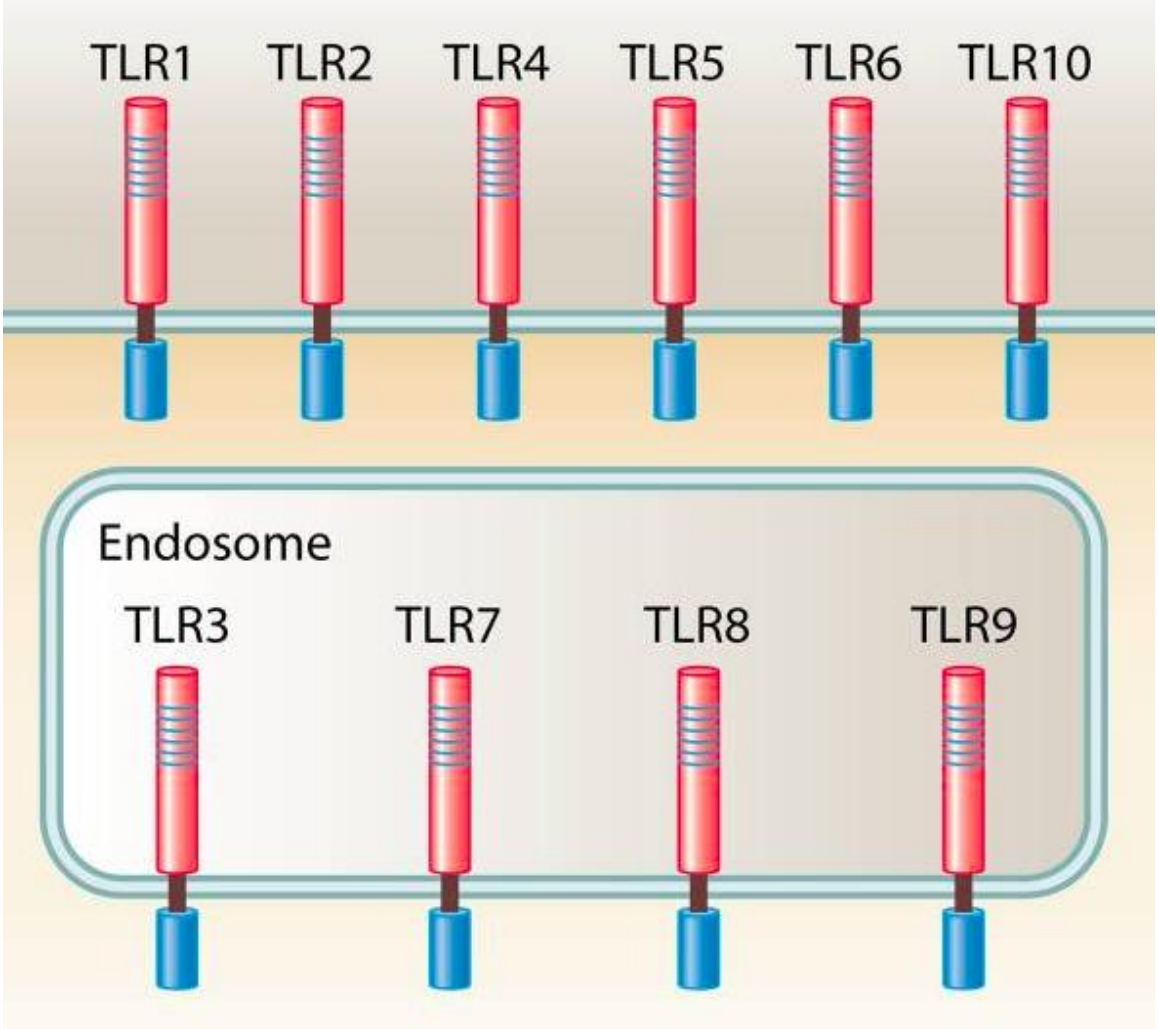

Figure 1.6: Toll-like Receptor Subcellular Localization. Modified from Mogensen, T. H., Clinical Microbiology Reviews, 2009[148].

1.4 The Microbiota and HIV-1 Susceptibility

The microbiota is a complex microbial ecosystem that rapidly colonizes its host during and after birth[104,105]. The microbiota develops from exposure to environmental microbes and becomes increasingly diverse through childhood[104,105]. Trillions of microbes, from bacteria, archaea, and even viruses colonize humans, with at least 1000 different known species of bacteria. Host factors such as genetics, sex, ethnicity, lifestyle, and diet all influence this diverse microbial environment[104,105].

The microbiota is comprised of both transient and resident microbes[104]. If looking at the skin, transient microorganisms temporarily live on the skin surface, whereas resident microorganisms are those in homeostatic balance with the host and comprise the commensal skin microbiota[104]. Over decades of study, it has been determined that the human microbiota is strongly associated with both health and the development of disease (reviewed in Wang *et al*, 2017)[105]. Microbial dysbiosis through perturbation of the commensal microbiota is also known to result in the development of various diseases[105].

As mentioned in Section 1.2.5, a hypothesis for variable HIV susceptibility in heterosexual men has been identified whereby penile microbial dysbiosis leads to localized penile inflammation. A series of studies were performed to facilitate this, using both penile coronal sulcus swabs from the RCT in Uganda as well as a cross-sectional cohort from the RCT to examine foreskin tissues[39–42]. These penile swabs were taken from uncircumcised and circumcised HIV negative men at trial enrollment, who were then followed for the duration of the two-year trial and re-swabbed at 6 months, 1-year, and 2-years post enrollment. Men were also monitored for HIV seroconversion.

Results from these studies showed that the odds of seroconversion increased upon detection of multiple cytokines on the coronal sulcus surface, with detectable IL-8 and monokine induced by interferon gamma (MIG) specifically associated with HIV acquisition[42]. Further, IL-8 levels were found to decrease following circumcision[42]. At six months post circumcision, IL-8 levels were significantly reduced and continued to decline afterward[42]. Coronal sulcus IL-8 levels were also correlated with the density of neutrophils and susceptible CD4+ T cell subsets (such as T helper 17 [Th17] cells) in the

foreskin tissue[42]. As well, the microbiota changed significantly after circumcision. Pre-circumcision, the microbiota contained 38 bacterial families, was more heterogeneous, and also was composed of several core community types[40]. One community type observed was dominated by the anaerobic bacterial families *Clostridiales* Family XI and *Prevotellaceae*, which have been identified as elevated in the human vagina during BV[40]. It was found that bacterial families predominantly composed of anaerobic genera were decreased in abundance in circumcised participants, while facultative anaerobic genera were increased in abundance[40]. It was also found that there were stark differences between the microbiota of uncircumcised and circumcised men[39]. Initially, men at baseline of control (uncircumcised) and treatment (circumcised) arms showed similar microbiota composition[39]. One-year post circumcision, the microbiota showed reduced total bacterial load and biodiversity[39]. Specifically, 12 anaerobic taxa decreased in prevalence and absolute abundance, with minor gains in aerobic taxa[39]. Lastly, it was found that men infected by HIV had significantly higher penile anaerobe abundances at baseline relative uninfected men[41]. These anaerobes included *Prevotella*, *Dialister*, *Mobiluncus*, *Murdochiella* and *Peptostreptococcus*[41]. It was also found that uncircumcised men with a greater absolute abundance of penile anaerobes had a greater concentration of chemokines (such as IL-8) at the coronal sulcus[41].

In sum, these results highlighted that circumcision profoundly shifts the penile microbiota, inflammatory cytokine abundance, and HIV target cell density at the level of the foreskin. This strongly suggests that these factors could be involved in variable male HIV susceptibility. Anaerobic bacteria have already been known to cause BV in females when in high abundance, and BV has been associated with vaginal inflammation and increased risk of HIV in females[102,103]. As such, it is suggested that the reduction in anaerobes may be the driving force behind circumcision's protective effect against HIV. From this, a plausible mechanism for HIV susceptibility can be developed involving host immune modulation. In uncircumcised men with high anaerobe abundance, localized secretion of chemokines like IL-8 could recruit neutrophils to the tissue. Neutrophils would act to recruit T cells to the tissue through release of chemokines, including the highly susceptible Th17 T cell subset. This would act to make the foreskin stochastically

more susceptible to HIV infection by virtue of increased immune cells present in the tissue.

Recently, a newly developed Bayesian classifier was used to extract species level data from the two cohorts discussed previously, highlighting the impact of penile anaerobes on local tissue inflammation and in turn, HIV susceptibility[43]. This study revealed that, as can be shown in Figure 1.7, there was a strong correlation between men with a greater proportional abundance of the anaerobe *Prevotella* in their microbiota and the risk of HIV seroconversion. Total bacterial density was also significantly associated with the risk of seroconversion, but this was not as strong of a relationship. Further, of the anaerobic genera associated with seroconversion, six species of anaerobes (*Peptostreptococcus anaerobius*, *Prevotella bivia*, *Prevotella disiens, Dialister propionicifaciens, Dialister micraerophilus*, and *Dialister succinatiphilus*) were identified and correlated with subpreputial IL-8 levels, α-defensins, the density of HIV target cells in foreskin tissue, and seroconversion. This provides strong evidence of a relationship between penile anaerobic species and seroconversion; however, this data remains observational and could be confounded by anaerobe co-occurrence. Controlled study of these anaerobic species using tissue models could provide evidence of a causal relationship and help elucidate the exact mechanism by which they impact HIV seroconversion. Additionally, this might guide development of novel targeted intervention strategies to eliminate these HIV associated bacteria from the penile microbiota.

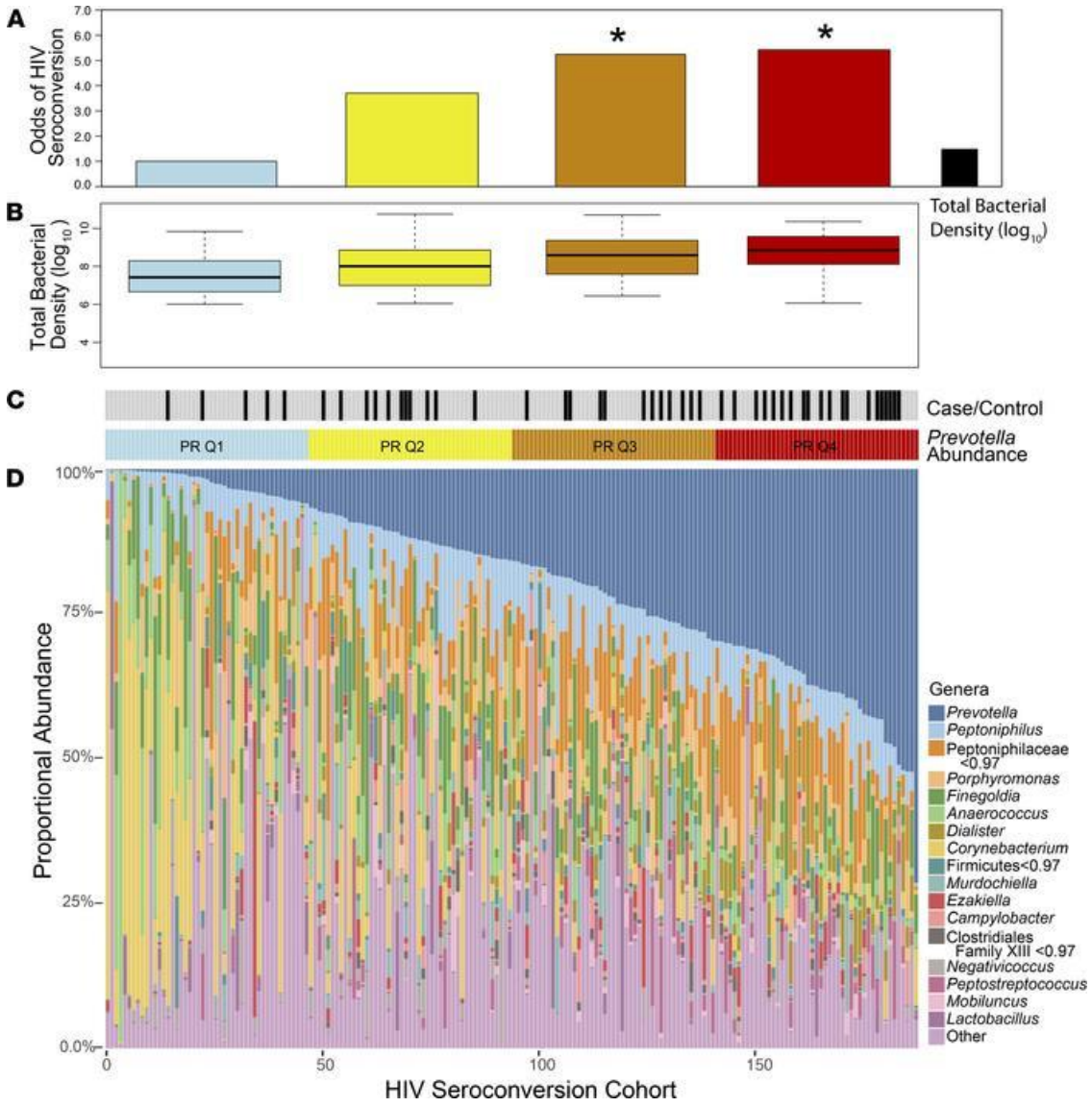

Figure 1.7: Microbiota Composition Stratified by *Prevotella* Proportional Abundance and Relation to HIV Risk Across Uncircumcised Men in Rakai, Uganda. (**A**) HIV risk increases alongside increasing *Prevotella* abundance and (**B**) total bacterial density. **C** shows case/control status in the study (each black bar represents one participant who seroconverted during the study; each grey bar a nonconverter) and *Prevotella* Quartiles. (**D**) Proportional abundances of the bacterial genera comprising the penile microbiota across the cohort tracked in the study (*n* = 188). Men were grouped via *Prevotella* proportional abundance quartiles so as to use case/control status to determine HIV risk across each quartile. PR Q, *Prevotella* quartile. From Prodger *et al*, JCI Insight, 2021[43].

1.5 Current Tissue Models and Limitations

Researchers have, in the past, created *in vitro* co-cultures to investigate microbial-human interactions. These *in vitro* models, however, quite often lacked sufficient complexity and presented many limitations in study design, which will be discussed below.

Previous *in vitro* models have often consisted of peripheral blood samples or monolayers of human cell lines inoculated with bacterial monocultures or bacterial products (e.g., LPS). This presents a wide variety of problems. One such problem is that cell lines or blood samples typically do not respond to commensal bacteria as well as primary cells isolated from tissue[149,150]. Monolayers also lack the complex cell-cell interactions and overall physiology that constitutes a tissue such as skin, while also impeding the addition of other cell types necessary to mimic the tissue (e.g., fibroblasts, melanocytes, immune cells)[151]. Submerged monolayers or blood cell suspensions also do not provide a physiologically relevant, dry surface for inoculation with a microbiota. One way to solve this limitation is through culturing a piece of surgically removed foreskin tissue, known as an explant. This strategy is also limited, however, as tissue viability and structure is gradually lost in culture due to cell migration[152]. This is problematic, as it is necessary to have a tissue remain stable over time to successfully study microbiota-tissue interactions. Finally, bacterial cell lysates applied to such models ignore skin-microbiota interactions, which are known to be imperative to skin barrier functioning and host processes (established in Sections 1.3.4 and 1.4)[153].

1.6 The Need for a Three-Dimensional, *In Vitro* Organotypic Foreskin Model

The studies relating the penile microbiota to HIV acquisition have thus far all been *in vivo* observational studies, limiting our ability to establish causality or explore the mechanics and relationship between the two. Additionally, anaerobes associated with HIV acquisition co-occur in the microbiota, limiting the ability to elucidate which specific species drive HIV susceptibility, or target species for intervention development. In order to empirically determine if and how the penile microbiota modulates the host

immune system and increases HIV susceptibility, it is necessary to generate an *in vitro* organotypic foreskin equivalent from primary skin cells. This foreskin model would bypass limitations imposed by previous work investigating tissue-microbiota interactions presented in Section 1.5. First, the skin model posited is a three-dimensional tissue that allows for complex interactions between the dermis, epidermis, and the cells that compose each of these. As the skin model is further refined and developed, additional cell types (e.g., melanocytes) and immune cells could be added to the tissue in a layer specific fashion, in sharp contrast to monolayers that do not permit this. Specifically, the dermal portion of the tissue mimic would provide an area for adding CD4+ T cells. The tissue model also presents a physiologically relevant dry surface for the culture of penile bacteria, in comparison to submerged monolayers that do not provide this. Additionally, primary cells that constitute the tissue would likely more accurately respond to commensal bacteria added to the top of the epidermal tissue surface[149,150]. Lastly, this model could present a more stable alternative to conventional explant cultures commonly used in HIV infection studies. Our group and others have observed that explant cultures deteriorate over time during culture, with the epithelium sloughing off and the dermis losing shape. Being able to develop a three-dimensional tissue mimic, as is the basis of this project, could remedy this problem in that the organotypic tissue may act to better maintain the physical epithelial barrier over time in addition to the previously mentioned benefits. This would permit the study of penile anaerobes selectively using a tissue that closely mimics *in vivo* foreskin tissue, without the caveats faced by current tissue models and explanted tissue itself.

1.7 Hypothesis and Specific Aims

Based on the lack of *in vitro* tissue models needed to study anaerobe-induced inflammation, I hypothesized that an *in vitro*, organotypic, 3D foreskin model could be developed and be able to model *in vivo* foreskin in structure and function. Specifically, I hypothesized that this organotypic tissue model would be able to mimic the skin in structure by generating a multilayer epithelium comprised of differentiated cells. It would

also retain relevant functional characteristics, including the ability to sense and respond to microbial products like LPS, while providing a mechanical barrier.

1.7.1 Specific Aims

Aim 1: Develop the 3D, *in vitro* organotypic foreskin model and characterize its structure relative fresh and seven-day explant-cultured foreskin tissues.

Aim 2: Characterize gene expression for microbial sensors, antimicrobial peptides, and the ability to secrete cytokines in response to bacterial ligand application by the organotypic foreskin model, relative fresh and explant cultured tissue.

Aim 3: Assess the barrier function of the organotypic model in comparison to fresh and seven-day explant-cultured foreskin tissues.

Chapter 2

2 Participants and Methodology

2.1 Participants

Two participant populations were enrolled in this study. One population consisted of adult men (≥18 years of age) undergoing circumcision for elective reasons (e.g., religious, cultural, or cosmetic) at the University Urology Associates (UUA) in Toronto, Ontario. Exclusion criteria included clinically apparent genital infection, recent antibiotic use (>30 days), and current hormone therapy. The second population consisted of boys (<18 years of age) undergoing circumcision at the London Health Sciences Centre (LHSC), London, Ontario, for either elective or medically indicated reasons (e.g., treatment of recurrent balanitis, phimosis, recurrent urinary tract infection [UTI], or balanitis xerotica obliterans [BXO]). Both adult and paediatric participants were excluded from the study if they displayed medical contraindications to circumcision surgery. Adult participants completed a behavioural questionnaire before surgery/sample collection. Paediatric participants or their substitute decision maker (SDM) completed a brief questionnaire regarding signs or history of genital infection and/or antibiotic use. All adult participants provided written consent; paediatric participants provided consent themselves if >16 years and assent if aged 8-16; and SDM of paediatric participants <16 years provided written consent. Formal ethics approval was obtained from institutional review boards (IRB) at the University of Toronto and the University of Western Ontario (protocol IDs 113008 and 111054, Western; Appendix A).

2.2 Sample Collection

Foreskin tissue was placed into a sterile 50 mL conical tube in the operating room and transported back to Western university within 4 hours of surgery. Segments of the harvested tissue were processed and stored in several ways, depending on requirements for future analysis, as schematically depicted in Figure 2.1, and described below.

Tissues were sectioned for immediate use in primary cell isolation (Section 2.3) and/or explant assays, cryopreserved for immunofluorescence microscopy (IF), or quantitative polymerase chain reaction (qPCR). For IF, two 3 x 3 mm sections of inner and outer foreskin tissue were placed in cryomolds, embedded in Tissue-Plus optimal cutting temperature embedding medium (OCT; Thermo Fisher Scientific) and were snap-frozen at -80°C. For qPCR, an eight-millimeter tissue biopsy punch (Integra Militex) was used to obtain a section that was placed into RNAlater (Invitrogen) at 4°C overnight and then frozen at -80°C. When RNAlater was not available, the qPCR punch biopsy was cryopreserved in a mixture of 90% heat-inactivated fetal bovine serum (HI FBS; Gibco) and 10% DMSO (dimethyl sulfoxide; MilliporeSigma) by placing in a Nalgene Mr. Frosty freezing unit (Thermo Fisher Scientific) overnight at -80 prior to long-term storage in liquid nitrogen. Samples frozen using this method were then placed into RNAlater-ICE (Invitrogen) and allowed to thaw at -20°C to preserve RNA quality when used for qPCR analysis. For culture of tissue explants, tissue samples were divided into 16 additional sections using an eight-millimeter tissue biopsy punch. Eight sections were cultured in Maintenance Medium (Table 2.8) for seven days prior to further assays ("seven-day explants"). The remaining eight pieces were taken as representative of fresh *in vivo* tissue. For both the freshly analyzed and seven-day explant tissues, four sections were subject to a permeability assay (below) and the other four subject to a Toll-like Receptor stimulation assay (below).

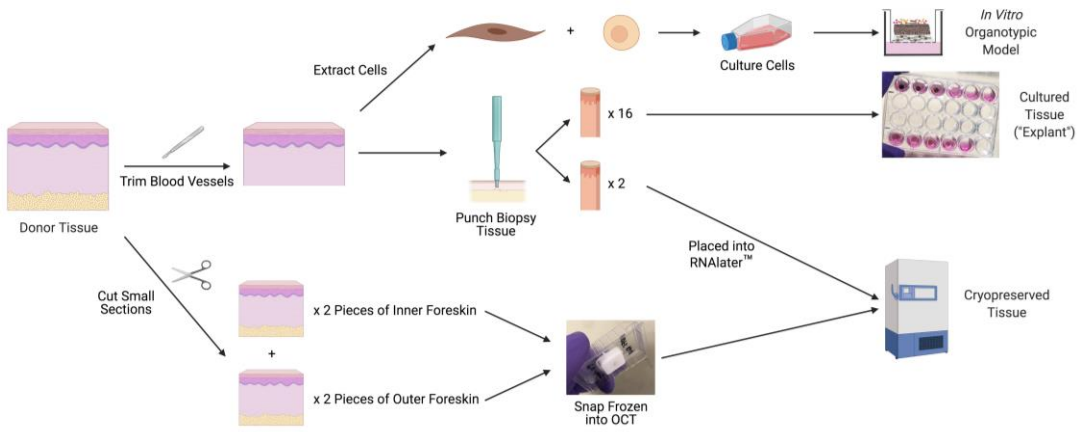

Figure 2.1: Summary of Foreskin Tissue Processing. Donor tissues receive varying treatment to generate organotypic, explant cultured, and frozen tissues for use in future analysis. Donor tissues first have two pieces of inner and outer foreskin excised using scissors (bottom), which are immediately frozen in OCT medium. The remaining foreskin tissues are trimmed of any remaining blood vessels. A portion of this tissue is then used for cell extraction (top) to generate organotypic foreskin tissues. The remaining tissue is then cut using a biopsy punch with two pieces placed into RNAlater and stored at -80°C for qPCR analysis, with remaining punch biopsies used for explant culture generation. Figure created with BioRender.com.

2.3 Isolation and Culture of Epidermal Keratinocytes and Dermal Fibroblasts

Tissues were processed according to the protocol established by Gangatirkar *et al*, 2007[154]. In brief, foreskin tissue samples were washed with 1X Dulbecco's phosphate buffered saline (DPBS; Gibco), with blood vessels removed thereafter. Tissues were then sectioned into pieces approximately 0.5 cm x 0.5 cm, covered in a 2.4 U/mL Dispase II solution (Gibco) at 4°C overnight followed with one hour at 37°C the next day to facilitate separation of the dermis from the epidermis. The dermis and epidermis were mechanically separated with forceps.

To isolate fibroblasts, dermal sections were placed into Dispase and collagenase (dissolved in 1X DPBS; 2.4 U/mL Dispase II, 780 U/mL collagenase type IV; collagenase from Gibco) and minced into smaller pieces with scissors. Minced dermal tissues were incubated in a 37°C, 5% CO_2 humidified incubator for two hours, with brief vortexing of the samples every 30 minutes. The resulting dermal suspension was diluted with three volume equivalents of DMEM Complete medium [Dulbecco's modified eagle medium (DMEM; Gibco) supplemented with 10% HI FBS (Gibco) and 1% penicillin-streptomycin (P/S; MilliporeSigma)], then filtered through a 70 µm cell strainer. The fibroblast suspension was then centrifuged at 114 x *g* for eight minutes, resuspended in DMEM Complete, and the number of Trypan Blue-excluding cells was determined (0.4% Trypan Blue; Gibco). Live cells were then plated at a density of 5.3×10^4 cells/cm^2.

To isolate keratinocytes, epidermal sheets were placed into a solution of 0.05% trypsin-ethylenediaminetetraacetic acid (EDTA; Gibco), minced with scissors, and left in a 37°C, 5% CO_2 humidified incubator for seven minutes. The resultant epidermal cell suspension was neutralized by adding two volume equivalents of a solution comprised of 20% HI FBS in 1X DPBS, then filtered through a 70 µm cell strainer. The keratinocyte suspension was then centrifuged at 114 x *g* for eight minutes and resuspended in keratinocyte serum-free medium (K-SFM) supplemented with 894 µL bovine pituitary extract (BPE), 2.8 µL recombinant epithelial growth factor (rEGF), and 2% Primocin (BPE and rEGF from Gibco, Primocin from InvivoGen; medium henceforth known as K-SFM Complete). These cells were then counted via Trypan Blue exclusion and plated at a density of 5.3×10^4 cells/cm^2.

Fibroblasts were maintained in DMEM Complete with medium changed every other day and passaged when 80-85% confluent. Fibroblasts were subcultured by rinsing cells with 1X DPBS, using a solution of 0.05% Trypsin-EDTA to dissociate cells from their cell culture vessel, neutralizing with DMEM Complete, centrifuging at 114 x *g*, resuspending, and replating at a ratio of 1:10. Fibroblasts were cryopreserved after proliferation (often at passage 4) by pelleting dissociated cells at 114 x *g* for 7 minutes, resuspending in cell freezing mixture (50% HI FBS, 40% DMEM Complete, and 10% DMSO), placing into a cell freezing unit, and freezing at -80°C.

Keratinocytes were allowed to reach 80-85% confluence, then subcultured routinely. Cells were maintained in K-SFM Complete with medium changed every other day and passaged when 80-85% confluent. Passages were accomplished by incubating cells with 0.5 mM EDTA in 1X DPBS, then incubating with Accutase (MilliporeSigma) to dissociate cells from their cell culture vessel, neutralizing with 20% HI FBS in 1X DPBS, centrifuging at 114 x *g* to remove serum, resuspending, and replating at a ratio of 1:2.

Cells were monitored via microscopy using a ZEISS Axio Observer.A1 inverted microscope.

2.4 Immortalization of Foreskin Keratinocytes

Primary human keratinocytes undergo cellular senescence after approximately 10 doublings. To maximize keratinocyte longevity for this project, it was necessary to immortalize these cells. To do this, primary keratinocytes were transduced with a replication-incompetent amphoteric retroviral vector encoding HPV16 E6 and E7 oncogenes, as well as a resistance gene for the antibiotic neomycin. These oncogenes, when successfully transduced into keratinocytes, extend the lifespan of the cell through production of E6 and E7 oncoproteins.

PA317 LXSN virus packaging cells were purchased to produce this retroviral vector (American Type Culture Collection [ATCC] CRL-2202). These cells contained the pLXSN16E6E7 insert, and when cultured, produce a retroviral vector which can be harvested from supernatant. To transduce keratinocytes, keratinocytes were washed with 1X DPBS, and a small volume (e.g., 1 mL per T25, 3 mL per T75) of transduction cocktail was added to the culture vessel (transduction cocktail contents found in Table 2.1). After six hours, additional K-SFM Complete was added to the cell culture vessel such that the amount of medium within the vessel was at the required level for typical cell culture (e.g., 9 mL medium needed for a T75, total volume with cocktail is 12 mL). 24 hours following the addition of the transduction cocktail, cell culture medium was replaced. 48 hours post transduction cocktail addition, K-SFM supplemented with

Geneticin (Gibco; a structural analog of neomycin; final concentration 50 µg/mL in medium), was added to the cell culture vessel to select for transduced cells. Transduced primary keratinocytes were then subcultured routinely as described in Section 2.3, but now grown only in K-SFM supplemented with the selection agent Geneticin as opposed to Primocin.

Table 2.1: Transduction Cocktail Recipe.

Reagent	Volume (µL)
Protamine Sulphate (1 µg/mL)	20
K-SFM Complete	1800
PA317 Packaging Cell Supernatant	200
Total Volume	**2,000 µL**

Transduced keratinocytes were harvested and snap frozen after completing selection in Geneticin supplemented media and compared to (if available) matched non-transduced keratinocytes immediately snap frozen before the immortalization procedure. Keratinocytes were thawed, and genomic DNA isolated using a DNeasy Blood and Tissue Kit (Qiagen) following the manufacturer's spin column protocol. Samples were analyzed spectrophotometrically for concentration and purity, then subject to polymerase chain reaction (PCR) amplification. PCR was performed using a SimpliAmp Thermal Cycler (Applied Biosystems) with the reaction components listed in Table 2.2, primers in Table 2.3 and reaction conditions in Table 2.4. PCR amplicons were then subject to gel electrophoresis for visualization of the HPV16 E6E7 amplicon. When available, comparison between non-transduced and transduced keratinocytes from the same patient was conducted. Amplicons were resolved by electrophoresis in a 1% Tris-acetate-EDTA (TAE) agarose gel stained with RedSafe (FroggaBio) for 45 minutes next to a 1 kilobase (Kb) Ready-to-use DNA ladder (Simply Biologics) and visualized using a Gel Doc EZ imager system with Image Lab 4.0.1 software (both from Bio-Rad Laboratories). Successfully transduced keratinocytes were cryopreserved after proliferation (often at passage 6). Dissociated cells were pelleted at 114 x *g* for 7 minutes, resuspended in cell

freezing mixture (80% K-SFM Complete, 10% HI FBS, and 10% DMSO), placed into a cell freezing unit, and frozen at -80°C.

Table 2.2: Transduction Verification PCR Reaction Components.

Component	Volume (µL)
2X KAPA HiFi HotStart Ready Mix (Kapa Biosystems)	13
Forward Primer (1 µM)	5
Reverse Primer (1 µM)	5
Keratinocyte Genomic DNA	2
Total Volume	**25 µL**

Table 2.3: Primers used for Transduction Verification PCR. The primer pair was obtained from Choi *et al*, 2017[155]

Gene of Interest	Primer sequences	
	Forward (5′ -3′)	Reverse (5′-3′)
HPV16 E6E7	CTAGCTAGCATGCACCAAAAGAGAACTGC	CCGGAATTCTTATGATGGTTTCTGAGAACAGATGGG

Table 2.4: Transduction Verification PCR Conditions.

Step	Thermocycler Temperature (°C)	Time	Number of Cycles
Initial Denaturation	95	3 min	1
1. Denaturation	95	30 s	35
2. Anneal	60	30 s	
3. Extend	72	1 min	
Final Extension	72	5 min	1
Storage	4	∞	-

2.5 Casting Organotypic Foreskin Models

Organotypic foreskins were prepared as described in the protocol established by Gangatirkar *et al*, 2007, with some modifications[154]. A summary of modifications is shown in Table 2.5, with the entire casting process shown below in Figure 2.2. For

development and testing of the *in vitro* organotypic foreskin model, keratinocytes between passage 10 and 14 were most routinely used, while fibroblasts between passage 4 and 25 were used. Each was used to cast organotypic foreskins one to two passages after thawing.

Table 2.5: Modifications to Organotypic Foreskin Development Protocol.

Change Number	Original Protocol (Gangatirkar *et al*, 2007)	New Method
1	Use cellular layer cell suspension concentration of 2.3 x 10^5 cells/mL when casting the collagen cellular layer.	Increase cellular layer cell suspension concentration to 3.28 x 10^5 cells/mL.
2	Immediately culture keratinocyte-seeded collagen in Epidermalization Medium.	Grow keratinocyte-seeded collagen for 10 days in K-SFM Complete medium, prior to the one week of culture in Epidermalization Medium.
3	Seed 30 µL of keratinocytes at 1.667 x 10^6 cells/mL onto the collagen surface.	Seed 50 µL of keratinocytes at 16.67 x 10^6 cells/mL onto the collagen surface.
4	Add the 30 µL keratinocyte suspension as a single droplet to the center of the collagen hydrogel.	Add the 50 µL droplet of keratinocytes as individual 10 µL droplets evenly across the surface of the collagen, rather than directly in the center.

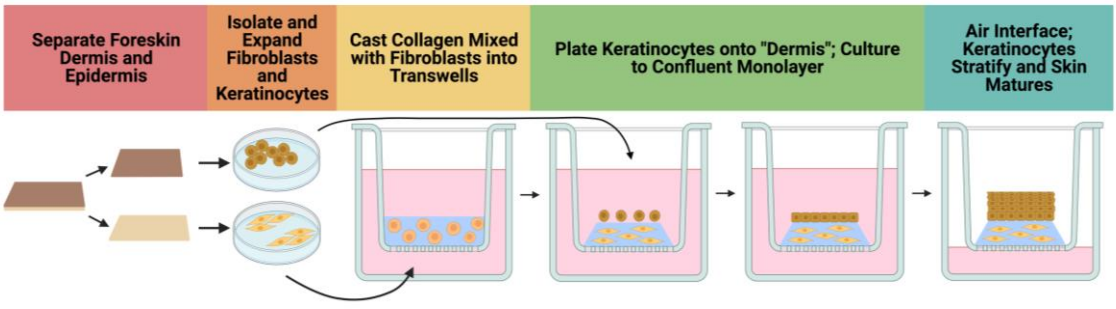

Figure 2.2: Overview of Methods used for Development of a 3D *In Vitro*, Organotypic Foreskin Model. Figure created with BioRender.com.

To create a dermal equivalent, acellular and cellular collagen layers were prepared and cast into 6-well plate Transwells (Corning). The 6-well Transwell membrane was composed of transparent polyethylene terephthalate and had a pore size of 3.0 µm. To prepare the initial acellular layer of collagen, pre-mix solution (Table 2.6) was added to bovine type 1 atelocollagen (Nutragen) and DMEM Complete as per the ratio established in Table 2.6 (next to "Acellular Collagen Layer"), all prepared and kept on ice. 1 mL of this mixture was cast into the apical chamber of 6-well Transwell inserts and allowed to polymerize for 30 minutes in a 37°C, 5% CO_2 humidified incubator. During this process, isolated primary foreskin fibroblasts were washed once with 1X DPBS, incubated for five minutes with 0.05% Trypsin-EDTA in a 37°C, 5% CO_2 humidified incubator, neutralized with DMEM Complete, centrifuged, resuspended, and counted via Trypan Blue exclusion. To prepare the cellular layer of collagen, a 3.28 x 10^5 cells/mL dilution was created and added to a combination of pre-mix and type 1 bovine atelocollagen as shown in Table 2.6, all on ice. 3 mL of this mixture was carefully added on the top of each polymerized acellular collagen layer and allowed to polymerize for two hours in a 37°C, 5% CO_2 humidified incubator. After polymerization of the cellular collagen layer, the Transwell inserts were placed into deep 6-well plates (Corning), and 15 mL of Cast Feed Medium (recipe as shown in Table 2.7) was added to the basal chamber of each well. The dermal equivalents were then kept in a 37°C, 5% CO_2 humidified incubator. 24 hours after casting the dermal equivalents, 3 mL of Cast Feed Medium was added to the apical Transwell compartment, with the dermal equivalents returned to the incubator for six further days of culture. Cast feed Medium was replaced every other day during this process.

Table 2.6: Organotypic Foreskin Casting Recipes. Reagent preparation is as described in Gangatirkar *et al*, 2007.

Recipe for:	Reagent	Volume (µL)		
		1 Well	**3 Wells**	**6 Wells**
Pre-mix	5X DMEM	395	1185	2400
	L-Glutamine	39	117	234
	Primocin	5	15	30
	$NaHCO_3$	120	360	730
	HI FBS	440	1320	2600
	Total Volume	**999 µL**	**2,997 µL**	**5,994 µL**
Acellular Collagen Layer	Pre-Mix	180 µL	540 µL	1,080 µL
	DMEM Complete	320 µL	960 µL	1,920 µL
	Collagen	500 µL	1,500 µL	3,000 µL
	Total Volume	**1 mL**	**3 mL**	**6 mL**
Cellular Collagen Layer	Pre-Mix	555 µL	1,665 µL	3,330 µL
	Fibroblast Cell Suspension (3.28 x 10^5 cells/mL)	945 µL	2,835 µL	5,670 µL
	Collagen	1,500 µL	4,500 µL	9,000 µL
	Total Volume	**3 mL**	**9 mL**	**18 mL**

Table 2.7: Cast Feed Medium Recipe. Reagent preparation is as described in Gangatirkar et al, 2007. Final solution is then filter sterilized using a 0.2 µm filter.

Reagent	Volume (mL)
5X DMEM	100
L-glutamine	10
$NaHCO_3$	13
Gentamicin or Primocin (optional)	0.5
HI FBS	50
dH_2O	340
Total Volume	**500 mL**

After a total of seven days culturing the dermal equivalent, immortalized primary foreskin keratinocytes were added apically to the dermal equivalent. Keratinocytes were incubated with 0.5 mM EDTA for five minutes, then incubated with Accutase enzyme for 14 minutes. The Accutase enzyme was diluted with a solution of 20% HI FBS in 1X DPBS, cells were counted via Trypan Blue exclusion, centrifuged at 114 x *g* for eight minutes, and then plated on top of the collagen layer as a 50 µL volume of concentrated

cells (1.67 x 10^7 cells/mL). This volume was dispersed evenly across the collagen gel surface, as five individual 10 µL droplets. Immediately after this, the collagen hydrogel was left undisturbed in a sterile tissue culture laminar flow cabinet for five minutes, then moved to a 37°C, 5% CO_2 humidified incubator for one hour to facilitate keratinocyte attachment to the collagen gel. After one hour of incubation, K-SFM Complete was added to the apical and basal chambers of Transwells and cultures incubated for 10 days in a 37°C, 5% CO_2 humidified incubator with medium changes every other day.

Following the 10-day incubation in K-SFM Complete, keratinocytes were viewed on the surface of the collagen layer using phase-contrast microscopy and assessed for confluence. If cells were not observed as a 100% confluent monolayer, they were incubated further and observed each day for confluence. At 100% confluence, K-SFM Complete was removed from the apical and basal Transwell aspects. 9 mL of Epidermalization Medium (recipe shown in Table 2.8) was then added to the basal compartment such that the medium touches the Transwell base without air-bubbles between the two. The apical aspect was left uncovered with culture medium, such that it was exposed to air continually and allowed to dry (or become "air-interfaced"). The air-interfacing procedure, in combination with switching to medium containing a higher concentration of calcium, allows the monolayer of keratinocytes to begin differentiation and stratification on the collagen gel[154]. These organotypic constructs were cultured for seven days with medium changes every other day in a 37°C, 5% CO_2 humidified incubator. All organotypic foreskins were mechanically agitated at room temperature outside of an incubator for 15 minutes every other day during this culture period using a Belly Button Shaker (IbI Scientific) at half power unless otherwise indicated. Mechanical agitation was used to simulate shear forces experienced by *in vivo* tissue.

Following the seven-day culture period in Epidermalization Medium, organotypic tissues were then incubated with Cornification Medium (recipe shown in Table 2.8) added to the basal Transwell aspect in place of Epidermalization Medium. Skin cultures were then cultured for seven days in a 37°C, 5% CO_2 humidified incubator with cornification medium changes every other day.

Lastly, following the seven-day incubation in Cornification Medium, organotypic cultures were then incubated with Maintenance Medium (recipe shown in Table 2.8) added to the basal Transwell aspect in place of Cornification Medium. Skin cultures were cultured for seven days in a 37°C, 5% CO_2 humidified incubator with medium changes every other day. At the completion of this incubation period, skin cultures had fully matured and were ready for further experimentation.

Table 2.8: Organotypic Foreskin Developmental Medium Recipes. Reagent preparation is as described in Gangatirkar et al, 2007. Final solution pH is adjusted to between 7.0 and 7.2 and is then filter sterilized using a 0.2 µm filter.

Reagent	Volume (mL)		
	Epidermalization Medium	Cornification Medium	Maintenance Medium
5X DMEM	75	50	50
$NaHCO_3$ Solution	9.75	6.5	6.5
5X Hams F12	25	50	50
L-Glutamine	10	10	10
Hydrocortisone	0.4	0.4	0.4
ITT	1	1	1
EOP	1	1	1
Adenine	1	1	1
Selenium	1	1	1
Gentamicin or Primocin (optional)	0.5	0.5	0.5
$CaCl_2$	1	1	1
HI FBS	1.5	10	5
Progesterone	1	-	-
dH_2O	380	380	380
Total Volume	**500 mL**		

2.6 Fresh Tissue and Explant Culture

Fresh tissue and explants were prepared by taking sections from foreskin tissue within four hours after circumcision surgery, after washing of the tissue with 1X DPBS and removal of visible blood vessels. Sections were cut evenly using an 8 mm tissue biopsy punch (Integra Militex) and placed onto the apical surface of SPONGOSTAN dental sponges (cut into thirds, one third per 24-well plate well; from Ethicon) or 24-well

Transwells (Corning). The 24-well Transwell membrane was composed of transparent polyethylene terephthalate and had a pore size of 0.4 µm. 600 µL of Maintenance Medium was added to each well of a 24-well plate with either a dental sponge or a Transwell insert. Medium was added such that the dental sponge was saturated with medium without submerging the tissue, or the Transwell membrane was in contact with basal chamber medium. Explants were either used in assays immediately (in Transwell inserts, as representative of *in vivo* state) or cultured for seven days on a dental sponge in a 37°C, 5% CO_2 humidified incubator, with medium changes every other day. At the end of the seven-day culture period, tissue explants were placed into 24-well Transwell inserts for further experimentation.

2.7 Tissue Sectioning and Immunofluorescence Microscopy

Organotypic foreskin cultures, but not fresh or explant-cultured tissues, were fixed overnight in 4% formaldehyde in piperazine-N,N′-bis(2-ethanesulfonic acid) (PIPES) Buffer, washed with 1X DPBS, and gradually dehydrated in a sucrose gradient (sucrose changed every other day; solutions used: 10%, 20%, 30%, and lastly a half-half mix of 30% sucrose and OCT medium). Organotypic foreskin tissues were again washed briefly with 1X DPBS to remove any remaining sucrose and blotted using Kimwipes (Kimtech Science) to dry the exterior surface. Organotypic and explant tissues were placed into OCT medium, frozen on dry ice, and stored at -80°C until processed for immunofluorescence microscopy.

Tissue blocks of organotypic, fresh, seven-day explant, and immediately frozen tissues were sectioned at -20°C using a Leica CM350 cryostat to a thickness of 10 µm and placed on Fisherbrand Colorfrost Plus microscope slides. Each block was sectioned to yield two slices per microscope slide. Regions just outside the tissue sections were circled with a hydrophobic PAP pen (Electron Microscopy Sciences). The tissue sections were then fixed using 200 µL of freshly made 3.7% formaldehyde in PIPES buffer for 10 minutes (PIPES Buffer recipe in Table 2.9). Tissue sections were then washed by dipping

slides three times sequentially in three Coplin staining jars filled with 1X DPBS, then blocked for 30 minutes using 100 µL Blocking Solution (recipe as per Table 2.10).

Table 2.9: PIPES Buffer Recipe. Combine $MgCl_2$, ethylene glycol-bis(β-aminoethyl ether)-N,N,N′,N′-tetraacetic acid (EGTA), and PIPES in a beaker with 500 mL of H_2O, and pH to 6.8 using NaOH. Following this, add H_2O to the solution such that the final volume is 630 mL. Solution is then filter sterilized after preparation using a 0.2 µm filter.

Reagent	Volume/Mass
0.9M $MgCl_2$	2.2 mL
0.25M EGTA	4 mL
PIPES	30.2 g
dH_2O	X mL
Total Volume	**630 mL**

Table 2.10: Blocking Solution Recipe. Solution is then filter sterilized after preparation using a 0.2 µm filter.

Reagent	Volume
Normal Donkey Serum (JIR)	50 mL
Triton X-100 (Sigma Aldrich)	500 µL
NaN_3 (Sigma Aldrich)	500 µL
1X DPBS (VWR)	449 µL
Total Volume	**51.449 mL**

Following this, tissue sections were incubated with 100 µL of mouse anti-human primary antibody for E-cadherin (1:50 in Blocking Solution) for one hour at 37°C (antibodies and dilutions in Table 2.11). Tissues were immediately washed after incubation, with 100 µL of donkey anti-mouse Alexa Fluor 647 (AF647) secondary antibody (1:400 in Blocking Solution) added to the tissue surface after and incubated for 30 minutes at room temperature. After this, tissues were washed in 1X DPBS, had 100 µL of rabbit anti-human primary antibody for claudin-1 (1:200 in Blocking Solution) added to their surface, and incubated for another hour at 37°C. This was followed with another wash, and subsequent incubation using donkey anti-rabbit AF546 secondary antibody (1:400 in Blocking Solution) following the steps before. Tissues were then stained for filaggrin by

incubating for one hour at 37°C with 100 µL of mouse anti-human AF488 primary antibody (1:50 in Blocking Solution). Following antibody incubations, 60 µL of DAPI-Fluoromount-G (Invitrogen) was added to the surface of the tissue sections. A cover slip was then placed on top of the microscope slide, and the cover slip edges sealed with clear nail polish. Slides were stored at 4°C until ready to be imaged with a Leica DM5500B fluorescence microscope equipped with CFP, GFP, DsR, and Y5 filter cubes.

Table 2.11: Antibodies used for Immunofluorescence Staining.

Target	Type	Clone	Supplier	Host Species	Dilution Factor	Fluorophore	Catalog and Lot Number
Human claudin-1	[a]1°	Poly	Abcam	Rabbit	1:200	None	Cat: ab15098 Lot: GR3248184-1
Human E-cadherin	1°	Mono	BD Biosciences	Mouse	1:50	None	Cat: 610181 Lot: 7187865
Human filaggrin	1°	Mono	Santa Cruz Biotechnology	Mouse	1:50	Alexa Fluor 488	Cat: SC-66192 Lot: H2019
Rabbit IgG*	[b]2°	Poly	Invitrogen	Donkey	1:400	Alexa Fluor 546	Cat: A10040 Lot: 1946340
Mouse IgG*	2°	Poly	Invitrogen	Donkey	1:400	Alexa Fluor 647	Cat: A31571 Lot: 2045337

*Binds both heavy and light IgG chains (H + L)

2.8 Toll-like Receptor, Tight Junction, and Defensin Gene Expression Analysis

Toll-like receptor, tight junction, and β-defensin mRNA levels were quantified between organotypic, explant cultured, and immediately frozen tissue. RNA extraction and purification were performed using an Aurum Total RNA Fatty and Fibrous Tissues Kit (Bio-Rad Laboratories). Tissues were placed into 1 mL of PureZOL, briefly minced with scissors, then homogenized on ice using a Fisher Scientific Model 100 Sonic

[a] Primary

[b] Secondary

Dismembrator in short five-second pulses on power setting four. The Aurum Total RNA Fatty and Fibrous Tissues Kit spin protocol was followed for RNA isolation. RNA concentration and purity were measured using a Nanodrop 2000c Spectrophotometer (Thermo Scientific).

cDNA was synthesized on a SimpliAmp Thermal Cycler (Applied Biosystems) from the previously extracted and purified RNA using an iScript cDNA Synthesis Kit (Bio-Rad Laboratories) following the manufacturer's protocol. Following this, cDNA was either stored at -20°C for later use, or immediately used for qPCR. cDNA was diluted to a concentration of 13.33 ng/µL (based on the starting amount of RNA in the reverse transcription step) in ultrapure water for use in the qPCR reactions. qPCR reactions included 20 ng of cDNA with the components listed in Table 2.12 and were performed on a QuantStudio 5 Real Time PCR System (Applied Biosystems). Primers and their optimized concentrations are listed in Table 2.13, while qPCR conditions are shown in Table 2.14. Copy numbers of target mRNA were determined through absolute quantitation using a seven-point standard curve and normalized in relation to glyceraldehyde 3-phosphate dehydrogenase (GAPDH) mRNA copy numbers. Double stranded standards used in the qPCR reactions are shown in Table 2.15. gBlocks Gene Fragment (Integrated DNA Technologies) standards were generated *in silico*. After analyzing primer binding sites, a region incorporating the primer binding sites (near the center of the standard) as well as part of the surrounding mRNA sequence was selected for standard generation such that final standard length was approximately 300-350 base pairs (bp).

Table 2.12: qPCR Reaction Components for Gene Expression Analysis.

Component	Volume (µL)
cDNA Template	1.5
SYBR Green PCR Master Mix (Applied Biosystems)	7.5
Forward Primer	0.75
Reverse Primer	0.75
dH_2O (DNase and RNase free)	4.5
Total Volume	**15 µL**

Table 2.13: Primer Sequences used for Gene Expression Analysis. Toll-like receptor primer sequences were obtained from Fitzner *et al*, 2008, while GAPDH primer sequences were obtained from Stupp *et al*, 2005[156,157]. Primer sequences for claudin-1 and β-defensin-1 were kindly provided by Luana Langlois (Laboratory of Dr. Gregor Reid), Western University. Source publications for these primers, in order, are as follows: Akizuki *et al*, 2018; Klag *et al*, 2018[158,159].

Target of Interest	Primer Sequences		Primer Concentration (μM)		Accession Number
	Forward (5′-3′)	Reverse (5′-3′)	Forward	Reverse	
TLR 1	CAGTGTCTGGT ACACGCATGGT	TTTCAAAAACC GTGTCTGTTAAG AGA	8	8	NM_003263
TLR 2	GGCCAGCAAAT TACCTGTGTG	AGGCGGACATC CTGAACC	16	16	NM_003264
Claudin-1	ATGAGGATGGC TGTCATTGG	ATTGACTGGGG TCATAGGGT	8	4	NM_021101.5
β-defensin-1	GGCCTCAGGTG GTAACTTTCT	TTCTTCTGGTCA CTCCCAGC	4	8	NM_005218.4
GAPDH	GAGCCACATCG CTCAGACAC	CATGTAGTTGA GGTCAATGAAG G	8	16	NM_002046.7

Table 2.14: qPCR Reaction Conditions for Gene Expression Analysis.

Step	Temperature (°C)	Time	Number of Cycles
Enzyme Activation	95	10 min	1
PCR	95	15 s	40
	X*	30 s	
	72	30 s	

*Annealing temperature of 62°C was used for reactions with TLR1, 64°C with TLR2, 60°C for claudin-1 and β-defensin-1, and 60°C for GAPDH.

Table 2.15: qPCR Reaction Standards for Gene Expression Analysis.

Target	Standard Sequence (5′-3′)	Length (bp)	Accession Number
Human TLR1, mRNA	TTTTGATTATTCTGGCACTTCCTTGAAGGCCTTGTC TATACACCAAGTTGTCAGCGATGTGTTCGGTTTTCC GCAAAGTTATATCTATGAAATCTTTTCGAATATGA ACATCAAAAATTTCACAGTGTCTGGTACACGCATG GTCCACATGCTTTGCCCATCCAAAATTAGCCCGTT CCTGCATTTGGATTTTTCCAATAATCTCTTAACAGA CACGGTTTTTGAAAATTGTGGGCACCTTACTGAGT TGGAGACACTTATTTTACAAATGAATCAATTAAAA GAACTTTCAAAAATAGCTGAAATGACTACACAGAT GAAGTCTCTGCAACAATTGGATATTAGCCAGA	350	NM_003263.4
Human TLR2, transcript variant 1, mRNA	TAACTACGTTTTCTAAGGAGCAACTTGACTCATTTC ACACACTGAAGACTTTGGAAGCTGGTGGCAATAAC TTCATTTGCTCCTGTGAATTCCTCTCCTTCACTCAG GAGCAGCAAGCACTGGCCAAAGTCTTGATTGATTG GCCAGCAAATTACCTGTGTGACTCTCCATCCCATG TGCGTGGCCAGCAGGTTCAGGATGTCCGCCTCTCG GTGTCGGAATGTCACAGGACAGCACTGGTGTCTGG CATGTGCTGTGCTCTGTTCCTGCTGATCCTGCTCAC GGGGGTCCTGTGCCACCGTTTCCATGGCCTGTGGT ATATGAAAATGATGTGGGCCTGGCTCCAGGCC	350	NM_001318787.2
Human claudin-1, mRNA	AAGCAACCCGTGCCTTGATGGTGGTTGGCATCCTC CTGGGAGTGATAGCAATCTTTGTGGCCACCGTTGG CATGAAGTGTATGAAGTGCTTGGAAGACGATGAG GTGCAGAAGATGAGGATGGCTGTCATTGGGGGTG CGATATTTCTTCTTGCAGGTCTGGCTATTTTAGTTG CCACAGCATGGTATGGCAATAGAATCGTTCAAGAA TTCTATGACCCTATGACCCCAGTCAATGCCAGGTA CGAATTTGGTCAGGCTCTCTTCACTGGCTGGGCTG CTGCTTCTCTCTGCCTTCTGGGAGGTGCCCTACTTT GCTGTTCCTGTCCCCGAAAAACAACCTCTTACCCA	350	NM_021101.5
Human β-defensin-1, mRNA	GCCAGTCGCCATGAGAACTTCCTACCTTCTGCTGTT TACTCTCTGCTTACTTTTGTCTGAGATGGCCTCAGG TGGTAACTTTCTCACAGGCCTTGGCCACAGATCTG ATCATTACAATTGCGTCAGCAGTGGAGGGCAATGT CTCTATTCTGCCTGCCCGATCTTTACCAAAATTCAA GGCACCTGTTACAGAGGGAAGGCCAAGTGCTGCA AGTGAGCTGGGAGTGACCAGAAGAAATGACGCAG AAGTGAAATGAACTTTTTATAAGCATTCTTTTAAT AAAGGAAAATTGCTTTTGA	300	NM_005218.4
Human GAPDH, transcript variant 1, mRNA	GCTCTCTGCTCCTCCTGTTCGACAGTCAGCCGCATC TTCTTTTGCGTCGCCAGCCGAGCCACATCGCTCAG ACACCATGGGGAAGGTGAAGGTCGGAGTCAACGG ATTTGGTCGTATTGGGCGCCTGGTCACCAGGGCTG CTTTTAACTCTGGTAAAGTGGATATTGTTGCCATCA ATGACCCCTTCATTGACCTCAACTACATGGTTTAC ATGTTCCAATATGATTCCACCCATGGCAAATTCCA TGGCACCGTCAAGGCTGAGAACGGGAAGCTTGTC ATCAATGGAAATCCCATCAC	300	NM_002046.7

2.9 Toll-like Receptor Function Analysis

To assess the function of Toll-like receptors, such as TLR4, a 4 μL volume of 100 ng/mL lipopolysaccharide (LPS, an agonist for TLR4; Invivogen) in endotoxin-free water was placed apically on organotypic, explant cultured, and fresh foreskin tissues on Transwell inserts. Maintenance Medium (9 mL for organotypic cultures, 600 μL for explants) was placed in the basal Transwell chamber, with tissues incubated in a 37°C, 5% CO_2 humidified incubator for 24 hours post LPS application. Basal medium from the culture was harvested at timed intervals (6, 12, and 24 hours) and stored at -80°C for further analysis of soluble immune mediators. An IL-8 enzyme-linked immunosorbent assay (ELISA) kit (Invitrogen) was used as per manufacturer's protocol, with samples diluted (1:100) prior to the procedure with provided sample diluent. Samples were then diluted 1:10 during the protocol with provided sample diluent, following the initial 1:100 dilution.

2.10 Tissue Marker and Tight Junction Analysis

The depth of the whole epithelial layer, as well as layers only staining positive for filaggrin (stratum corneum), and E-cadherin (whole epithelium) were determined. Additionally, the proportion of the epidermal layer that stained positive for the junction proteins claudin-1 and E-cadherin was also determined.

To determine tissue depth measurements, a minimum of three fields of view (FOV) of similar size (within a tissue) were obtained from whole tissue section immunofluorescence microscope images using ImageJ. FOVs were selected from regions without breaks or staining artefacts. ROIs were then put through a workflow designed based on Edfeldt *et al*, 2020 using CellProfiler cell image analysis software[160,161]. Briefly, each FOV was outlined and the epidermis segmented by drawing apical and basal lines (following the apical epithelial border and basal membrane, respectively) with a CellProfiler pipeline. A third line was manually drawn onto images denoting the area at which the stratum corneum begins, based on filaggrin staining. The distances between the

apical, basal, and filaggrin lines were then determined using a CellProfiler pipeline that measures the shortest distance between each pixel on the apical line to the basal line, apical line to filaggrin separator line, basal line to filaggrin separator line, and vice versa. The average total thickness of the epithelium was determined through this method, alongside the region between the basement membrane and stratum corneum, and the stratum corneum itself (Figure 2.3).

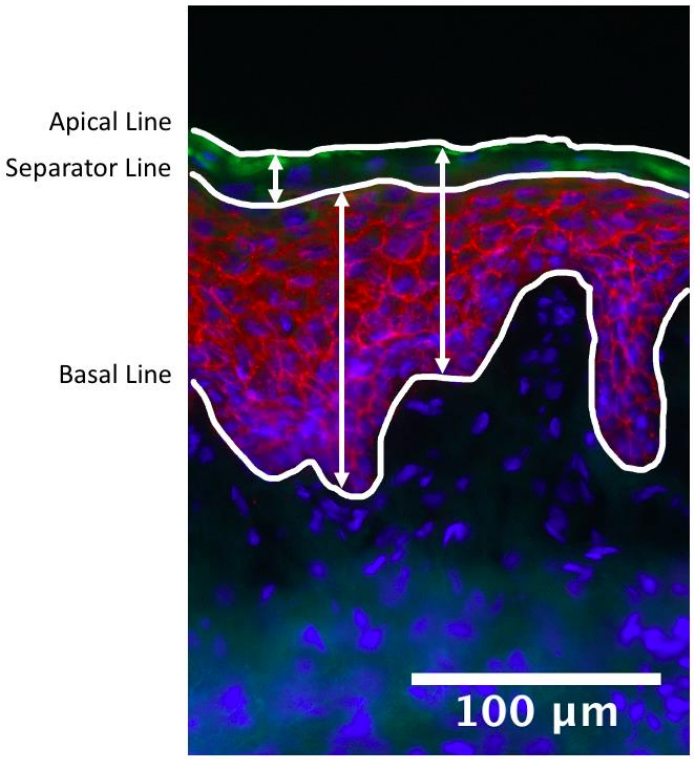

Figure 2.3: Process for Determination of Tissue Thickness Measures. Tissues have an apical, basal, and separator line drawn on their surface. The average mean thickness measure is then determined between the apical and separator lines, basal and separator lines, and finally between apical and basal lines. The shortest distance between the two lines examined is calculated per pixel of each line and averaged to determine this value.

Percent area coverage (immunoreactivity quantification) was determined using ImageJ, as follows (Figure 2.4). Four-colour whole tissue section immunofluorescence microscope images obtained from Section 2.7 were split into individual colour channels, with the individual channels for E-cadherin and claudin-1 saved for analysis. The resultant saved images were converted to an 8-bit format, then into greyscale. A representative image for each marker was used in ImageJ to determine image thresholds with the "Adaptive Thresholding" plugin. The "Pixel Block Size" parameter was optimized such that the net-like structure of each marker was captured without picking up non-positive signals. The "Subtraction" parameter was then optimized thereafter to help refine the selection of pixels, such that background noise in the image was eliminated. These two values were kept and used for the script described later in this section. Next, the area outside the greyscale tissue image was circled manually using the "Free Selection" tool and eliminated. Images were then subject to the "Percent Signal Coverage Determination" script (described in Buchanan *et al*, in press) using the manually determined "Adaptive Thresholding" values for "Pixel Block Size" and "Subtraction" described earlier[162]. These two thresholding values were kept consistent across all tissues used in the study so as to permit comparison. The script used in this study provided an output describing the total area covered with positive staining and had to be adjusted as indicated by the scripts publishers so as to ensure the correct percent area coverage was determined. The total area for positive marker staining in the whole image was then divided by the area of the tissue to facilitate this. Tissue area was manually determined by circling the region of positive staining three separate times in ImageJ using the "Freehand Selection" tool.

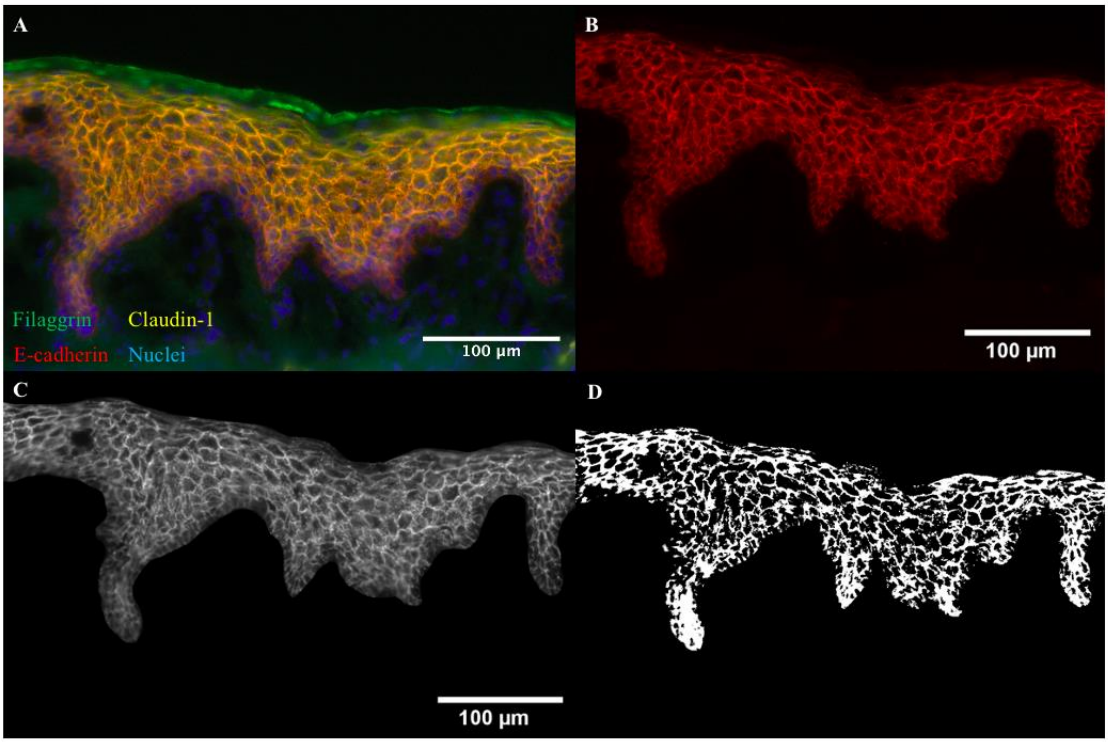

Figure 2.4: Immunofluorescent Image Immunoreactivity Quantification Steps. (**A**) 16-bit four-colour immunofluorescent image prior to quantification. (**B**) Immunofluorescent image is split into only one channel, then (**C**) converted to 8-bit, converted to grayscale, and then subject to manual background removal. (**D**) Binary image after processing with immunoreactivity pipeline script, highlighting areas of positive E-cadherin immunoreactivity.

2.11 Tight Junction Functional Analysis

Organotypic, explant-cultured, and fresh tissues was subject to a permeability assay as described by Sayedyahossein *et al*, 2016 to assess tight junction functionality and skin barrier integrity[163]. Explanted tissues were placed into 24-well Transwell inserts with the epidermis side up, had their edges sealed with a 1:1 (vol/vol) mixture of white petrolatum and paraffin oil (MilliporeSigma), and were fed basally with Maintenance Medium. A single 10 µL drop of 10,000 kDa AF594-conjugated dextran (Invitrogen; dissolved in 1X DPBS) was added to the center surface of the tissue of interest. *In vitro* tissues were incubated with a 10 µL droplet of 0.3 mg/mL dextran after tissue sealing, while explanted

tissues were incubated with an 8 µg/mL solution of dextran to account for differences in culture medium volume required for each tissue type. Tissues were covered using aluminum foil with a large Kimwipe (Kimtech Science) taped on basally to block light reflection and incubated for 24 hours in a 37°C, 5% CO_2 humidified incubator. Small 100 µL volumes of basal medium were removed at timed intervals (6, 12, 24 hours), transferred to a covered black microplate, and retained in the incubator until all timepoints were complete. The fluorescence intensity of the collected samples was then determined using a Cytation 5 imaging reader (Gen5 3.02 software; both from BioTek) to quantify the amount of dextran that penetrated through the tissue and into the basal medium below the Transwell. Experiments contained control tissue without dextran tracer (negative controls) and medium without tissue or tracer (blank); positive controls consisted of either medium with dextran either spiked directly into medium or pipetted onto the apical side of empty Transwell inserts with medium in the basal chamber. Samples of basal medium were taken from negative and positive controls at the same time points as experimental Transwells (i.e., containing tissues). To quantify percent permeation, raw fluorescence values from each experimental Transwell were normalized to a time-matched positive control, following either Equation 2.1 or 2.2 (dependent on controls available).

Equation 2.1:

$$\left(\frac{\text{Experimental Well Medium} - \text{Average Tissue Negative Control}}{\text{Average Medium Only Positive Control} - \text{Average Medium Only Negative Control}}\right) \times 100\%$$

Equation 2.2:

$$\left(\frac{\text{Experimental Well Medium} - \text{Average Tissue Negative Control}}{\text{Transwell Positive Control at 24 hours} - \text{Average Medium Only Negative Control}}\right) \times 100\%$$

2.12 Data Analysis

Data was analyzed and graphs assembled using GraphPad Prism (version 8.4.3; GraphPad Software Inc.) and Stata SE (version 17; StataCorp LLC). Each dataset obtained in this study was screened for outliers using the robust regression and outlier removal (ROUT) method (Q = 1%). Data is presented as mean ± standard deviation, and statistical testing done when sample sets contained at minimum three biological replicates. When directly comparing means between two independent groupings, unpaired two-tailed *t*-tests were used. Comparing two related groupings was done using paired two-tailed *t*-tests. A random effects model was used to examine tissue permeability over time. A confidence level of 95% was selected for each statistical test. Lastly, comparisons were made in this study between organotypic foreskins and adult foreskin tissues where possible (as organotypic foreskins are composed of isolated adult foreskin cells), although this was not possible in all cases. Where such comparisons could not be made, paediatric foreskin tissue was used as a substitute.

Chapter 3

3 Results

3.1 Participants

Tissue samples were obtained from two cohorts: (1) adult men (≥18 years of age; *n* = 10) undergoing elective circumcision, with no signs or history of genital infections, recent antibiotic use, or hormone therapy; and (2) boys (<18 years of age; *n* = 43) undergoing circumcision for either elective or medically indicated reasons (e.g., treatment of recurrent balanitis, phimosis, recurrent urinary tract infection, or balanitis xerotica obliterans). A summary of adult participant demographics is provided in Table 3.1, while paediatric participant demographics are provided in Table 3.2. Demographics for specific participant tissues used for 3D organotypic foreskin development or explant culture are shown in Table 3.3 and Table 3.4 for adult (*n* = 3) and paediatric (*n* = 5) participants, respectively. Two cohorts were assessed in this study as elective cosmetic circumcision, our main source of foreskin tissue prior to the coronavirus disease 2019 (COVID-19) pandemic, was no longer permitted due to pandemic-associated restrictions. Medically indicated circumcision, as occurred for most paediatric participants, was permitted and thus became our main source of foreskin tissue during the pandemic.

Table 3.1: Adult Cohort Demographics (*n* = 10).

Demographic	Value	
Age (yrs; median, range; *n* = 9)		24 (20-48)
Ethnicity	White	8/10 (80.0%)
	African, Caribbean, or other Black	0/10 (0.0%)
	East Asian	0/10 (0.0%)
	South Asian	0/10 (0.0%)
	Latin American	1/10 (10.0%)
	First Nations	0/10 (0.0%)
	Other/Mixed Ethnicity	1/10 (10.0%)
Sexually Active		9/10 (90.0%)
Indication for Circumcision	Partial Inability to Retract Foreskin	3/10 (30.0%)
	Complete Inability to Retract Foreskin	3/10 (30.0%)
	Cosmetic	4/10 (40%)

Table 3.2: Paediatric Cohort Demographics (*n* = 43).

Demographic	Value	
Age (yrs; median, range; *n* = 43)		8.09 (0.94-17.33)
Ethnicity (*n* = 41)	Caucasian	29/41 (70.7%)
	Asian	6/41 (14.6%)
	African American	2/41 (4.9%)
	Middle Eastern	4/41 (9.8%)
	Other	0/41 (0.00%)
Sexually Active (*n* = 42)		1/42 (2.4%)
Indication for Circumcision (*n* = 43)	Elective	5/43 (11.6%)
	Recurrent UTI[c]	1/43 (2.3%)
	Balanitis	2/43 (4.7%)
	BXO[d]	0/43 (0.0%)
	Phimosis	32/43 (74.4%)
	Other	3/43 (7.0%)

[c] UTI, Urinary Tract Infection

[d] BXO, Balanitis Xerotica Obliterans

Table 3.3: Demographics of Adult Participants Included in this Study. Demographic information for adult participants who took part in the study through tissue donation. Tissues were used for either 3D organotypic foreskin development or explant culture.

Deidentified Participant	Demographic Value	
ADLT[e] 001	Age	21
	Ethnicity	White
	Sexually Active	Yes
	Indication for Circumcision	Cosmetic
ADLT 002	Age	25
	Ethnicity	White
	Sexually Active	Yes
	Indication for Circumcision	Partial Inability to Retract Foreskin; Cosmetic
ADLT 009	Age	No Response
	Ethnicity	Latin American/White
	Sexually Active	Yes
	Indication for Circumcision	Complete Inability to Retract Foreskin

[e] ADLT, Adult

Table 3.4: Demographics of Paediatric Participants Included in this Study.

Demographic information for paediatric participants who took part in the study through tissue donation. Tissues were used for either 3D organotypic foreskin development or explant culture.

Deidentified Participant	Demographic Value	
PED[f] 037	Age	8.98
	Ethnicity	Caucasian
	Sexually Active	No
	Indication for Circumcision	Phimosis
PED 039	Age	1.78
	Ethnicity	Caucasian
	Sexually Active	No
	Indication for Circumcision	Phimosis
PED 040	Age	14.15
	Ethnicity	Caucasian
	Sexually Active	No Response
	Indication for Circumcision	Phimosis
PED 041	Age	8.17
	Ethnicity	African American
	Sexually Active	No
	Indication for Circumcision	Elective
PED 043	Age	8.09
	Ethnicity	Caucasian
	Sexually Active	No
	Indication for Circumcision	Phimosis

[f] PED, Paediatric

3.2 Isolation and Culture of Foreskin Epidermal Keratinocytes and Dermal Fibroblasts

Cells were isolated from foreskin tissues as described in Gangatirkar *et al*, 2007, with modifications made through troubleshooting highlighted in Table 3.5.

Table 3.5: Cell Isolation and Culture Troubleshooting.

Cell Isolation Issue	Change to Protocol	Result
Tissue epidermis not peeling off after Dispase II incubation at 4°C.	Add one extra incubation step (1 hour; 37°C) before mechanical separation of tissue layers.	Tissue layers now easily separate from one another with minimal effort; yields whole epidermal sheets.
	Increase Dispase II volume for incubation to ensure whole tissue is covered.	
Few keratinocytes or fibroblasts survive plating and exhibit slowed growth.	Centrifuge cells at slower speed for longer time [114 x *g* (500 RPM[g]), 8 minutes; from 524 x *g* (1500 RPM), 5 minutes].	Increased cell attachment, less cell death after isolation, and faster cellular proliferation.
	Plate all isolated cells into smaller cell culture vessel (e.g., one well of a 24-well plate) instead of multiple cell culture vessels.	
Keratinocytes difficult to detach from cell culture vessels.	Incubate cells with 0.5 mM EDTA in 1X DPBS before adding detachment enzyme.	Almost all keratinocytes detach from cell culture vessels.
	Incubate with Accutase enzyme instead of 0.05% or 0.25% Trypsin-EDTA solutions.	
Few keratinocytes survive passaging protocols; slow growth once passaged.	Centrifuge cells at slower speed for longer time [114 x *g* (500 RPM), 8 minutes; from 524 x *g* (1500 RPM), 5 minutes].	More cells attach to cell culture vessels after passaging. Increased growth rate.
	Incubate with Accutase enzyme instead of 0.05% or 0.25% Trypsin-EDTA solutions.	
Fibroblasts or keratinocytes do not appear in their respective cell culture vessel. Cells are indistinguishable between small foreskin tissue remnant/debris.	Incubate cell culture vessel without any media changes/disruptions.	Cells should become visible and begin dividing within 2-3 weeks post isolation.

[g] RPM, Revolutions per Minute

3.3 Immortalization of Foreskin Keratinocytes

Isolated foreskin keratinocytes were transduced with a retroviral vector encoding HPV16 E6 and E7 oncogenes to prolong the ability to propagate these cells for developing the organotypic foreskin model. Cells were retained pre-transduction as well as post transduction for comparison to one another. This comparison would ensure the donor's isolated keratinocytes were not previously infected with HPV16 before the study commenced, which could impact the isolated keratinocytes phenotype in a non-controlled way. Additionally, this confirms successful cell transduction through amplification of the viral insert.

Isolated foreskin keratinocytes that underwent the immortalization procedure were cultured with Geneticin antibiotic to select for transduced cells and were harvested for PCR comparison when little to no cellular death was observed during culture. Figure 3.1 shows an initial test of the procedures used to extract genomic DNA and amplify the HPV16 E6E7 insert on a transduced paediatric sample with no matched non-transduced keratinocytes. Cells were transduced at passage 1 and harvested 22 days later at passage 3. The insert amplified in this test was verified as the HPV16 E6E7 insert (773 base pairs) through sequencing the PCR amplicon and comparing this sequence via *in silico* alignment to the HPV16 E6E7 insert.

If available, non-transduced, snap frozen keratinocytes were compared to transduced keratinocytes as shown in Figure 3.2. Transduced cells from ADLT 001 and 002 were used for developing and troubleshooting the 3D organotypic foreskin model, while transduced paediatric cells (PED 010, 022, 023, 024, 025, 028) were frozen with patient-matched fibroblasts for future use.

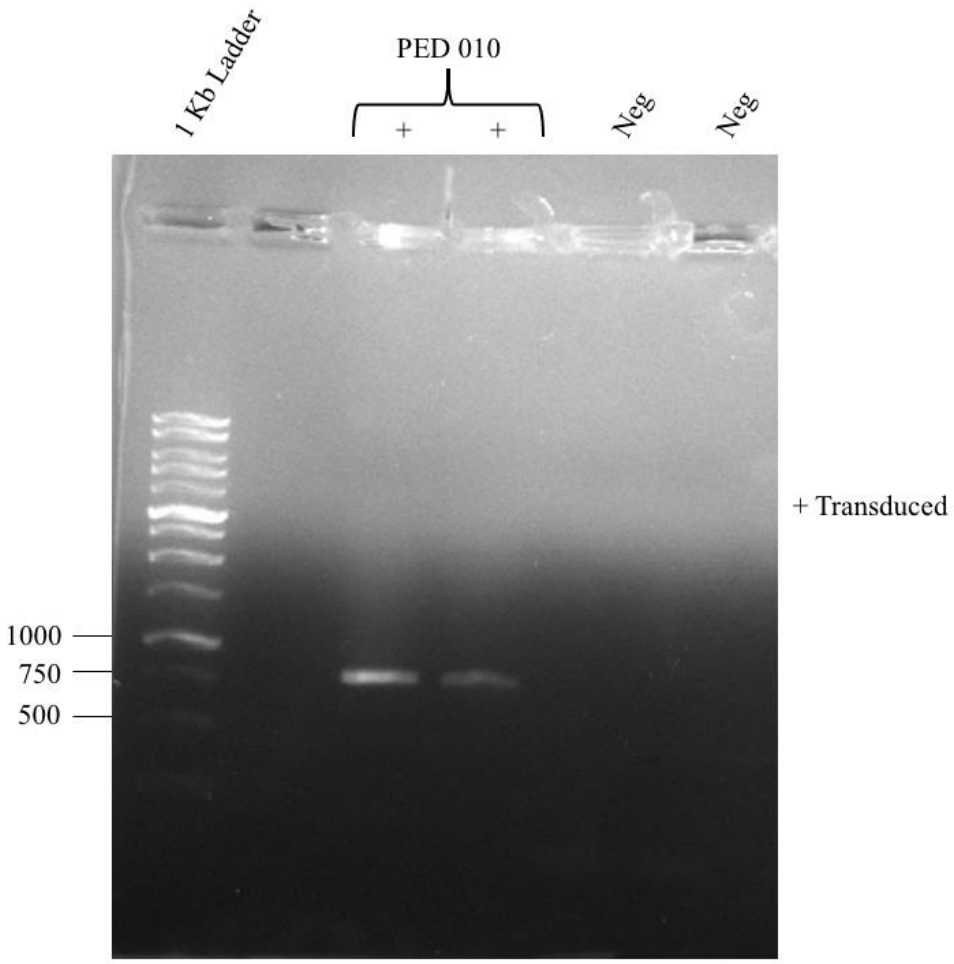

Figure 3.1: Initial Test of the Keratinocyte Transduction PCR Verification Procedure. Genomic DNA isolated from transduced PED 010 keratinocytes subject to PCR amplification for the HPV16 E6E7 insert. Amplicon was run on a 1% agarose gel and compared to a commercially available DNA ladder for amplicon size. Amplicon was subject to sequencing and *in silico* sequence alignment analysis to verify amplicon identity. Amplicon size, 773 bp; Neg, negative control (no DNA included in PCR step); +, transduced cell PCR product.

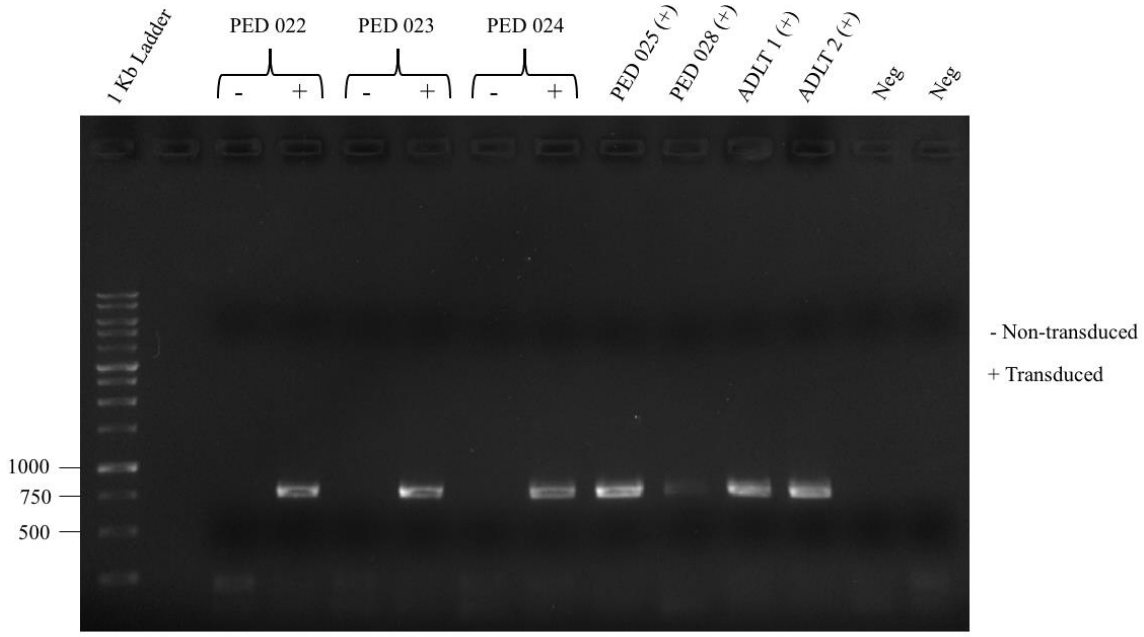

Figure 3.2: Verification of Keratinocyte Transduction via PCR. Genomic DNA isolated from non-transduced and transduced paediatric and adult keratinocytes was subject to PCR amplification for the HPV16 E6E7 insert. Amplicon was run on a 1% agarose gel and compared to a commercially available DNA ladder for amplicon size. Amplicon size, 773 bp; Neg, negative control (no DNA included in PCR step); -, non-transduced cell PCR product; +, transduced cell PCR product.

3.4 Developing Organotypic Foreskin Models

Artificial foreskin tissues were created as described in Gangatirkar *et al*, 2007, with modifications made through troubleshooting highlighted in Table 3.6. The stages of organotypic foreskin model development are shown in Figure 3.3, alongside a representative image of cross-sectioned, immunofluorescently stained mature organotypic foreskin. In this figure, it is shown that the collagen matrix embedded with fibroblasts actively contracts over one week of culture in Cast Feed Medium (Figure 3.3A and B). Additionally, keratinocytes used to seed the surface (using the modifications in Table 3.3) are also observed to form a fully confluent monolayer on the surface of the collagen, as the apical surface becomes opaque and white in colouration (in sharp contrast to the reddish-pink collagen apical surface; Figure 3.3C and D). Examination of microscopy images show organotypic foreskins have multiple layers of cell nuclei (blue) throughout the tissue epidermal region (Figure 3.3E) that express both E-cadherin and filaggrin. Filaggrin can be found in the more apical aspect of the model, similar to matured terminally differentiated keratinocytes *in vivo*. In comparison to foreskin tissue immediately frozen after circumcision surgery (representative images in Figure 3.4), organotypic foreskins express E-cadherin and filaggrin proteins in similar suprabasal layers as compared to *in vivo* tissue. It is also possible to identify each of the epithelial layers in the immediately frozen foreskin tissue, and, although less clearly, in the organotypic epidermis. Cell layers were identified based on morphology, and the location of the basal collagen layer (“dermis”) and apical filaggrin staining (stratum corneum). E-cadherin expression also appears more diffuse throughout the organotypic model, in comparison to the cell surface expression (net-like) in the immediately frozen tissue.

Table 3.6: Organotypic Foreskin Model Troubleshooting Summary.

Organotypic Foreskin Development Issue	Change to Protocol	Result
Minimal cellular collagen contraction; fibroblasts very sparse within the collagen hydrogel.	Increase cellular layer cell suspension concentration from 2.3×10^5 cells/mL to 3.28×10^5 cells/mL.	Collagen contracts by ¼ its original size after seven days of culture. Fibroblasts now more tightly packed together in the collagen hydrogel.
Keratinocytes not growing on cellular collagen surface.	Grow keratinocyte seeded collagen for one week in K-SFM Complete medium, prior to one week of culture in Epidermalization Medium.	Keratinocytes now growing and forming patches of cells on the top of cellular collagen layer.
Keratinocytes growing on cellular collagen surface but forming patches instead of a confluent monolayer.	Increase keratinocyte concentration in seeding procedure. Instead of seeding 30 µL of cells at 1.667×10^6 cells/mL, seed 50 µL of cells at 16.67×10^6 cells/mL.	Keratinocytes now forming homogenous, confluent monolayer visible to the naked eye across the entire surface of the cellular collagen.
	Add the 50 µL droplet of keratinocytes as individual 10 µL droplets evenly across the surface of the collagen, rather than directly in the center.	
	Increase growth time of the dermal equivalent in K-SFM Complete medium from seven to 10 days.	

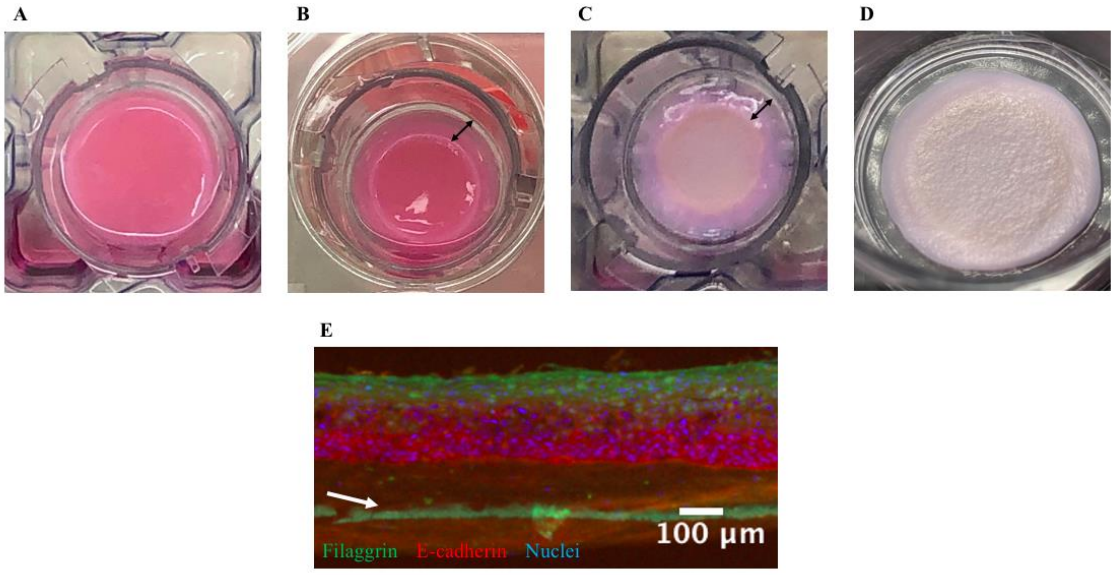

Figure 3.3: Developmental Stages of the Organotypic Foreskin Model. (**A**) Collagen and fibroblast mixture after having been cast into a 6-well Transwell. (**B**) Collagen and fibroblast mixture after seven days of culture; arrow shows the contraction of collagen away from the Transwell periphery. (**C**) Collagen surface after having been seeded with keratinocytes and cultured for 10 days until reaching 100% confluence. (**D**) Fully mature 3D organotypic foreskin. (**E**) Representative image of a fully matured organotypic foreskin cryosectioned, immunofluorescently stained, and imaged to examine presence of structural markers. Filaggrin (green) staining highlights terminally differentiated keratinocytes of the stratum corneum; E-cadherin (red) staining highlights maturing keratinocytes and adherens junction presence; Nuclear staining (blue) highlights cell nuclei. Note that collagen fibres may autofluoresce green, alongside the Transwell membrane located basally (white arrow). Organotypic constructs were cultured without mechanical agitation.

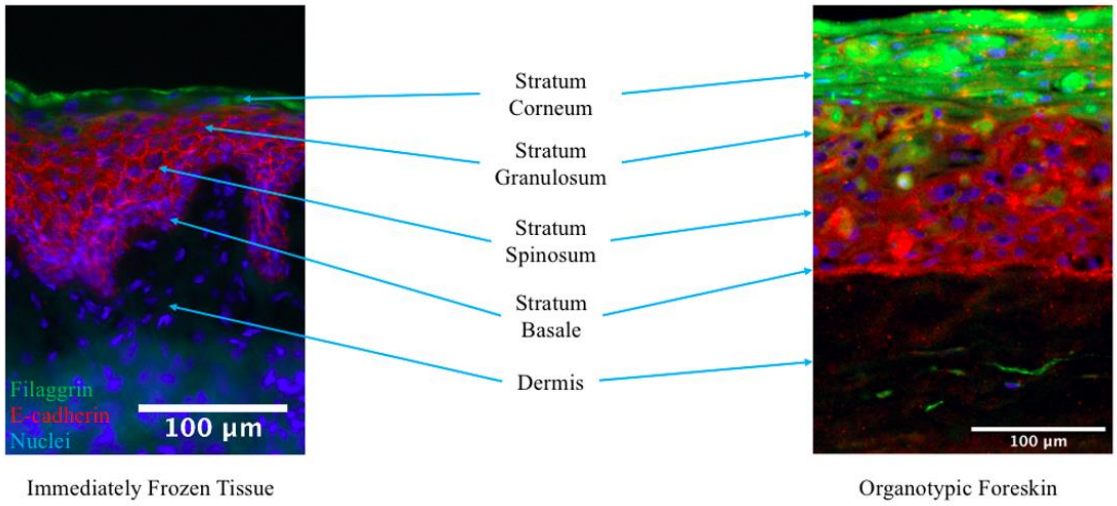

Figure 3.4: Immunofluorescence-based Comparison between Paediatric Foreskin Tissue Frozen Immediately after Circumcision and Organotypic Foreskin. Sections of paediatric foreskin and organotypic foreskin are compared to highlight the presence or absence of constituent skin layers. Both tissues are stained for filaggrin (green; terminally differentiated keratinocytes), E-cadherin (red; maturing keratinocytes and adherens junctions) and nuclei (blue). Note that collagen fibers may autofluoresce green. Organotypic foreskin was cultured without mechanical agitation.

To ensure we had the correct comparator for organotypic foreskins, immunofluorescence images were quantified using the previously described depth quantification pipeline (Chapter 2.10). Adult and paediatric participant thickness and immunoreactivity metrics were compared between tissues isolated from the inner vs. outer aspects of the foreskin (Figure 3.5). Quantification included (1) E-cadherin immunoreactivity thickness, (2) filaggrin immunoreactivity thickness, (3) Total epithelial thickness, and (4) the proportion of the epithelium immunoreactive for E-cadherin. Tissues immediately frozen after circumcision were examined in this analysis. Immediately frozen paediatric inner and outer foreskin tissues show no detectable difference in overall thickness for the E-cadherin layer (inner: 35.7 ± 20.0 µm, outer: 34.8 ± 2.5 µm; $p = 0.9$; Figure 3.5A), filaggrin layer (inner: 12.5 ± 6.6 µm, outer: 14.9 ± 4.4 µm; $p = 0.5$; Figure 3.5B), total epithelium (inner: 48.2 ± 24.8, outer: 59.6 ± 24.3; $p = 0.5$; Figure 3.5C) or E-cadherin

immunoreactivity (inner: 38.0 ± 13.1%, outer: 34.1 ± 11.8%; $p = 0.6$; Figure 3.5D). Preliminary results for adult tissues suggest that they may show some difference between inner and outer foreskin for E-cadherin (inner: 55.8 µm, outer: 99.3 µm), filaggrin (inner: 14.1 µm, outer: 24.1 µm), and total epithelial thickness (inner: 69.9 µm, outer: 123.5 µm), as well as E-cadherin immunoreactivity (inner: 35.8%, outer 21.0%).

Adult immunofluorescence images were subsequently quantified using the depth quantification pipeline based on the observed differences between paediatric and adult foreskins, and because organotypic foreskins were made with adult cells (Figure 3.6). As cells used to construct the organotypic foreskin were from both the inner and outer foreskin, both of these measures were included on the same graph. These inner and outer foreskin measures were from the same participant. Adult foreskin tissues either immediately frozen after circumcision or cultured for seven days as an explant were compared to organotypic foreskins. The organotypic foreskin produced a similar thickness of cells expressing E-cadherin when compared to fresh tissue (117.9 µm and 77.5 ± 30.8 µm, respectively), and a thicker layer of cells expressing filaggrin (46.7 µm and 19.1 ± 7.1 µm, respectively; Figures 3.6A and B). The organotypic model also produced a measurable total epithelial layer when compared to fresh tissues (168.5 µm and 96.7 ± 37.9 µm, respectively; Figure 3.6C). The organotypic model and fresh tissues showed E-cadherin immunoreactivity as well (55.6% and 28.4 ± 10.4%, respectively; Figure 3.6D). Of note, I was unable to quantify seven-day cultured explant tissue through this approach (Figure 3.6A, B, C, and D). As adult foreskin tissues were difficult to source during the latter portion of this study due to the COVID-19 pandemic, these two datasets are incomplete (Figure 3.5 and Figure 3.6). More biological replicates are required to draw statistical conclusions from these results.

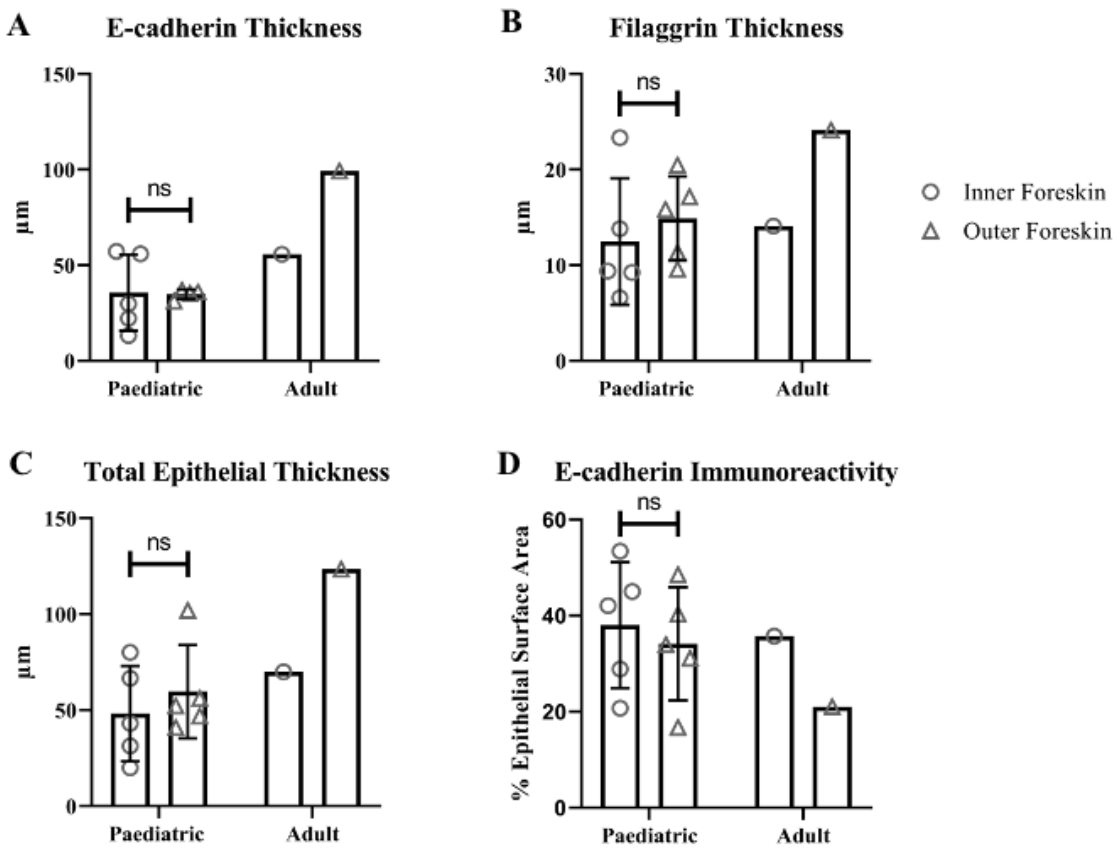

Figure 3.5: Quantifying Layer Thickness and E-cadherin Immunoreactivity between Adult and Paediatric Inner and Outer Foreskin Tissues. The thickness of (**A**) E-cadherin, (**B**) filaggrin, and (**C**) the epithelial layer was quantified between inner (*n* = 3 paediatric, *n* = 1 adult) and outer (*n* = 3 paediatric, *n* = 1 adult) foreskin tissue immediately frozen after circumcision surgery. (**D**) The percent surface area coverage by E-cadherin pixels was then quantified for these tissue images. Shown are mean values and standard deviation. Each point was obtained from three fields of view (**A**, **B**, **C**) or one representative section of a complete image (**D**). Statistical comparisons made by unpaired *t*-test. ns, non-significant.

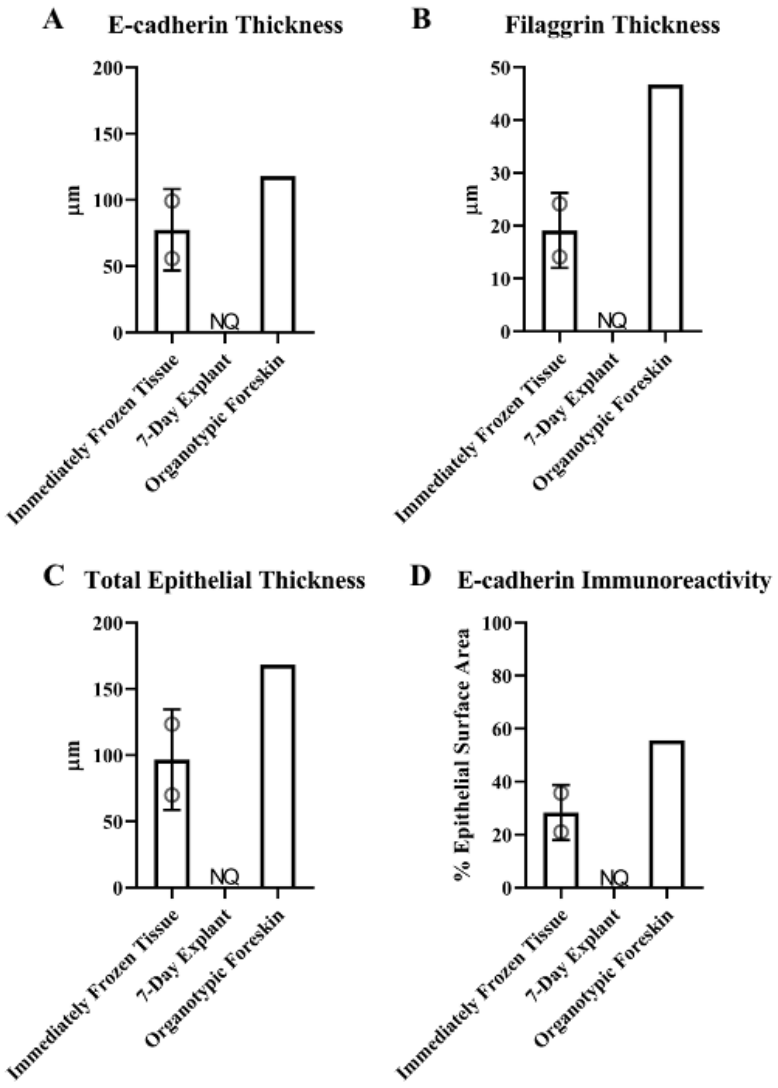

Figure 3.6: Quantifying Layer Thickness and E-cadherin Immunoreactivity between Adult Foreskin Tissues and the Mature *In Vitro* Organotypic Foreskin Model. The thickness of (**A**) E-cadherin, (**B**) filaggrin, and (**C**) the epithelial layer was quantified between foreskin tissue immediately frozen after circumcision surgery (1 participant, $n = 2$ samples; inner and outer foreskin), tissue cultured for seven days in medium (1 participant, $n = 1$), and an organotypic foreskin tissue ($n = 1$). (**D**) The percent surface area coverage by E-cadherin pixels was then quantified for these tissue images. Shown are mean values and standard deviation. Each point was obtained from three fields of view (**A**, **B**, **C**) or one representative section of a complete image (**D**). NQ, not quantifiable.

3.4 Characterizing Innate Immune Defense Capability and Functionality

To quantify the abundance of mRNAs for genes involved in innate immune defense, qPCR experiments were optimized for primer concentration and annealing temperature using a standard curve. The optimized mean reaction efficiency and linearity for the standard curve are shown in Table 3.7. The qPCR assay for TLR1 had an efficiency of 99.8 ± 3.5%, and linearity of 0.991 ± 0.005. TLR2 qPCR assay efficiency was 94.1 ± 1.8%, with linearity at 0.998 ± 0.001. β-defensin-1 efficiency and linearity were 104.3 ± 1.1% and 0.996 ± 0.001 respectively. GAPDH efficiency and linearity were 92.8 ± 2.5% and 0.998 ± 0.001, respectively.

Following this, the gene expression levels of TLR1, TLR2, β-defensin-1, and GAPDH were quantified in fresh foreskin tissue, tissue cultured in medium for seven days, and organotypic foreskins (Figure 3.7). The number of mRNA copies calculated for these genes were normalized across tissues by determining the number of copies per 10,000 copies of GAPDH. This was performed so as to examine the effect of culturing on the expression of these innate immune system genes. There was no detectable difference between fresh or seven-day explant cultured tissue $\log_{10}$ copy numbers for TLR1, TLR2, or β-defensin-1 mRNA (p = 0.3, 0.6, and 0.9 respectively; Figure 3.7). Lastly, organotypic foreskins appear to show a decrease in TLR1 copy numbers compared to fresh and seven-day explant tissue, but similar TLR2 and β-defensin-1 copies compared to fresh tissue. PED fresh tissue copy numbers were 3.3 ± 0.8 for TLR1, 3.0 ± 0.6 for TLR2, and 4.3 ± 0.4 for β-defensin-1. PED seven-day explant copy numbers were 2.6 ± 0.1 for TLR1, 2.7 ± 0.2 for TLR2, and 4.2 ± 0.8 for β-defensin-1. Lastly, ADLT organotypic foreskin copy numbers were 2.1 ± 0.1 for TLR1, 3.0 ± 0.4 for TLR2, and 4.2 ± 0.4 for β-defensin-1.

Table 3.7: Optimized qPCR Reaction Efficiency and Standard Curve Linearity for TLR1, TLR2, β-defensin-1, and GAPDH. Efficiency of amplification as measured with a standard curve, as well as standard curve linearity are shown for successful qPCR assays used to detect copies of TLR1 (*n* = 10), TLR2 (*n* = 9), β-defensin-1 (*n* = 8), and GAPDH (*n* = 3). Shown are mean values and standard deviation.

Gene	Reaction Efficiency	Linearity
TLR1	99.78 ± 3.54%	0.991 ± 0.005
TLR2	94.13 ± 1.82%	0.998 ± 0.001
β-defensin-1	104.34 ± 1.06%	0.996 ± 0.001
GAPDH	92.77 ± 2.46%	0.998 ± 0.001

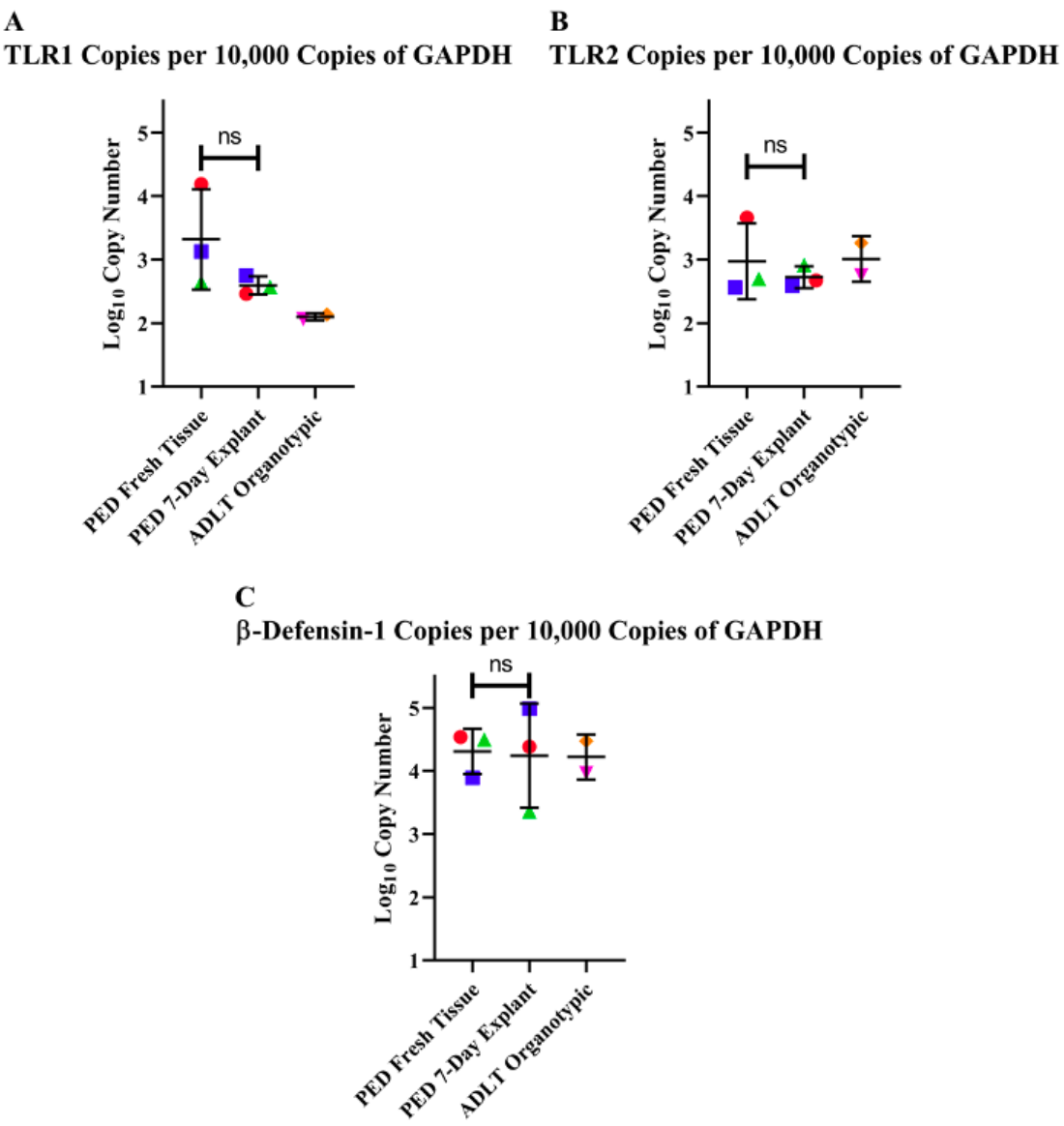

Figure 3.7: Innate Immune System Gene Expression Comparison between Paediatric Explant-Cultured and Adult Organotypic Foreskin Tissues over Culture Time. The $\log_{10}$ copy number of (**A**) TLR1, (**B**) TLR2, and (**C**) β-defensin-1 was quantified between fresh (n = 3, paediatric), seven-day cultured (n = 3, paediatric) and organotypic (n = 2, adult) foreskin tissues. Matched tissues are indicated by same-point colouration and shape across groupings. Shown are mean values and standard deviation. Each point was obtained from three technical replicates (**A**, **B**, and **C**). Statistical comparisons made by paired t-test. ns, non-significant.

Changes in expression of innate immune defense genes after exposure to LPS (100 ng/mL) were quantified across fresh, seven-day, and organotypic tissues (Figure 3.8). There were too few biological replicates to include data from organotypic foreskin tissues in statistical analyses. There was no detectable difference in the mean $\log_{10}$ copy numbers for TLR1, TLR2, or β-defensin-1 (p = 0.2, 0.1, and 0.7, respectively) between fresh foreskin tissues stimulated with LPS and their unstimulated controls (Figure 3.8). This was also the case for LPS stimulated seven-day explant foreskin tissues and unstimulated controls (p = 0.6, 0.4, and 0.7 respectively). Organotypic foreskins appeared to show no difference in mean $\log_{10}$ copy numbers for these same genes when comparing LPS stimulated and unstimulated tissue.

Tissues examined in the TLR1 analysis (no LPS vs. with LPS) included PED fresh tissue (3.5 ± 1.4 vs. 2.4 ± 0.6), PED seven-day explant tissue (2.8 ± 0.5 vs. 2.7 ± 0.1) and. organotypic foreskins (2.1 ± 0.05 vs. 1.8 ± 0.3). Tissues examined in the TLR2 analysis included PED fresh tissue (3.2 ± 0.8 vs. 2.5 ± 0.5), PED seven-day explant tissue (3.4 ± 0.3, vs. 3.1 ± 0.6), and organotypic foreskins (3.0 ± 0.4 vs. 2.7 ± 0.1). Tissues examined in the β-defensin-1 analysis included PED fresh tissue (4.4 ± 0.5 vs. 4.4 ± 0.2), PED seven-day explant tissue (4.5 ± 0.5 vs. 4.6 ± 0.8), and organotypic foreskins (4.2 ± 0.4 vs. 4.1 ± 0.5).

Additional organotypic cultures are required (Figure 3.7 and 3.8) to allow statistical analysis of this data set in comparison to other tissue types.

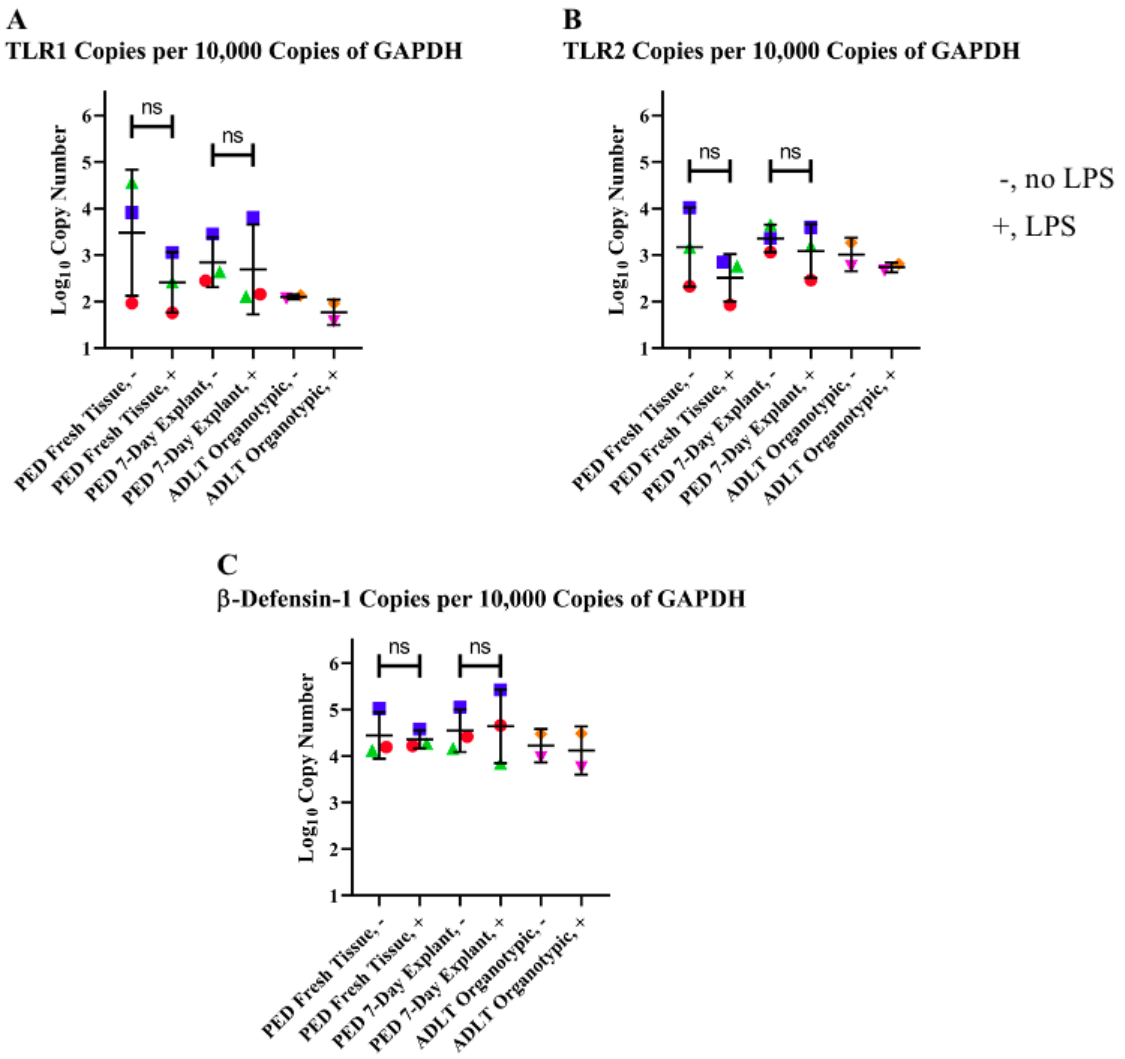

Figure 3.8: Innate Immune System Gene Expression Comparison between Paediatric Explant-Cultured and Adult Organotypic Foreskin Tissues Exposed to LPS. The $\log_{10}$ copy number for (**A**) TLR1, (**B**) TLR2, and (**C**) β-defensin-1 was quantified between fresh (n = 3, paediatric), seven-day cultured (n = 3, paediatric) and organotypic (n = 2, adult) foreskin tissues exposed to LPS and compared to matched no-LPS controls. Matched tissues are indicated by same-point colouration and shape across groupings. Shown are mean values and standard deviation. Each point was obtained from three technical replicates (**A**, **B**, and **C**). Statistical comparisons made by paired *t*-test. ns, non-significant.

In addition to innate immune gene expression, the effect of LPS on release of the chemokine IL-8 into basal chamber medium was assessed. At 6 hours (Figure 3.9A), fresh paediatric tissue did not secrete detectable IL-8 irrespective of LPS exposure. Seven-day explants stimulated with LPS for 6 hours did not appear to show any difference in $\log_{10}$ IL-8 secretion (3.9 ± 0.07, no LPS vs. 4.1 ± 0.4, LPS). Organotypic foreskin showed increased IL-8 secretion when stimulated with LPS for 6 hours (0, no LPS vs. 3.6, LPS,). 12 hours of LPS exposure (Figure 3.9B) did not cause differences in IL-8 secretion in fresh (3.8 ± 0.3, no LPS vs. 3.7 ± 0.1, LPS) and seven-day cultured explant (4.4 ± 0.2 no LPS; 4.1 ± 0.2) foreskin. Additionally, the organotypic foreskin at 12 hours secreted more IL-8 compared to unstimulated controls (2.6, no LPS vs. 4.0 ± 0.7, LPS). 24 hours of LPS exposure (Figure 3.9C) did not induce differences in fresh (4.7 ± 0.03, no LPS vs. 4.5 ± 0.2, LPS) and seven-day cultured explant (4.8 ± 0.01, no LPS vs. 4.2 ± 0.8, LPS) IL-8 secretion. The organotypic tissue also secreted IL-8 at a level comparable to unstimulated control tissues (3.7, no LPS; 3.3 ± 0.5, LPS). More biological replicates are required (Figure 3.9A, B, and C) to make any statistical conclusions regarding the impact of LPS at the given concentration and the secretion of soluble immune mediator IL-8.

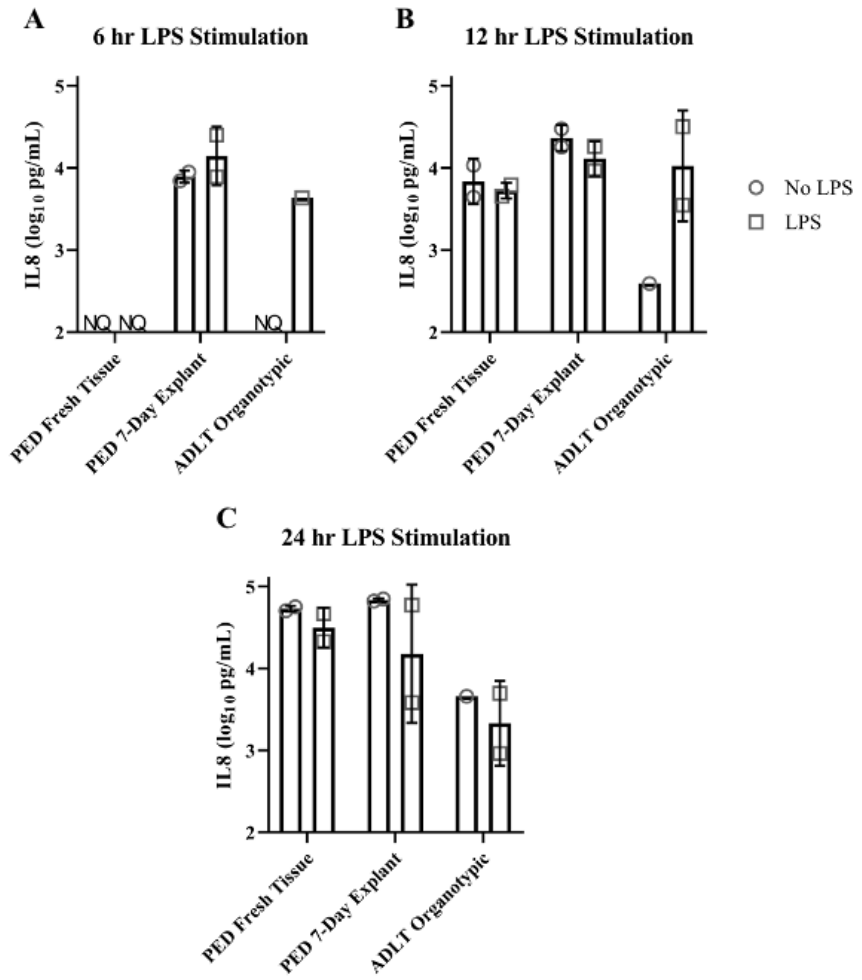

Figure 3.9: IL-8 Secretion as Compared Between Paediatric Explant-Cultured and Adult Organotypic Foreskin Tissues Stimulated with LPS. The $\log_{10}$ IL-8 concentration in basal compartment medium was quantified at (**A**) 6 hours, (**B**) 12 hours, and (**C**) 24 hours post LPS administration. These values were compared to matched non-stimulated controls. (**A**, **B**, and **C**) This comparison was between fresh (n = 2, paediatric) and seven-day cultured foreskin tissue (n = 2, paediatric); as well, the adult *in vitro* model was compared to these tissues (**A**: n = 1 unstimulated and stimulated; **B**: n = 1 unstimulated, n = 2 stimulated; **C**: n = 1 unstimulated, n = 2 stimulated tissues). Shown are mean values and standard deviation. Each point was obtained from three technical replicates (**A**, **B**, and **C**). Samples were not included in this dataset if they showed IL-8 contamination in their corresponding basal medium-only negative control. NQ, not quantifiable.

3.5 Characterizing Tissue Barrier Functionality

Foreskin tissue immediately frozen after circumcision and seven-day cultured tissue were subject to immunofluorescent staining and imaging so as to discern the presence of tight junction marker claudin-1 in tissue cultured with or without LPS (representative four-colour images shown in Figure 3.10, foreskin tissue comparison in Figure 3.11). To compare across paediatric and adult participants as before, inner and outer paediatric and adult foreskin tissues were immunostained and quantified in terms of claudin-1 epithelial immunoreactivity, as shown in Figure 3.12. There was no detectable difference in the immunoreactivity of claudin-1 between inner (47.9 ± 13.9%) and outer (48.8 ± 16.5%) paediatric foreskin tissues ($p = 0.9$). It appeared as though there was increased claudin-1 immunoreactivity for adult inner foreskin compared to the outer foreskin (46.9% vs. 26.8%), but more biological replicates are required to know if this is representative of all men.

Note that I was unable to immunostain LPS stimulated organotypic cultures due to COVID-19 pandemic-mediated time constraints and restrictions (Figure 3.11). Similarly, it was not possible to quantify organotypic foreskin cultures using the established pipelines mentioned in Chapter 2 for the same reason.

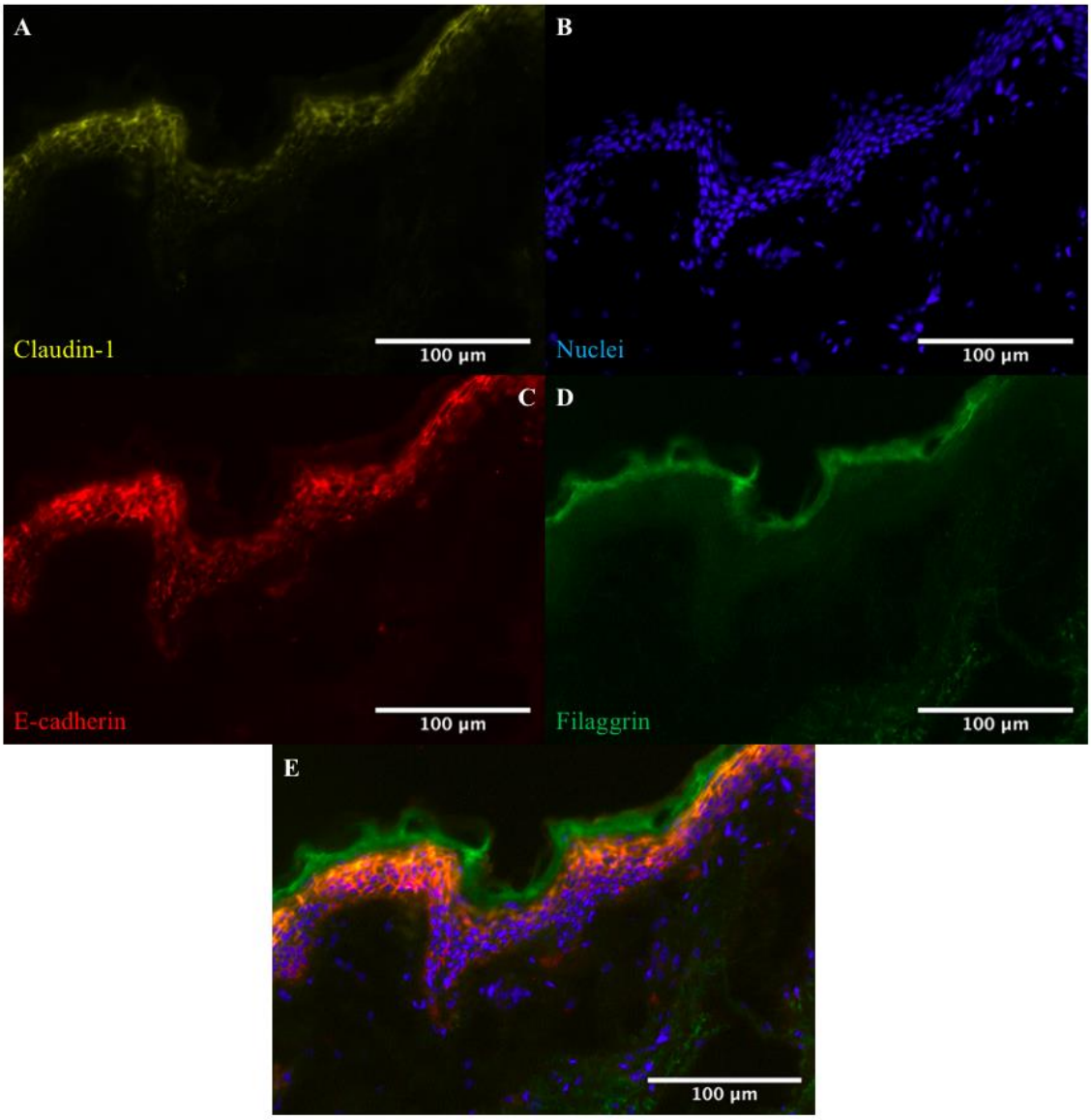

Figure 3.10: Representative Immunofluorescent Images of Immediately Frozen Foreskin Tissues. Representative Foreskin tissues from one paediatric participant are shown. Individual (**A**) Yellow, (**B**) blue, (**C**) red, and (**D**) green channels are shown for image **E**.

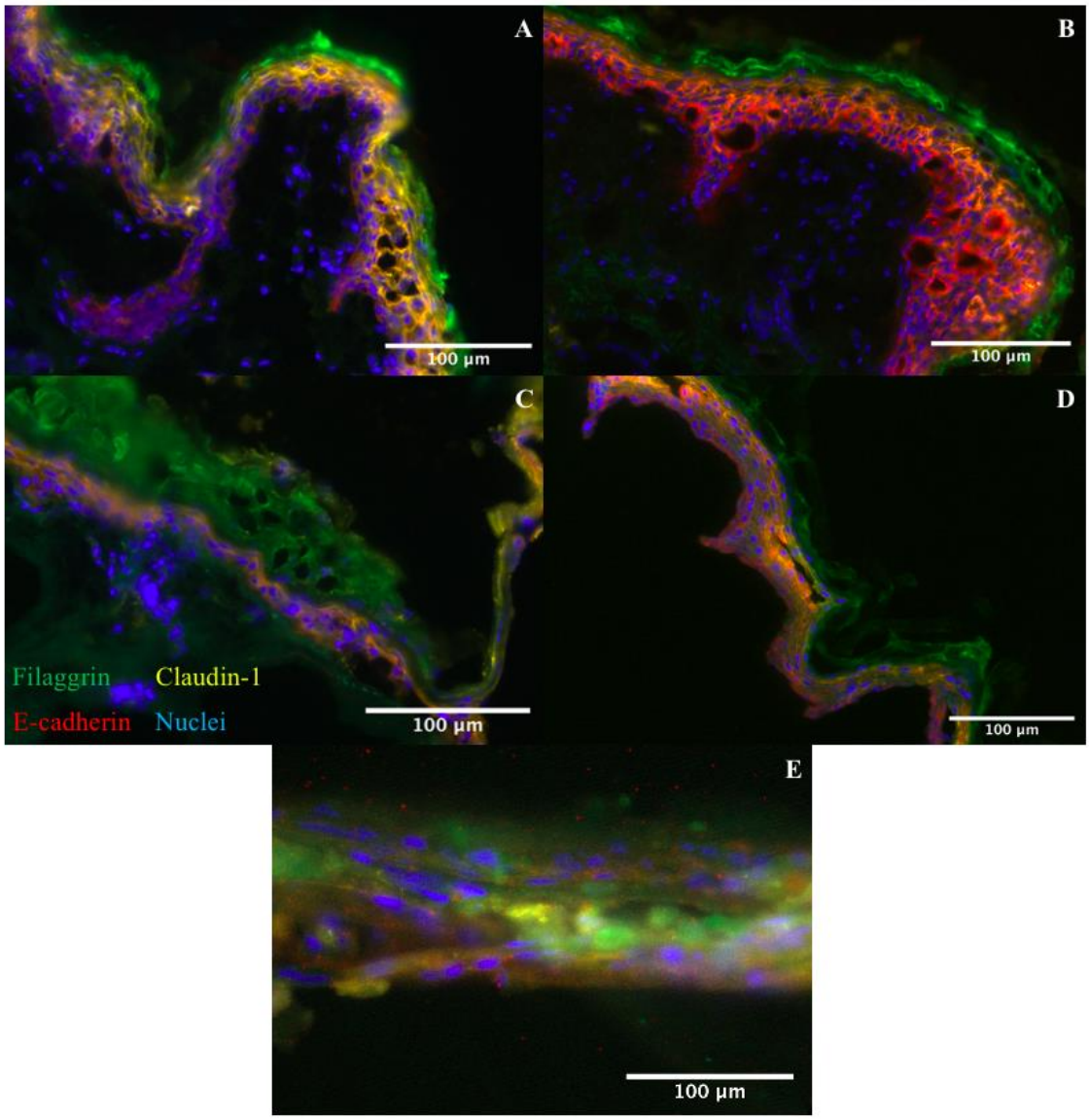

Figure 3.11: Representative Immunofluorescent Imaging of Foreskin Explant Tissues Cultured either without or with LPS. Representative images of fresh cultured foreskin tissue either cultured without (**A**) or with (**B**) LPS are shown next to that of seven-day cultured explant tissue cultured without (**C**) or with (**D**) LPS. **E** shows a representative image of an organotypic foreskin culture without LPS exposure.

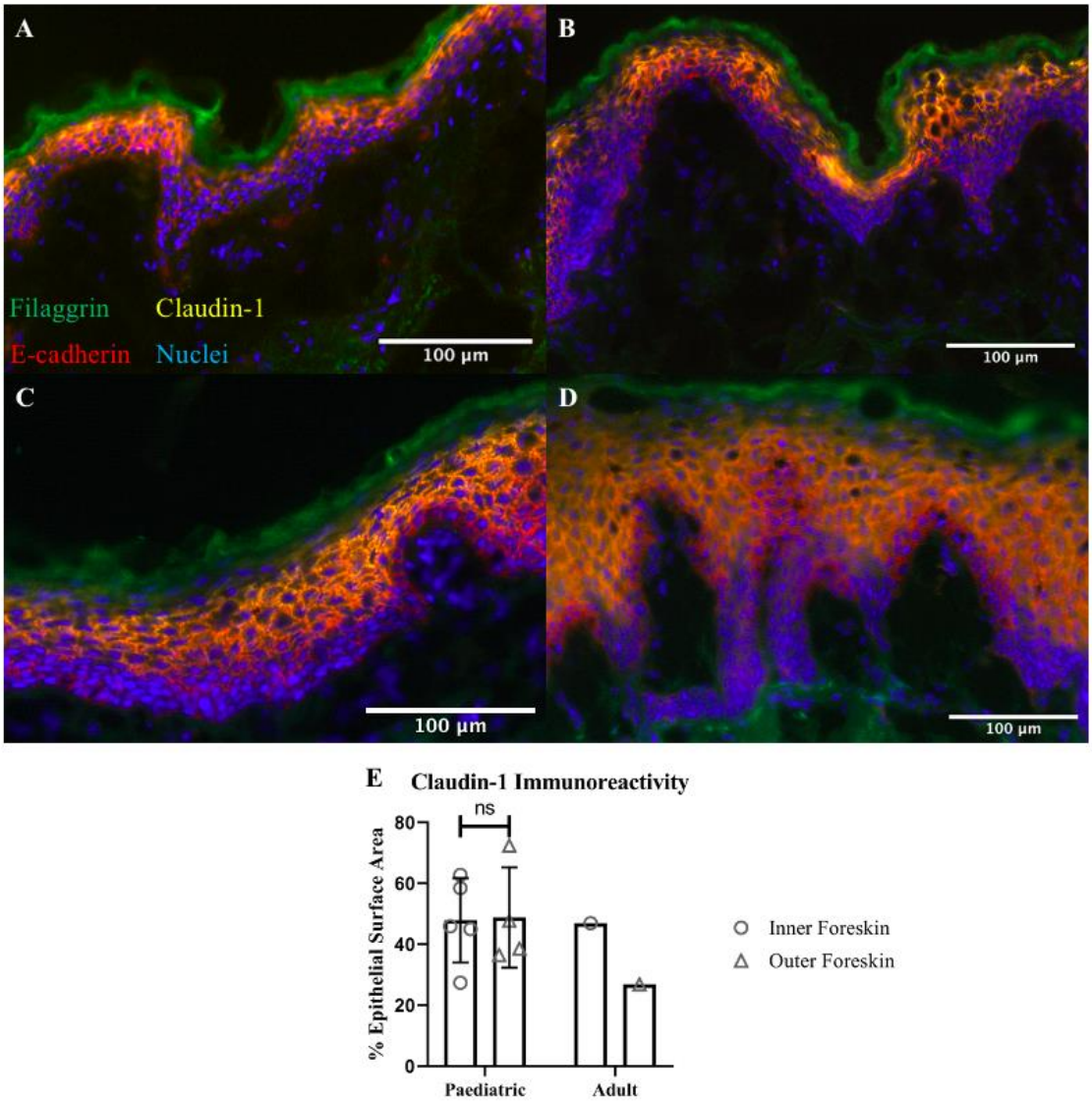

Figure 3.12: Claudin-1 Immunoreactivity Comparison between Paediatric and Adult Inner and Outer Foreskin Tissues. Representative images of paediatric inner (**A**) and outer (**B**) foreskin tissues are shown next to that of adult inner (**C**) and outer (**D**) foreskin tissues. Tissues were frozen immediately after circumcision surgery. (**E**) The percent surface area coverage by claudin-1 pixels was quantified between inner (n = 5 paediatric, n = 1 adult) and outer (n = 4 paediatric, n = 1 adult) foreskin tissue immediately frozen after circumcision surgery. Shown are mean values and standard deviation. Each point was obtained from one representative section of a complete image. Statistical comparison made by unpaired *t*-test. ns, non-significant.

Tissues were then subject to an optimized (efficiency and linearity of the standard curve shown in Table 3.8) qPCR assay to determine the number of mRNA copies for the tight junction protein claudin-1 in fresh, seven-day cultured, and organotypic foreskin tissues (Figure 3.13). The efficiency and linearity of this assay was 94.4 ± 2.3% and 0.998 ± 0.001, respectively.

Table 3.8: Optimized qPCR Reaction Efficiency and Standard Curve Linearity for Claudin-1. Efficiency of amplification as measured using a standard curve, as well as standard curve linearity are shown for successful qPCR assays used to detect copies of claudin-1 (n = 8). Shown are mean values and standard deviation.

Gene	Reaction Efficiency	Linearity
Claudin-1	94.4 ± 2.3%	0.998 ± 0.001

There were no statistically significant, detectable differences in claudin-1 mRNA between tissue types (p = 0.7; Figure 3.13). Organotypic foreskins appeared to show similar claudin-1 mRNA copies as snap frozen, fresh, and seven-day explant cultured tissues. Tissues used in the analysis had $\log_{10}$ claudin-1 mRNA copy numbers of 3.2 ± 0.2 (PED fresh tissue), 3.0 ± 0.3 (PED seven-day explant), and 3.3 ± 0.2 (ADLT organotypic). Next, the effect of LPS on claudin-1 mRNA was assessed (Figure 3.14). There were no detectable, statistically significant differences between fresh tissues, as well as seven-day explants across LPS treatment (p = 0.9 fresh tissues; p = 0.5 seven-day explant tissues). As well, organotypic foreskins appeared to show no difference in claudin-1 copy numbers when stimulated with LPS. Log_{10} claudin-1 mRNA copy numbers (no LPS vs. with LPS) include 3.2 ± 0.1 vs. 3.2 ± 0.1 (PED fresh tissue), 3.1 ± 0.5 vs. 3.1 ± 0.5 (PED seven-day explant), and 3.3 ± 0.2 vs. 3.1 ± 0.1 (ADLT organotypic).

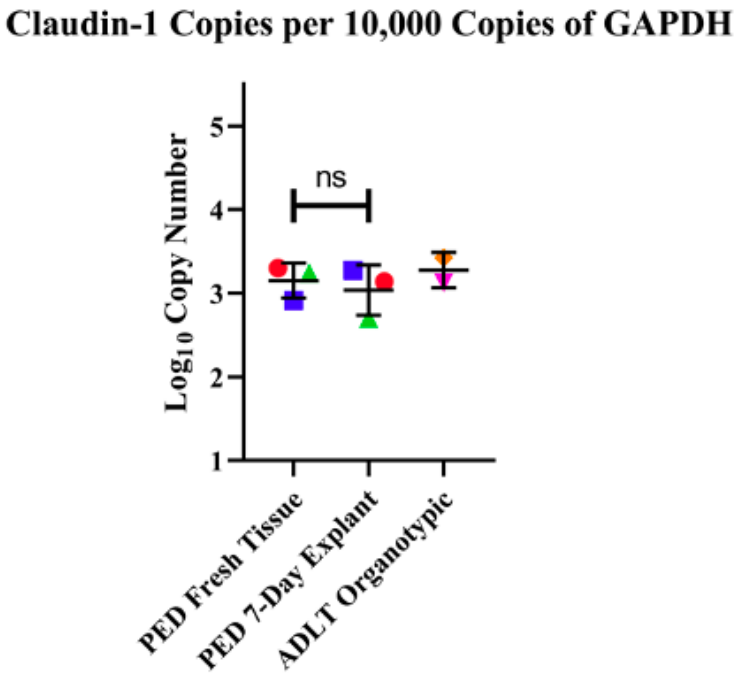

Figure 3.13: Claudin-1 Gene Expression Comparison between Paediatric Foreskin Tissue and Adult Organotypic Foreskins. The $\log_{10}$ copy number for claudin-1 was quantified between fresh (*n* = 3, paediatric), seven-day cultured (*n* = 3, paediatric) and *in vitro* organotypic (*n* = 2 adult) foreskin tissues. Shown are mean values and standard deviation. Each point was obtained from three technical replicates. Matched tissues are indicated by same-point colouration and shape across groupings. Statistical comparison made by paired *t*-test. ns, non-significant.

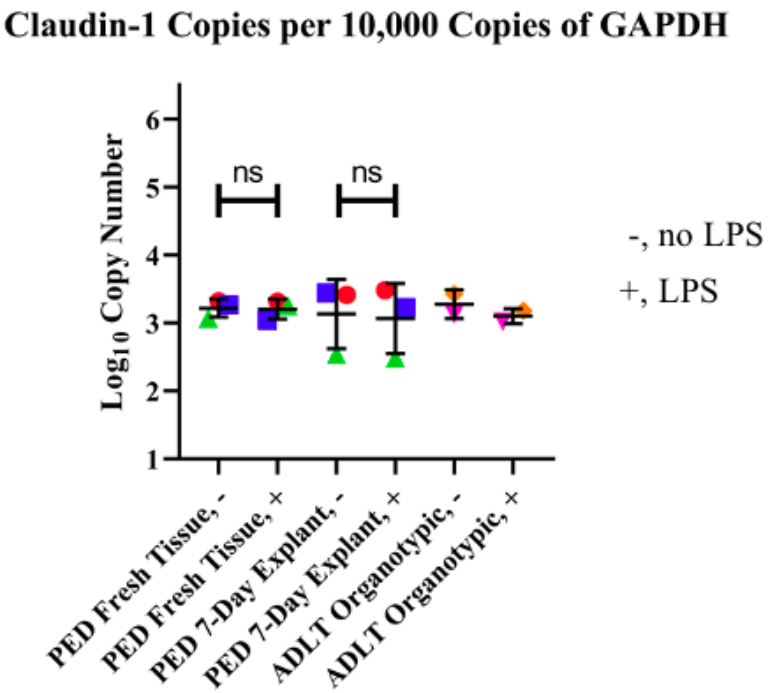

Figure 3.14: Claudin-1 Gene Expression Comparison between Paediatric Foreskin Tissues and Adult Organotypic Foreskins Exposed to LPS. The $\log_{10}$ copy number for claudin-1 was quantified between fresh (n = 3, paediatric), seven-day cultured (n = 3, paediatric) and organotypic (n = 2 adult) foreskin tissues exposed to LPS and compared to matched no-LPS controls. Shown are mean values and standard deviation. Each point was obtained from three technical replicates. Matched tissues are indicated by same-point colouration and shape across groupings. Statistical comparisons made by paired *t*-test. ns, non-significant.

To determine the barrier capability of fresh, seven-day cultured, and organotypic foreskin, tissues were tested on their ability to exclude a high molecular weight fluorescent tracer molecule (dextran) applied apically to the stratum corneum over a period of 24 hours (basal media sampled at 6, 12 and 24 hours; Figure 3.15A). Fresh foreskin tissue permeability is not significantly different over time (0.16 ± 0.28% permeation per hour, $p = 0.6$), whereas seven-day explant tissue does increase in permeability over time (1.4 ± 0.2% permeation per hour, $p = 0$). Similarly, organotypic tissue permeability also increases over time (1.5 ± 0.4% permeation per hour, $p = 0$). Tissues included in this analysis (mean ± standard deviation) included PED fresh tissue at 6, 12, and 24 hours (13.8 ± 2.5%, 13.2 ± 2.7%, and 16.3 ± 12.1%, respectively), PED seven-day explant tissue at 6, 12, and 24 hours (34.4 ± 30.7%, 44.7 ± 27.3%, and 59.6 ± 20.8%), and lastly organotypic foreskins (45.4 ± 21.8%, 63.8 ± 33.1%, and 74.8 ± 27.4%). Organotypic foreskin cultures used in the analysis are shown in Figure 3.15B and C. Organotypic foreskins in both images appear disorganized with no clear tissue structure or expression of E-cadherin, claudin-1, or filaggrin.

The preliminary results highlighted in this chapter suggest organotypic foreskins can mimic the stratification of *in vivo* tissue, while retaining the expression of innate immune mediators and adherens junctions that play a role in maintaining tissue structure. As well, they provide a sterile, physiologically relevant surface suitable for bacterial inoculation. This is in stark contrast to seven-day cultured foreskin tissue, which loses tissue integrity and does not provide a sterile environment to inoculate the foreskin microbiota for long-term culture.

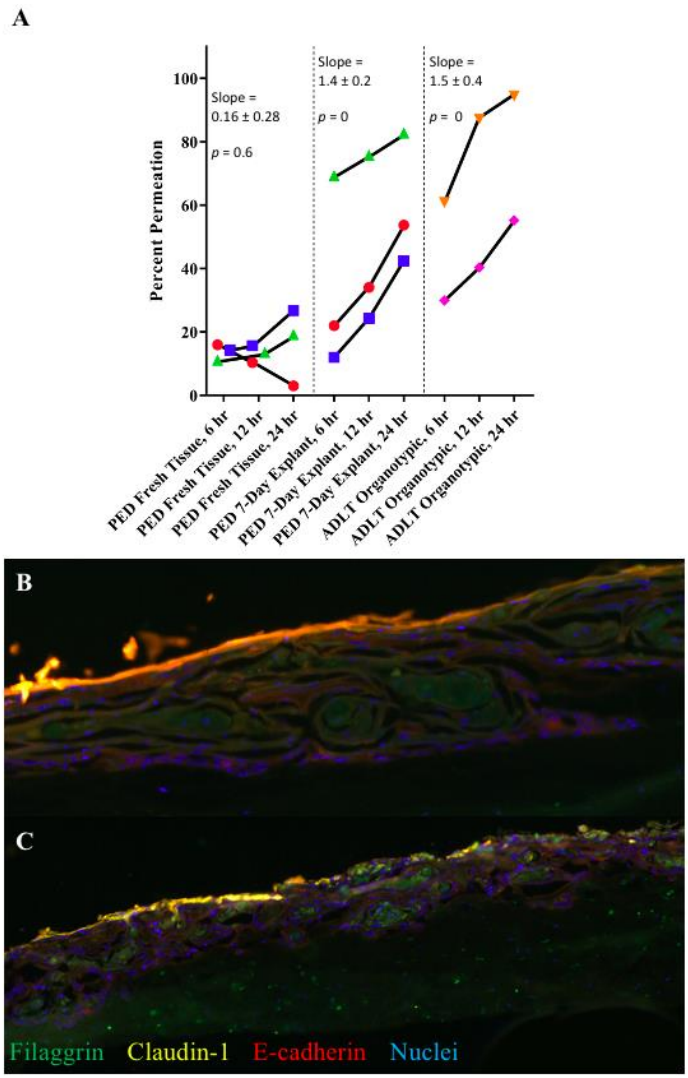

Figure 3.15: Permeability Comparison between Paediatric Foreskin Tissues and Adult Organotypic Foreskins. The percent permeation by 5 kDa fluorescent dextran applied to the stratum corneum was quantified for fresh (n = 3 paediatric) and organotypic (n = 2 adult) foreskin tissues (**A**). Each point in **A** represents a single participant assayed in triplicate, and matched tissues are indicated by same-point colouration and shape across groupings. **B** and **C** shows representative images of the organotypic foreskin cultures used for this assay (ADLT 001 is shown in **B**, represented by pink data points in **A**; ADLT 002 is shown in **C**, represented by orange data points in **A**). Statistical comparisons were made with a random effects model.

Chapter 4

4 Discussion

4.1 Cell Isolation and Culture

Primary fibroblasts and keratinocytes were isolated from both adult and paediatric foreskin tissues as described in Chapter 2. Troubleshooting was required to optimize this procedure. First, mechanical separation of the dermis from the epidermis after overnight Dispase II incubation was not successful in most cases, especially with paediatric tissues. Changes were made (Chapter 3) which included adding an additional 37°C, 1-hour incubation step after 4°C overnight incubation with Dispase II, and also increasing Dispase II volume during the incubation. Both paediatric and adult tissue layers were able to be more easily separated after this which is attributable to both enzyme kinetics and the selective (collagen type IV) proteolytic activity of Dispase II[164]. The 37°C incubation step can increase the enzyme-catalyzed collagen Type IV breakdown rate at the basement membrane[165]. By increasing the volume of the enzyme solution, the entire tissue surface (dermis side up) was in greater overall contact with the enzyme, increasing Dispase II access (and thus enzyme activity) to its collagen Type IV substrate at the basement membrane[166]. Some pieces (particularly those from paediatric participants) still exhibited little to no layer separation, however. Future directions may include further optimization of the time the tissue spends in contact with Dispase enzyme at each reaction temperature above, or empiric testing of mixed incubation temperatures and times on tissue separation. Alternatively, incubation overnight using cold 0.25% trypsin without EDTA could be done as this has also been shown to separate the dermis and epidermis of newborn mouse skin[167].

During keratinocyte isolation, keratinocyte viability was initially very low. Few keratinocytes were able to survive the plating procedure, and those that did exhibited slow growth. To increase cell viability, cells were centrifuged at a lower speed (114 vs. 524 x *g*) and plated at a higher density than recommended in the original protocol by Gangatirkar et al, 2007 (5.3×10^4 vs. 2.6×10^4 cells/cm^2). By decreasing centrifugation

speed, keratinocytes were able to be pelleted and separated from the 0.05% Trypsin-EDTA enzyme solution used to extract cells from the epidermal sheet while reducing cellular damage[168]. Although, to my knowledge, the specific centrifugation speed at which keratinocytes experience damage has not been published, this has been documented in other, more fragile cells such as adipocytes (504 – 2016 x *g* [1500 – 3000 RPM] for three minutes damaged and lysed cells)[169]. Plating cells at a higher density allowed for a higher concentration of cell-produced growth factors in the medium used to culture the cells, increasing growth and proliferation. To further improve this process, primary keratinocytes could be cultured with irradiated 3T3 feeder cells (cells unable to divide) which are primarily used in culture applications to provide additional growth factors in cell culture medium[170]. Additionally, increases in K-SFM Complete growth factors BPE and rEGF may increase the proliferative ability of primary isolated keratinocytes without relying on 3T3 fibroblast produced growth factors[171–173].

Keratinocytes were also difficult to detach from cell culture vessels with trypsin, and upon any detachment, viability and growth were low and slow once replated. This was suspected to be due to firm adherence of the keratinocytes to the cell culture vessel plastic, and cellular damage due to long trypsin incubation followed by centrifugation. Both the use of trypsin and centrifugation at high speeds can reduce cell viability[168,174]. Cells that are damaged during these processes may additionally require a recovery period after replating before they start to divide once again. Literature review indicated that incubating the keratinocyte cell monolayer with a solution of 0.5 mM EDTA in 1X DPBS before enzyme treatment would help to dissociate cell-cell and cell-substrate interactions,[175]. In addition, Accutase enzyme was added to cell culture vessels after EDTA to further dissociate cells. Accutase is composed of proteolytic and collagenolytic enzymes allowing it to mimic both trypsin and collagenase but at a greater efficiency, allowing its use at lower concentrations; this, according to the manufacturer, results in gentler and less toxic cell dissociation (Innovative Cell Technologies, Inc.). Afterward, cells were centrifuged at 114 x *g* (700 RPM) for 8 minutes compared to the original 524 x *g* (1500 RPM) for 5 minutes to decrease cellular damage[168]. Keratinocytes that were once firmly attached were able to be detached and replated successfully at higher densities when subject to this technique.

Lastly, keratinocytes may oftentimes not be visible or distinguishable from dead cells and small cellular debris remaining after the filtration step during cell isolation. Increased undisturbed culture time was necessary to promote cell growth and proliferation. It was suspected that these cells were damaged during the isolation protocol and required time to undergo growth after plating in cell culture vessels. By leaving the keratinocytes in the cell culture vessel over a period of 2-3 weeks with no disturbance or media change, cells started dividing and forming distinct colonies distinguishable from cellular debris. This could be due to low cell viability and density after isolation and thus decreased secretion of cell growth factors imperative for stimulating cell growth and proliferation. Additionally, cells may have been stripped of surface receptors due to trypsin treatment during isolation which may reduce initial cellular response to factors that require surface receptors[176]. Future directions and optimizations at this stage include plating isolated keratinocytes onto irradiated 3T3 fibroblast feeder cells for growth factor secretion, or possibly using an enzyme that does not strip cells of surface receptors during the isolation procedure. This may increase the concentration of cell growth factors necessary for keratinocyte recovery and proliferation, while maintaining the receptors to detect them. This could thus speed up the time between isolation and establishment of a healthy, confluent culture of cells.

4.2 Immortalization of Foreskin Keratinocytes

Primary human keratinocytes undergo cellular senescence after approximately 10 doublings[177]. To maximize keratinocyte longevity for this project, it was necessary to immortalize these cells such that they can continue dividing and surpass this limitation. To do this, primary isolated keratinocytes were infected with a replication incompetent retroviral vector encoding HPV16 E6 and E7 oncogenes, as well as a resistance gene for the antibiotic neomycin, as shown in Figure 4.1[178]. The packaging cell line used for this vector has helper virus DNA containing several alterations crucial for ensuring it remains replication incompetent, such as removal of a small portion of the 5′ long terminal repeat (LTR), replacement of the 3′ LTR with a simian virus 40 (SV40) polyadenylation signal, and deletion of the retroviral packaging signal[178]. This acts to ensure the vector does not

generate helper virus, and safeguards against packaging signal transfer between the vector insert and retrovirus genome[178]. Should RNA containing helper virus genes get packaged into virions, these alterations prevent their transmission as many of the signal elements required for reverse transcription and integration are missing[178]. There is additionally a stop codon inserted into the vector insert *gag* start codon, preventing production of helper virus by thwarting recombination between the vector sequence and the helper virus genome (containing the viral packaging signal)[178]. It would thus be highly unlikely for replication competent virus to be generated in our study. At least one recombination event in a short region of homology at the 5′ end of the vector and one nonhomologous recombination event between the vectors 3′ end and the helper virus genome would be necessary to do so[178].

The E6 and E7 oncogenes, when successfully transduced into keratinocytes, extend the lifespan of the cell through production of E6 and E7 oncoproteins[179]. E6 oncoprotein will induce tumour suppressor p53 degradation, while activating human telomerase reverse transcriptase (hTERT), the catalytic subunit of telomerase (Figure 4.2)[180,181]. E7 oncoprotein inhibits the tumour suppressor protein retinoblastoma (pRb; Figure 4.2)[179–181]. In combination, it is the activation of hTERT by E6 and degradation of pRb by E7 that induces cellular immortalization[180]. Geneticin antibiotic was applied to culture medium and used to select transduced cells as it selects against eukaryotic cells through blocking peptide synthesis, and resistance can be conferred through expression of a neomycin resistance gene[182–184]. As a result, successfully transduced cells exhibited Geneticin resistance through incorporation of the neomycin resistance gene, while non-transduced cells were broadly eliminated from the culture.

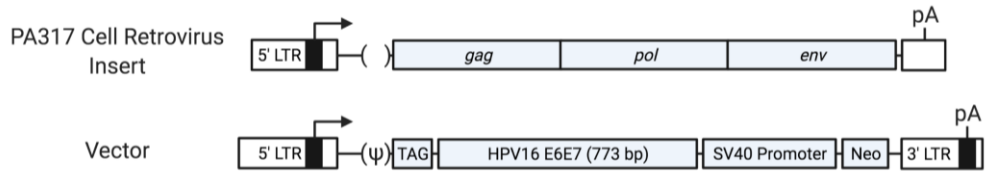

Figure 4.1: PA317 Cell Inserts used in the Generation of Retroviral Vectors for Keratinocyte Transduction. The PA317 fibroblast cell genome contains two sequences. The PA317 Cell Retrovirus Insert (top) is the genome of a deleted helper virus incorporated into the genome of the PA317 fibroblast cell, and supplies proteins Gag, Pol, and Env in *trans* for use in retrovirus generation. The helper virus genome also lacks a packaging sequence (ψ), preventing its transcript from being packaged into the mature retrovirus virions. A portion of the helper virus 5′ LTR is also missing to prevent recombination events between the two sequences. The vector (bottom) incorporated into the PA317 cell genome contains a packaging signal so that its transcript will be incorporated into mature retrovirus virions, as well as genes that will be inserted into the genome of a successfully transduced cell (up to 4 kb in length). The retrovirus insert contains a SV40 polyadenylation signal to replace the 3′ LTR so as to prevent recombination and also block second strand synthesis. TAG indicates the *gag* start codon in the bottom vector sequence has changed to a stop codon. Arrows indicate transcription start sites; LTR, the retroviral long terminal repeat; pA, the replacement of the 3′ long terminal repeat with a Simian Virus 40 polyadenylation signal. Adapted and modified from Miller, A. D., Molecular Therapy, 2002. Figure created with BioRender.com.

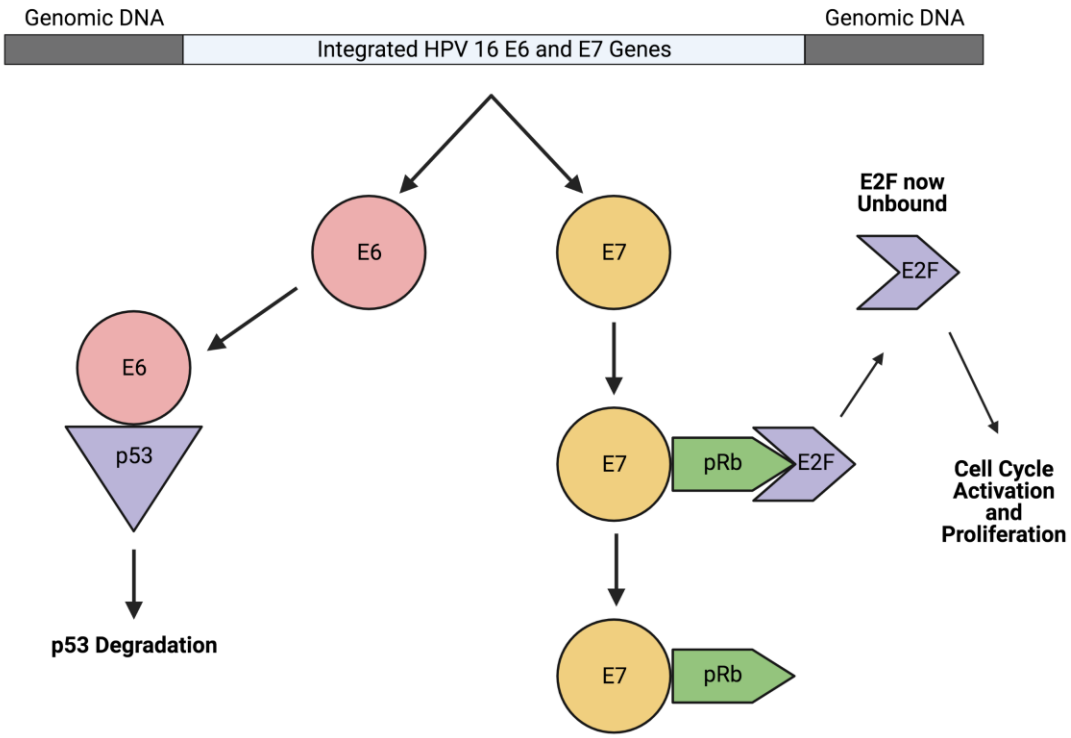

Figure 4.2: Effect of HPV16 E6 and E7 Oncoproteins on Tumour Suppressor Proteins. E6 oncoprotein binds to tumour suppressor protein p53, promoting its degradation. E7 oncoprotein binds to tumour suppressor protein retinoblastoma (pRb) while it is complexed with the E2 transcription factor (E2F), causing the release of E2F and subsequently cell cycle activation. Adapted and modified from Ruttkay-Nedecky *et al*, International Journal of Oncology, 2013. Figure created with BioRender.com.

Cells were retained pre-transduction as well as post transduction for comparison to one another. This comparison would verify the donor's isolated keratinocytes were not previously infected with HPV16 before the study commenced, which could impact the isolated keratinocytes phenotype in a non-controlled way. Additionally, this confirms successful cell transduction through amplification of the viral insert.

Transduced keratinocytes were subject to PCR analysis to verify the presence of the HPV16 E6E7 insert in the keratinocyte genome[155]. Non-transduced and transduced keratinocytes were compared by PCR amplification of the E6E7 sequence and resolving any produced amplicon by gel electrophoresis. Additionally, verification of amplicon identity (Figure 3.1) through sequencing and comparison to the viral insert *in silico* was used to verify presence of the correct sequence. Transduced keratinocytes (Figure 3.2) showed sharp bands at 773 base pairs, indicating successful integration of the HPV16 E6E7 sequence into their genome. Non-transduced, matched keratinocytes lacked any bands in their respective lanes of the agarose gel (Figure 3.2). This suggests cells were successfully transduced and possibly immortalized for this project. It is, however, possible that the viral insert was not present in the non-transduced cell lanes of the agarose gel due to degradation of isolated genomic DNA or PCR amplicon. Future comparisons could include a housekeeping gene in the keratinocyte genome like β-Glucuronidase (GUSB) to verify the presence or absence of PCR product in each lane of the agarose gel[185]. As well, it is possible that these cells are not fully immortalized despite introduction of the E6E7 sequence. The retroviral vector (based off of Moloney Murine Leukemia virus) used in this study does not introduce the E6E7 insert into a specific part of the keratinocyte genome; instead, there are weak preferences for insertion into gene coding regions and strong preferences for transcription start sites and CpG rich regions raising the possibility that it is introduced into a non-transcribed region[186]. This is hopefully mitigated by rigorous selection in Geneticin antibiotic. Western blotting could be used to detect E6, E7, and downstream proteins (e.g., pRb, hTERT, p53) in the cell lysate to help confirm successful transcription and translation of functional proteins. However, alternative approaches may be better suited for this project. E7 protein can disrupt skin barrier integrity through altering claudin expression (an important epithelial barrier aspect investigated in this study)[187]. As well, at later cell passages E6 and E7 oncoprotein immortalization disrupts the karyotype of the cells, while earlier passages retain low tumourigenicity and have karyotypes similar to that of non-immortalized cells[188]. Modulation of rEGF concentration in culture medium may increase keratinocyte primary cell longevity up to 20 passages without immortalization as shown by Ahmed *et al*, 2006 in ovarian epithelial cells[189,190]. As well, culture of keratinocytes could be

conducted in the presence of the Rho kinase inhibitor Y-27632 which has been shown to extend the neonatal foreskin keratinocyte passage number to 150[191,192]. These methods could permit the mass culture of primary non-transduced keratinocytes required for skin model development. In contrast, a different system of cellular immortalization could be used that does not rely on HPV16 E6 and E7 proteins. Most importantly, these would need to inactivate tumour suppressor genes involved in inducing cellular senescence[193]. As suggested by Matsumura *et al*, 2004, the use of SV40 T antigen alongside overexpression of the hTERT catalytic subunit can be effective at inducing cell immortalization[194]. Additional alternatives include p53 siRNA expression while overexpressing the hTERT catalytic subunit[195,196]. This also provides a more defined genetic background that mimics keratinocytes with finite proliferative capacity[195,196]. Of interest, keratinocytes could be grown, in the future, on a soft culture substrate to help cells retain their stem-like phenotype[197]. Substrates such as polydimethylsiloxane (PDMS) are less stiff than tissue culture plastic and have been demonstrated to reduce premature keratinocyte senescence when the Young's elastic modulus for the substrate is either 1.5 or 15 kilopascals (kPa)[197]. This could provide a cell culture substrate-based alternative to immortalization techniques discussed earlier.

Although not used to generate organotypic foreskins in this thesis, I have generated three sets of paediatric transduced keratinocytes and banked these alongside matched non-transduced keratinocytes and fibroblasts. In the future, these will permit (1) creation and testing of organotypic foreskins using these paediatric cells, providing a better match comparator to the paediatric tissues and explants used in this study; (2) comparison of organotypic models generated using immortalized and non-immortalized cells to determine the effect of immortalization on key aspects of innate immunity and barrier function; and, (3) investigation and comparison of alternative immortalization approaches to current methods through use of non-transduced cells. Furthermore, during my thesis adult keratinocytes from one additional individual were transduced and banked alongside matched fibroblasts. These additional banked cells will allow for the creation of additional organotypic foreskins that can be used in to bolster biological replicates in the current work. Finally, these banked adult and paediatric cells can be used to determine if there are any differences in innate immune function, tissue structure, or barrier function

between organotypic foreskins generated from adult and paediatric tissues. This information is important, as while adult skin in a more relevant model for sexually transmitted infections, paediatric foreskins are substantially more readily available than adult foreskins.

4.3 Generation of the Organotypic Foreskin Model

Artificial foreskin tissues were created as described in Gangatirkar *et al*, 2007, with modifications made through troubleshooting highlighted in Table 3.6[154]. As can be seen in Figure 3.3, fibroblasts are actively remodeling the collagen matrix they are placed in, qualitatively observed through collagen gel contraction. The fibroblasts can be viewed through phase contrast microscopy at all stages of model development, although this becomes progressively more difficult to do so when keratinocytes start to proliferate on the collagen surface and reduce light penetration. Initially, cellular collagen contraction was minimal, and fibroblasts were quite sparse within the collagen hydrogel. Fibroblast cell concentration was thus increased from 2.30×10^5 cells/mL to 3.28×10^5 cells/mL ($\sim 10^5$ cells/mL increase) during casting. This notably increased collagen contraction such that the hydrogel decreased by $1/5^{th}$ of its original size (contraction of approximately 15-20%), and increased fibroblast density when viewed by phase contrast microscopy. While these fibroblasts can be viewed through phase contrast microscopy, they are difficult to resolve through immunofluorescent microscopy as there are few blue stained nuclei present within the dermal mimic (Figure 3.4). In this comparison, there are many nuclei shown within the *in vivo* dermis, while the dermal mimic of the organotypic tissue has only one observable nucleus. While this may indicate reduced organotypic dermal fibroblasts, many of the cells identified in the dermis *in vivo* are immune cells[160], which are absent in the organotypic tissues at this point in time. To accurately compare the number of fibroblasts in the organotypic model to *in vivo* tissue, future comparison could include immunostaining for vimentin, a cytoskeletal marker expressed within fibroblasts[198,199]. However, vimentin is not specific for fibroblasts and is also expressed within macrophages, T cells, and neutrophils in the dermis[198–201]. By combining immunostaining for immune cell markers such as CD3, CD4, CD14, CD1a, langerin,

CD1c, CD141, CD68, and CCR5 with vimentin, we could more accurately delineate the immune cell populations of *in vivo* tissue from that of fibroblasts[198,202–205]. If complexed with Haematoxylin and Eosin (H & E) staining, this may help provide an additional layer of confidence in fibroblast identification by eliminating other cell types based on morphology or staining patterns[199]. Once immune cell populations are added to the organotypic tissue model, this combination of immunostaining and H & E staining could help visualize the resident cells of the artificial dermis.

Keratinocytes, once added to the dermal mimic surface, form a confluent monolayer as the apical surface becomes opaque and white in colouration (in sharp contrast to the reddish-pink collagen surface; Figure 3.3C). Initially, I was only able to generate dermal mimics with patches of keratinocytes located on their apical surface, but modification of seeding and culture protocols allowed for confluent monolayer development. Initially, cells were added in a single small volume (30 µL), high cell concentration (1.667×10^6 cells/mL) droplet to the surface of the collagen layer. Cells did not spread across the large surface area of the collagen gel, and as such they often formed a small, centrally located cell aggregate on its surface. This was due to the central location of the cell droplet, and immediate culture in Epidermalization Medium meant to allow the cells to stratify. Adding multiple small-volume (10 µL) cell droplets across the surface of the hydrogel, increasing their concentration by one order of magnitude, and culturing the cells for one week in K-SFM Complete medium allowed cells to attach to the gel, grow to form colonies, and spread across the gel surface. This resulted in an almost confluent monolayer consisting of multiple large patches of cells visible to the naked eye. To further optimize this, keratinocyte culture time in K-SFM Complete was extended to 10 days to allow further proliferation (fully confluent monolayer shown in Figure 3.3C).

The fluorescence image of the mature organotypic foreskin in Figure 3.3D shows formation of a multilayer epithelium on the surface of the dermal equivalent collagen, as can be seen by multiple nuclei throughout the epidermis. The structural junction protein E-cadherin is also located in this area, which suggests formation of functional adherens junctions[206–208]. Finally, terminally differentiated keratinocytes appear present on the apical organotypic model surface due to positive staining for filaggrin[61–63].

Representative images of foreskin tissue immediately frozen after surgery and an organotypic foreskin were compared at higher magnification in Figure 3.4. Organotypic foreskins are indeed composed of a multilayer epithelium and express E-cadherin and filaggrin proteins in regions similar to that of *in vivo* foreskin tissue. Based on cell morphology and the presence of filaggrin staining in the stratum corneum, it is possible to identify the layers of the epithelium as each layer contains cells of distinct shape (discussed in Chapter 1). These layers are clearly identified for the *in vivo* tissue shown in this figure, which shows the stratum basale, spinosum, granulosum, and corneum as expected. Cell morphology in the organotypic model is more difficult to visualize due to the diffuse cytoplasmic and membrane localization of E-cadherin throughout the organotypic tissue, whereas *in vivo* tissue E-cadherin is localized to the cell membrane. This does not permit close comparison of cell morphology necessary to identify each unique layer of the epithelium. However, stratum corneum location can be inferred through the apical presence of the protein filaggrin and by the location of the stratum basale (indicated by the presence of cuboidal cells at the clearly defined dermal-epidermal junction). This limits identification of the stratum spinosum and granulosum.

Immunostaining the organotypic tissue with antibodies specific for early and late keratinocyte markers of proliferation would help in identifying each distinct layer more accurately and clearly[209]. Early markers of proliferation include cytokeratin 14 which is expressed in the cells of the stratum basale, as well as cytokeratin 10, found in the stratum spinosum and granulosum[209]. Late markers include cytokeratin 2 found in the upper spinous and granular layers, and involucrin found in early stages of keratinocyte terminal differentiation[209,210]. While this helps resolve the basal and apical layers, it still makes identification of the stratum spinosum and granulosum difficult as there are no markers specific to their constituent cells[209]. Optimizing the organotypic foreskin culture may help localize E-cadherin expression to the cell membrane and aid in epidermal layer visualization.

This pattern of immunostaining could additionally be a result of the increased duration of formalin fixation necessary for preparing organotypic foreskin tissues for cryosectioning. This is undertaken as collagen hydrogels have a high water content, which results in a

hardness differential between the hydrogel and freezing medium it is embedded in[211]. As observed in preliminary work, formalin fixation over 24 hours seemed to result in diffuse E-cadherin immunoreactivity in immediately frozen *in vivo* foreskin when compared to non-fixed immediately frozen foreskin. Replacement of formalin with a different fixative or empirical testing of varied fixation times and formalin concentrations may remedy this issue. Alternatively, tissues could be placed into ascending concentrations of sucrose solution while still in culture, then a mixture of sucrose and OCT[212]. This renders the frozen hydrogel homogenous with OCT and reduces the hardness differential between the two substances[212].

Lastly, E-cadherin is expressed at the organotypic foreskin apical and lateral surfaces weakly, but strongly at the basal surface. This is in contrast to apicolaterally expressed E-cadherin in the *in vivo* tissue. If not an artefact of tissue fixation, this could indicate that diffuse expression is due to altered cell signaling pathways important for localization of structural junction proteins[213–215]. This is important for model development as *in vitro* studies have indicated E-cadherin mediated adhesion between cells is a prerequisite in the formation of tight junctions and desmosomes, with tight junctions specifically examined in this study[213,214]. Future study is necessary to discern the exact reason for this observation and to implement corrective measures, such that the organotypic tissue model may more accurately mimic *in vivo* skin.

The COVID-19 pandemic substantially disrupted the availability of tissues during this project. As a result, paediatric tissues were used for explant and immediately frozen comparators to organotypic foreskins generated with cells isolated from adults. To determine if this was an appropriate comparison, different tissue parameters were compared between paediatric participants and one adult foreskin tissue available (Figure 3.5). In these graphs, it is shown that immediately frozen paediatric inner and outer foreskin tissues showed no difference in their overall thickness for the E-cadherin layer, filaggrin layer (stratum corneum), or the total epithelium as defined by the pipeline used. Preliminary results for adult tissues suggest that they may show some difference in inner and outer foreskin thickness for the E-cadherin, filaggrin, and total epithelial layers compared to each other and paediatric tissues. Additional adult and paediatric *in vivo* and

organotypic foreskins are necessary to draw accurate conclusions about use of comparator groups in this and future studies.

When quantifying tissue parameters between *in vivo*, explant, and organotypic tissues as in Figure 3.6, it is clear that the organotypic model is composed of cell layers that express the protein E-cadherin (Figure 3.6A), as well the protein filaggrin (Figure 3.6B). It is also able to produce multiple layers of cells similar to that of the *in vivo* epithelium, as revealed through measuring the total epithelial thickness (Figure 3.6C). However, one difference observed is that, while the organotypic model had a layer of E-cadherin as thick as *in vivo* tissue, it had a much thicker filaggrin layer, resulting in greater overall epithelial thickness. A thicker organotypic filaggrin layer may be due to reduced desquamation due to a lack of physical abrasion in culture, compared to what *in vivo* skin would experience. More biological replicates are required to draw statistical conclusions from these results (Figure 3.6) and be able to compare between tissues examined. One limitation in the E-cadherin thickness measure is the presence of rete ridges at the dermoepidermal junction in *in vivo* tissue. These are not present in organotypic tissue, simplifying the depth measurement, but their presence within *in vivo* tissue limits quantification as they may occur at higher frequency in some parts of the tissue than others. It may be more accurate to determine the median depth of each *in vivo* FOV and separate each depth into quintiles and determine which quintile the organotypic model is most comparable to. As well, paediatric organotypic foreskins need to be generated to compare to adult organotypic foreskins. This comparison could, in the future, determine the feasibility in comparing organotypic foreskins to either adult or neonate tissue.

Lastly, organotypic tissue may produce more E-cadherin than that of *in vivo* tissue, although this again cannot be confidently said due to lack of biological replicates amongst both groups, and the diffuse cytoplasmic localization of E-cadherin throughout the organotypic tissue. In contrast, seven-day explant cultured tissue contained large holes throughout its suprabasal epidermal layers and poor immunoreactivity. Seven-day cultured tissue loses its ability to maintain its architecture at some point during the culture period, while also losing expression of E-cadherin protein (Figure 3.6A, B, C, and D). Thus, it can be shown through these preliminary results that organotypic foreskin tissue

may be able to mimic *in vivo* tissue architecture and E-cadherin expression more closely than seven-day cultured explant tissues.

4.4 Characterizing Innate Immune Capability

To examine innate immune capability, tissues were examined for: (1) mRNA expression of TLR1, TLR2, and β-defensin-1 during culture and after challenge with TLR agonist LPS; and (2) secretion of the chemokine IL-8 upon challenge with LPS. Expression of mRNA for innate immune proteins was normalized to GAPDH, which has been shown to be stably expressed in post mortem skin tissues[216]. GAPDH served as a measure of a gene expressed at similar levels between cells, but while this may be similarly expressed in explanted and fresh skin, it may not be in organotypic tissues. As well, there is a growing trend in using more than one stably expressed reference gene when normalizing cell or tissue level qPCR data[185]. While information regarding multiple reference genes for analysis of human skin tissue is scarce, further selection and validation of reference genes could be conducted in the future on both paediatric, adult, and organotypic foreskin samples. By selecting a large enough number of similarly expressed reference genes, we could ensure more accurate comparisons of normalized target mRNA across tissues examined in this study.

To quantify the number of mRNA copies for TLR1, TLR2, and β-defensin-1, qPCR experiments were optimized in terms of primer concentration and annealing temperature using a synthetic double-stranded DNA oligonucleotide-based standard curve[217]. The optimized mean reaction efficiency and linearity for each standard curve are shown in Table 3.7. The mean efficiency for each (TLR1, TLR2, β-defensin-1, and GAPDH) qPCR assay falls within the 90-110% efficiency guideline recommended for use of absolute quantification[218]. The assay linear dynamic range was high for the qPCR assays conducted as, aside from TLR1, each had a mean linearity greater than 0.995. In contrast, the qPCR assay for TLR1 had a mean linearity of 0.991 ± 0.005. Often in absolute quantification it is assumed that the standard and sample have the same efficiency, but this may not be the case[219]. In the future, to assess if efficiency is similar between the

standard and samples (two different targets), samples can be serially diluted similar to the oligonucleotide standard and the cycle threshold value determined per sample to establish a sample-based standard curve. This will allow for direct comparison to the oligonucleotide standard and permit troubleshooting should the sample-based standard curve differ in efficiency.

There was no detectable difference in TLR1, TLR2, or β-defensin-1 mRNA abundance between immediately snap frozen, seven-day cultured explant, and organotypic foreskin tissues. It can be reasonably assumed from this that expression did not differ between the cells of the tissue, but it is not known if mRNA examined was from living or apoptotic cells. As highlighted before in analyzing tissue structure, the seven-day explant loses tissue integrity and does not stain for E-cadherin (Figure 3.5, Figure 3.10). It is possible that the rate of apoptosis in the explant differs from the other tissues. Differences in induction of apoptosis may result in increases or decreases in mRNA yield per total number of cells in the tissue. This may be due to global degradation of mRNA that occurs near the initiation of apoptosis[220]. The presence of degraded intermediate mRNA of different lengths from cells at different stages of apoptosis may artificially change the quantity of mRNA copies of any of the genes examined in the study. This could be an upward or downward change in the copies expressed per 10,000 copies of GAPDH, depending on which target mRNAs have started degrading within the tissue sample. It is integral, in the future, that matched tissues be immunostained for markers of apoptosis such as apoptosis regulatory proteins caspase-3, B-cell lymphoma 2 (Bcl-2), or p53[221]. This will allow the amount of tissue level apoptosis in all tissues to be examined so as to validate this assay. It is also possible that GAPDH mRNA copies are decreasing within the seven-day explant, leading to increased target mRNA copies when normalized to it. This could be remedied by including more reference genes and comparing GAPDH numbers across fresh and seven-day tissues. We could alternatively immunostain foreskin tissue sections or perform Western blotting to determine protein level expression of TLRs or β-defensin-1.

Additionally, there was no detectable difference in expression of TLR1, TLR2, or β-defensin-1 mRNA copy numbers between fresh cultured, seven-day cultured explant, and

organotypic tissues stimulated with LPS and their matched unstimulated controls. Once more, careful analysis of stimulated and non-stimulated tissues at matched time points for markers of apoptosis is necessary to verify the identity of the population of cells examined in this analysis. One limitation experienced when stimulating organotypic tissues is the dispersion of aqueous LPS on their large, dry apical surface. While LPS covered the moist explant apical surface, the droplet added to the organotypic model did not seem to disperse on the surface of the tissue. This acts to limit the amount of tissue in contact with the LPS, and therefore may result in a reduced or minimal response from the organotypic tissue. Future directions include scaling the LPS droplet volume up such that it matches the droplet/surface area ratio of the explant tissue and ensuring the organotypic tissue surface area is in full contact with LPS. Lastly, examination of β-defensin-1 could be complemented with that of β-defensin-2, which has been shown through Northern blotting to sometimes upregulate in expression upon fresh skin tissue exposure to LPS[222]. It may be possible that LPS alone is not sufficient to induce expression of the genes examined, and that additional stimulatory factors (like the cytokine IL-1) are necessary for this as these factors are also required in some cases for β-defensin-2 expression[222].

Tissues were then examined for their ability to respond to stimulation with the TLR4 agonist LPS through quantifying secretion of the chemokine IL-8[148,223]. Fresh foreskin tissue obtained after circumcision surgery, tissue cultured in medium for seven days, and organotypic foreskins were exposed to a 100 ng/mL solution of LPS in endotoxin-free water, with culture medium harvested and tested for IL-8 (Figure 3.9). At 6 hours (Figure 3.9A), fresh paediatric tissue did not secrete detectable IL-8 (lower limit of quantification = 15.6 pg/mL; limit of detection = 2.0 pg/mL), regardless of LPS exposure, while IL-8 secretion was upregulated at 12 and 24 hours regardless of LPS exposure. This is in contrast to seven-day explanted tissue, which produced similar IL-8 levels regardless of IL-8 exposure throughout the entire 24-hour time period (Figure 3.9B). In sharp contrast to both fresh tissue and seven-day explants, the LPS-stimulated organotypic model secreted more IL-8 at the 6-hour time point relative the unstimulated tissue. IL-8 levels increased to similar levels across stimulated and non-stimulated tissues past 6 hours. Additionally, IL-8 levels decreased over time in comparison to the cultured explant tissues, suggesting it was downregulated after peaking at 12 hours of LPS exposure.

These results could be the due to the presence of microbiota-associated bacteria on the fresh and possibly seven-day explant tissues, which would be absent from the sterile organotypic foreskin tissues. Fresh tissue explants were not transported or cultured in media containing antibiotic after surgery. It is possible that bacteria still present during culture modulated IL-8 secretion, similar to what occurs during multi-species biofilm formation in gingival tissue (a stratified squamous epithelium just like the foreskin)[224]. As a result, our measures of IL-8 secretion for fresh tissue after the first six hours could be artificially elevated due to possible bacterial overgrowth or biofilm formation, limiting our ability to compare to seven-day explants and the organotypic foreskin. The seven-day cultured explant tissue was cultured in medium containing antibiotics for the seven-day culture period to limit bacterial and fungal overgrowth, but residual biofilm-associated bacteria may remain during this period and modulate IL-8 secretion. The organotypic tissue was sterile at baseline, which may explain the large increase in IL-8 compared to the other models at the 6-hour time point. This suggests the organotypic foreskin could be used to study the effects of microbes on the foreskin tissue, as the organotypic foreskin is sterile during culture and is not influenced by microbiota-associated bacteria unless it is artificially inoculated or loses sterility. For future assays, foreskin tissue could be transported from the surgical site to the laboratory in a bactericidal and fungicidal antibiotic-antimycotic solution such as Primocin. Tissue could then be washed several times before use with 1X DPBS, which in combination with antibiotic-antimycotic exposure could eliminate a proportion of the patient's bacterial and fungal microbiota and any possible undesired tissue immune modulation. We could also swab foreskin tissue explants after antibiotic-antimycotic treatment and determine the residual microbial load prior to conducting the assays described within this study.

In the future, comparing the function of TLR4 to mRNA expression and protein levels may help discern if changes in expression are related to altered function across tissue types. While data has been generated for gene expression of TLR1 and 2, it has not been for TLR4. Western blotting or immunofluorescent microscopy may also help in quantifying tissue protein expression for different TLRs and relating it to gene expression.

4.5 Characterizing Tissue Barrier Function

Tissue barrier function was analyzed using several different methods. First, immediately frozen and explant cultured tissues were examined for the presence of tight junction protein claudin-1. The amount of immunoreactivity per immunofluorescence image was then quantified *in silico* between adult and paediatric tissues. This was repeated on tissues stimulated with a 100 ng/mL solution of LPS, to examine if experimental TLR4 stimulation could enhance production of barrier proteins. Enhancement of the epidermal barrier occurs with peptidoglycan-mediated TLR2 stimulation on cultured keratinocytes, prompting this investigation[225]. Lastly, a permeability assay was conducted on fresh, seven-day cultured, and organotypic tissues to establish the functionality of tight junctions in each tissue[226].

Immunofluorescence imaging of foreskin immediately frozen after surgery alongside cultured explants demonstrated that over culture time, organized tissue architecture and integrity was lost (Figure 3.11). After one day of culture, fresh tissue appeared to develop multiple holes within the suprabasal epidermis, which was enhanced in seven-day cultured tissue regardless of LPS exposure (Figure 3.11A, B, C, D). Seven-day cultured explant tissue appeared to have fewer nuclei in the suprabasal epidermis when compared to immediately frozen and fresh cultured tissues, which could be indicative of cell migration or death during the culture period. With previous organotypic foreskins, poor cell surface localization of E-cadherin prompted us to subject these organotypic cultures to short, low RPM shaking to replicate shear stress and possibly enhance cell-cell adherens junction formation. This was prompted through examining studies showing that microflow-induced shear stress modulates keratinocyte physiology and enhances E-cadherin and ZO-1 colocalization at the cell-cell junction[227–231]. Regrettably, organotypic cultures subject to mechanical agitation did not exhibit definable tissue structure (Figure 3.11E). Lastly, claudin-1 immunoreactivity qualitatively decreased and was nearly absent in the majority of seven-day cultured explant tissues compared to fresh tissue (Figure 3.11A, C). This was in contrast to LPS stimulated fresh tissue and seven-day explants, which appeared to retain claudin-1 immunoreactivity in some portions of the tissue (Figure 3.11B, D). Mechanically agitated organotypic foreskins did not exhibit

quantifiable (through our methods) claudin-1 immunoreactivity, with immunoreactivity appearing diffuse and non-specific. Explant cultures may, over time, start to lose functional tight junction protein claudin-1 which could be due to cell migration from the tissue. Previous publications have reported that, over the first few days of explant culture, keratinocytes migrate away from the tissue, soon followed by fibroblasts, which begin migration several days later[152]. Cell migration itself is facilitated by forming new adhesive connection to other cells and substrate while reducing previous connections[232]. Consequently, the non-uniform expression of adhesion proteins within a tissue due to migration (e.g., desmosomes, tight junctions, and adherens junctions) may alter permeability of the tissue itself[232]. During our study, organotypic foreskin did not show robust claudin-1 expression presumably due to mechanical agitation, severely reducing the ability to make comparisons between other tissues. Despite this, it can be seen that the non-mechanically agitated organotypic model can express E-cadherin in a similar way to that of immediately frozen tissue (Figures 3.4 and 3.10). Expression of E-cadherin is also qualitatively and quantitatively maintained within organotypic foreskins while that of seven-day tissue is lost, suggesting that cells are migrating away from explant cultured tissues while they are not from organotypic foreskins. Further investigation, such as by analyzing tissue cell populations through culture, is necessary to draw this conclusion.

Next, there was no detectable difference in claudin-1 immunoreactivity between paediatric inner and outer tissues (Figure 3.12A, B, E). Additionally, adult inner and outer foreskin tissues may show differences in expression between one another and paediatric tissues, but more biological replicates are required to confidently determine this (Figure 3.12C, D, E). It could be possible that similarity in claudin-1 expression between paediatric participants and differences shown between the adult participant is the result of age differences or puberty. Paediatric participants included in this analysis were of median age 8.17 yrs (range: 1.78 – 14.15 yrs), only one was within the range at which puberty begins, and all had phimosis (Table 3.4). This is in sharp contrast to the adult participant (Table 3.3, ADLT 009) who has gone through puberty and, although not before surgery, may have been able to retract their foreskin. Careful analysis of these factors and the role they play may be able to determine the reasoning for any differences exhibited between and within adult and paediatric tissues.

Fresh, seven-day explant cultured, and organotypic foreskin tissues were then subject to qPCR to detect claudin-1 mRNA copy numbers. This was performed so as to evaluate culture effects on claudin-1 expression. Additionally, this analysis was performed using the same tissue types but stimulated with LPS, as well as matched unstimulated controls to examine if TLR4 stimulation could upregulate claudin-1 gene expression as peptidoglycan can by stimulating TLR2[225]. The qPCR assay was optimized such that the mean efficiency was between 90-110% and linearity greater than 0.995, which ensured accuracy and guaranteed reaction efficiency fell within recommended guidelines for use of absolute quantification (Table 3.8)[218]. Over culture, expression of claudin-1 did not change between fresh cultured, seven-day cultured, and organotypic tissues (Figure 3.13). As mentioned previously, the population of cells in the tissue analyzed via qPCR must be verified as non-apoptotic so as to ensure the measure obtained is an accurate representation of tissue gene expression and not skewed by the presence of apoptosis-induced mRNA degradation intermediates. It is also, as mentioned previously, possible that GAPDH mRNA copies decrease within the seven-day explant which could skew normalized claudin-1 transcript numbers. This could be remedied by including more reference genes and comparing GAPDH numbers across fresh and seven-day tissues. There was additionally no detectable difference in claudin-1 mRNA copies in fresh, seven-day cultured explant, and organotypic tissues exposed to LPS and their matched tissue controls (Figure 3.14).

Tissue permeability was quantified through use of a dextran tracer exclusion assay. Dextran was chosen as the molecule to examine permeability as it is a non-digestible sugar that is not known to undergo transcytosis by epithelial cells[226]. Pinocytosis of dextran has been reported by epithelial cells, but this is negligible due to its slow rate in comparison to paracellular transport[226]. As can be shown in Figure 3.15A, time was a significant predictor of seven-day explant permeability, but not fresh tissue permeability. This could be due to tissue integrity and barrier function loss as noted earlier which could be the result of cell migration out of the seven-day explant tissue, but not fresh tissue. Of note, one participant had significantly more permeability at 12 and 24 hours (PED 041: age 8 yrs, African American) than the other two (PED 040: age 14 yrs, Caucasian; PED 037: age 9 yrs, Caucasian) in each grouping. Each participant underwent circumcision to

treat phimosis during this study. These data raise the question that participant ethnicity may be correlated to permeability measures (in comparison to age or indication for circumcision), which could restrict tissue comparisons from paediatric participants of different ethnicity. To discern whether or not this is the case, it would be necessary to have a larger sample size and more information on ethnicity. This could help ensure better generalizability of results in the future when generating foreskin models from different ethnic groups.

In contrast, time was a significant predictor of organotypic foreskin permeability. When examining the two organotypic tissues used in this experiment, it can be noted that ADLT 001 had lower permeability at all timepoints compared to ADLT 002, suggesting there may be donor-to-donor variability even in the organotypic model. These data also suggest that the organotypic model has relatively poor barrier function. However, this poor function may be due to mechanical agitation of the tissues during culture, and not reflective of the model if grown statically. Mechanical agitation most likely disrupted the structure of the tissues examined, as can be shown in immunofluorescence images of ADLT 001 and 002 (Figure 3.15B and C, respectively). Restricting mechanical agitation to the end stage of development (culturing in maintenance medium) or replacing it with a surface level fluid microflow may reduce integrity loss and enhance tight junction expression and localization[231]. As well, the passage number of the cells used to generate organotypic models may influence permeability, as it is known that HPV16 E6E7 immortalized cells may display altered karyotypes at high passage numbers[188]. ADLT 001 was seeded with passage 14 keratinocytes, while ADLT 002 was seeded with passage 10 keratinocytes. It is also possible that HPV16 E7 expression in immortalized cells altered tight junction expression, and may have reduced the ability to form a functional, sealed epithelial barrier even without mechanical agitation[187]. Investigation into alternative immortalization techniques may be necessary to remedy this.

Based on these results, the tracer exclusion experimental technique has been optimized to the extent that it that has the possibility discriminate between optimal and suboptimal barrier functionality (i.e., distinguish between participants organotypic foreskin tissues and between fresh and seven-day explant tissues). Once additional organotypic foreskin

tissues are produced, this method can be used to screen them for permeability next to matched explant tissues to examine any differences in overall barrier function.

4.6 Future Long-Term Directions

In order to refine the organotypic foreskin tissue model and allow it to more closely mimic *in vivo* foreskin tissue, many different short- and long-term goals need to be met. While short-term goals are listed within this discussion already, this section will focus those in the long-term.

To enhance the tissue-level accuracy of the organotypic foreskins, several different approaches could be undertaken. First, additional cells like melanocytes could be incorporated in the tissue model where appropriate. Melanocytes, for example, could be added to the keratinocyte cell suspension and seeded onto the cellularized collagen described in the study. Second, the organotypic foreskin tissues could be cultured using a medium perfusion system similar to that established by Strüver *et al*, 2017[233]. This system, when used with our foreskin models, may supplement diffusion-based medium feeding by providing convection effects to the basal aspect of the tissue. As well, the continual flow of medium against the basal aspect would transmit mechanical stress to the tissue model, which could augment mRNA and protein level expression of skin structural and barrier markers.

While tissue structure is an important aspect to modify in the future, another significant facet of this work will be the incorporation of immune cells with the foreskin tissue model to facilitate the study of tissue-microbiota interactions. This will be a challenging aspect, involving the isolation, independent culture, and then integration of immune cells with the organotypic foreskin dermal layer and basal medium. Technically, this will require knowledge of how to culture multiple different cell types each with their own varying culture conditions (e.g., fibroblasts, keratinocytes, melanocytes, and varying subsets of immune cells). It will also require isolation of immune cells (that differ in frequency within the blood) from same-participant blood samples, requiring large

aliquots of blood to facilitate the extraction process. As well, this aspect will require seeding immune cells at physiologically relevant densities in the foreskin model. Once the immune cell integration process is completed, it will be followed with incorporation of microbes on the tissue model, and eventually replication competent HIV.

When incorporating the microbiota, it will be of interest to examine possible differences that high and low HIV risk microbiota induce on organotypic foreskins that contain immune cells. This could help delineate microbiota-based differences in foreskin immune activation. As well, inoculating suspect bacteria onto the organotypic foreskin cultures would help solve the issue of bacterial co-occurrence that has obscured study of the exact species of anaerobes implicated in uncircumcised heterosexual male HIV susceptibility.

Lastly, high HIV risk bacterial species could be examined in studies looking at microbiome alteration using the organotypic foreskins generated in this study. Narrow spectrum pharmacologic agents could be developed and initially tested on the foreskin model to examine their effect on eliminating high risk bacteria. As well, study on the effects of microbiota supplementation or transplantation could be conducted to see if one can alter the penile microbiota through this approach, compared to alternatives like circumcision or topical antimicrobial use.

The tissue model could also, if an artificial hypodermis is incorporated similar to Sugihara *et al*, 1991, be used for the formation of full skin equivalents and used for study of the microbiota on other portions of the body[234]. This organotypic full skin equivalent could possibly, with modification and significant testing, be used as a treatment modality for deep skin injuries (e.g., chronic ulcers).

Chapter 5

5 Conclusion

In vitro organotypic foreskins have been generated and compared to foreskin tissue frozen immediately after circumcision and seven-day cultured explant tissues. Organotypic foreskins form multilayer epithelia capable of expressing E-cadherin (an adherens junction protein) as well as filaggrin (a marker of keratinocyte terminal differentiation). More work is required to compare the stratification of organotypic tissues to that of explant cultured tissues and ensure they are able to mimic the unique epidermal layers present in stratified squamous keratinized epithelia. Organotypic tissues were also shown to express genes for innate immune sensors TLR1 and TLR2, and the antimicrobial peptide β-defensin-1. Similar to fresh and seven-day explant tissues, organotypic tissues did not alter expression of these innate immune genes when stimulated with LPS. However, in contrast to fresh and seven-day explant tissues, organotypic tissue appeared to increase secretion of the chemokine IL-8 in response to LPS stimulation, although these results are preliminary, and more replicates are required to confidently state this. Lastly, a method to reliably discern optimal and suboptimal tissue barrier function has been optimized for use with organotypic tissues. Preliminary permeability results indicate mechanical agitation during maturation leads to poor tissue structure and high permeability of organotypic foreskins, and that seven-day explants have reduced barrier function compared to fresh tissues. Further investigation of tissue permeability in relation to mechanical agitation and current immortalization techniques is required to discern whether these play a role in altered organotypic foreskin barrier function.

While more work is required to improve this tissue model, the organotypic foreskin model described does present a promising option for exploring the effects of long-term culture with foreskin anaerobes on foreskin innate immunology. Preliminary results suggest organotypic foreskin tissues provide a physiologically relevant environment for the culture of the foreskin microbiota (a dry, cornified surface that is sterile prior to inoculation). As well, preliminary evidence suggests organotypic foreskins retain

expression of innate immune mediators, as well as adherens junctions that play a role in maintaining tissue structure. This is in contrast to foreskin tissue cultured for seven-days, which loses tissue integrity and does not provide a dry, sterile environment to inoculate the foreskin microbiota for long-term culture.

References

1. German Advisory Committee Blood (Arbeitskreis Blut), Subgroup 'Assessment of Pathogens Transmissible by Blood'. Human Immunodeficiency Virus (HIV). *Transfus Med Hemother* **43**, 203–222 (2016).
2. Sharp, P. M. & Hahn, B. H. Origins of HIV and the AIDS Pandemic. *Cold Spring Harbor Perspectives in Medicine* **1**, a006841–a006841 (2011).
3. Centers for Disease Control (CDC). Kaposi's sarcoma and Pneumocystis pneumonia among homosexual men--New York City and California. *MMWR Morb. Mortal. Wkly. Rep.* **30**, 305–308 (1981).
4. Bhatti, A. B., Usman, M. & Kandi, V. Current Scenario of HIV/AIDS, Treatment Options, and Major Challenges with Compliance to Antiretroviral Therapy. *Cureus* (2016) doi:10.7759/cureus.515.
5. Greene, W. C. A history of AIDS: looking back to see ahead. *Eur. J. Immunol.* **37 Suppl 1**, S94-102 (2007).
6. AIDSinfo | UNAIDS. https://aidsinfo.unaids.org/.
7. WHO | Data and statistics. *WHO* http://www.who.int/hiv/data/en/.
8. James, S. L. *et al.* Global, regional, and national incidence, prevalence, and years lived with disability for 354 diseases and injuries for 195 countries and territories, 1990–2017: a systematic analysis for the Global Burden of Disease Study 2017. *The Lancet* **392**, 1789–1858 (2018).

9. Roth, G. A. *et al.* Global, regional, and national age-sex-specific mortality for 282 causes of death in 195 countries and territories, 1980–2017: a systematic analysis for the Global Burden of Disease Study 2017. *The Lancet* **392**, 1736–1788 (2018).
10. Vidya Vijayan, K. K., Karthigeyan, K. P., Tripathi, S. P. & Hanna, L. E. Pathophysiology of CD4+ T-Cell Depletion in HIV-1 and HIV-2 Infections. *Front Immunol* **8**, (2017).
11. Angeletti, P. C., Zhang, L. & Wood, C. The Viral Etiology of AIDS-Associated Malignancies. *Adv Pharmacol* **56**, 509–557 (2008).
12. Poorolajal, J., Hooshmand, E., Mahjub, H., Esmailnasab, N. & Jenabi, E. Survival rate of AIDS disease and mortality in HIV-infected patients: a meta-analysis. *Public Health* **139**, 3–12 (2016).
13. Arts, E. J. & Hazuda, D. J. HIV-1 antiretroviral drug therapy. *Cold Spring Harb Perspect Med* **2**, a007161 (2012).
14. Autran, B. *et al.* Positive effects of combined antiretroviral therapy on CD4+ T cell homeostasis and function in advanced HIV disease. *Science* **277**, 112–116 (1997).
15. Komanduri, K. V. *et al.* Restoration of cytomegalovirus-specific CD4+ T-lymphocyte responses after ganciclovir and highly active antiretroviral therapy in individuals infected with HIV-1. *Nat. Med.* **4**, 953–956 (1998).
16. Lederman, M. M. *et al.* Immunologic responses associated with 12 weeks of combination antiretroviral therapy consisting of zidovudine, lamivudine, and ritonavir: results of AIDS Clinical Trials Group Protocol 315. *J. Infect. Dis.* **178**, 70–79 (1998).

17. Yoong, D., Bayoumi, A. M., Robinson, L., Rachlis, B. & Antoniou, T. Public prescription drug plan coverage for antiretrovirals and the potential cost to people living with HIV in Canada: a descriptive study. *cmajo* **6**, E551–E560 (2018).
18. Rintamaki, L. S., Davis, T. C., Skripkauskas, S., Bennett, C. L. & Wolf, M. S. Social Stigma Concerns and HIV Medication Adherence. *AIDS Patient Care and STDs* **20**, 359–368 (2006).
19. Kalichman, S. C. & Grebler, T. Stress and Poverty Predictors of Treatment Adherence among People with Low-Literacy Living with HIV/AIDS. *Psychosom Med* **72**, 810–816 (2010).
20. Kalichman, S. C. & Rompa, D. Functional health literacy is associated with health status and health-related knowledge in people living with HIV-AIDS. *J. Acquir. Immune Defic. Syndr.* **25**, 337–344 (2000).
21. Garey, L. *et al.* Anxiety, depression, and HIV symptoms among persons living with HIV/AIDS: the role of hazardous drinking. *AIDS Care* **27**, 80–85 (2015).
22. Arrivillaga, M., Ross, M., Useche, B., Alzate, M. L. & Correa, D. Social position, gender role, and treatment adherence among Colombian women living with HIV/AIDS: social determinants of health approach. *Rev Panam Salud Publica* **26**, 502–510 (2009).
23. Willie, T. C., Overstreet, N. M., Sullivan, T. P., Sikkema, K. J. & Hansen, N. B. Barriers to HIV Medication Adherence: Examining Distinct Anxiety and Depression Symptoms among Women Living with HIV Who Experienced Childhood Sexual Abuse. *Behavioral Medicine* **42**, 120–127 (2016).

24. Mellins, C. A., Kang, E., Leu, C.-S., Havens, J. F. & Chesney, M. A. Longitudinal study of mental health and psychosocial predictors of medical treatment adherence in mothers living with HIV disease. *AIDS Patient Care STDS* **17**, 407–416 (2003).

25. Azar, P. *et al.* Drug use patterns associated with risk of non-adherence to antiretroviral therapy among HIV-positive illicit drug users in a Canadian setting: a longitudinal analysis. *BMC Infect. Dis.* **15**, 193 (2015).

26. Ingersoll, K. The impact of psychiatric symptoms, drug use, and medication regimen on non-adherence to HIV treatment. *AIDS Care* **16**, 199–211 (2004).

27. Waldrop-Valverde, D., Jones, D. L., Weiss, S., Kumar, M. & Metsch, L. The effects of low literacy and cognitive impairment on medication adherence in HIV-positive injecting drug users. *AIDS Care* **20**, 1202–1210 (2008).

28. Dlamini, P. S. *et al.* HIV stigma and missed medications in HIV-positive people in five African countries. *AIDS Patient Care STDS* **23**, 377–387 (2009).

29. Simbayi, L. C. *et al.* Internalized stigma, discrimination, and depression among men and women living with HIV/AIDS in Cape Town, South Africa. *Soc Sci Med* **64**, 1823–1831 (2007).

30. Shaw, G. M. & Hunter, E. HIV Transmission. *Cold Spring Harb Perspect Med* **2**, (2012).

31. Cohen, M. S., Shaw, G. M., McMichael, A. J. & Haynes, B. F. Acute HIV-1 Infection. *N Engl J Med* **364**, 1943–1954 (2011).

32. Hladik, F. & McElrath, M. J. Setting the stage: host invasion by HIV. *Nat. Rev. Immunol.* **8**, 447–457 (2008).

33. LeMessurier, J. *et al.* Risk of sexual transmission of human immunodeficiency virus with antiretroviral therapy, suppressed viral load and condom use: a systematic review. *CMAJ* **190**, E1350–E1360 (2018).

34. Porter, K. A. *et al.* Understanding the Intersection of Young Age, Mucosal Injury, and HIV Susceptibility. *AIDS Research and Human Retroviruses* **32**, 1149–1158 (2016).

35. Scott, H. M. *et al.* Age, Race/Ethnicity, and Behavioral Risk Factors Associated with Per-Contact Risk of HIV Infection Among Men Who Have Sex with Men in the United States. *J Acquir Immune Defic Syndr* **65**, 115–121 (2014).

36. Auvert, B. *et al.* Randomized, controlled intervention trial of male circumcision for reduction of HIV infection risk: the ANRS 1265 Trial. *PLoS Med.* **2**, e298 (2005).

37. Gray, R. H. *et al.* Male circumcision for HIV prevention in men in Rakai, Uganda: a randomised trial. *Lancet* **369**, 657–666 (2007).

38. Bailey, R. C. *et al.* Male circumcision for HIV prevention in young men in Kisumu, Kenya: a randomised controlled trial. *Lancet* **369**, 643–656 (2007).

39. Liu, C. M. *et al.* Male circumcision significantly reduces prevalence and load of genital anaerobic bacteria. *MBio* **4**, e00076 (2013).

40. Price, L. B. *et al.* The effects of circumcision on the penis microbiome. *PLoS ONE* **5**, e8422 (2010).

41. Liu, C. M. *et al.* Penile Anaerobic Dysbiosis as a Risk Factor for HIV Infection. *mBio* **8**, (2017).

42. Prodger, J. L. *et al.* Chemokine Levels in the Penile Coronal Sulcus Correlate with HIV-1 Acquisition and Are Reduced by Male Circumcision in Rakai, Uganda. *PLoS Pathog.* **12**, e1006025 (2016).

43. Prodger, J. L. *et al.* Penile bacteria associated with HIV seroconversion, inflammation, and immune cells. *JCI Insight* **6**, (2021).

44. Fanales-Belasio, E., Raimondo, M., Suligoi, B. & Buttò, S. HIV virology and pathogenetic mechanisms of infection: a brief overview. *Ann Ist Super Sanita* **46**, 5–14 (2010).

45. Checkley, M. A., Luttge, B. G. & Freed, E. O. HIV-1 Envelope Glycoprotein Biosynthesis, Trafficking, and Incorporation. *J Mol Biol* **410**, 582–608 (2011).

46. Trovato, M., D'Apice, L., Prisco, A. & De Berardinis, P. HIV Vaccination: A Roadmap among Advancements and Concerns. *International Journal of Molecular Sciences* **19**, 1241 (2018).

47. Gorry, P. R. & Ancuta, P. Coreceptors and HIV-1 Pathogenesis. *Curr HIV/AIDS Rep* **8**, 45–53 (2011).

48. Cuevas, J. M., Geller, R., Garijo, R., López-Aldeguer, J. & Sanjuán, R. Extremely High Mutation Rate of HIV-1 In Vivo. *PLOS Biology* **13**, e1002251 (2015).

49. Fernàndez, G., Clotet, B. & Martínez, M. A. Fitness Landscape of Human Immunodeficiency Virus Type 1 Protease Quasispecies. *Journal of Virology* **81**, 2485–2496 (2007).

50. Yu, F. *et al.* The Transmission and Evolution of HIV-1 Quasispecies within One Couple: a Follow-up Study based on Next-Generation Sequencing. *Scientific Reports* **8**, 1404 (2018).

51. Grivel, J.-C., Shattock, R. J. & Margolis, L. B. Selective transmission of R5 HIV-1 variants: where is the gatekeeper? *J Transl Med* **9**, S6 (2011).

52. Keele, B. F. & Derdeyn, C. A. Genetic and antigenic features of the transmitted virus. *Curr Opin HIV AIDS* **4**, 352–357 (2009).

53. Salazar-Gonzalez, J. F. *et al.* Genetic identity, biological phenotype, and evolutionary pathways of transmitted/founder viruses in acute and early HIV-1 infection. *J Exp Med* **206**, 1273–1289 (2009).

54. Wang, L. *et al.* Visualization of HIV T Cell Virological Synapses and Virus-Containing Compartments by Three-Dimensional Correlative Light and Electron Microscopy. *J Virol* **91**, (2017).

55. Feldmann, J. & Schwartz, O. HIV-1 Virological Synapse: Live Imaging of Transmission. *Viruses* **2**, 1666–1680 (2010).

56. Bracq, L., Xie, M., Benichou, S. & Bouchet, J. Mechanisms for Cell-to-Cell Transmission of HIV-1. *Front. Immunol.* **9**, (2018).

57. Ménager, M. M. & Littman, D. R. Actin Dynamics Regulates Dendritic Cell-Mediated Transfer of HIV-1 to T Cells. *Cell* **164**, 695–709 (2016).

58. McDonald, D. Dendritic Cells and HIV-1 Trans-Infection. *Viruses* **2**, 1704–1717 (2010).

59. Jolly, C. & Sattentau, Q. J. Human Immunodeficiency Virus Type 1 Virological Synapse Formation in T Cells Requires Lipid Raft Integrity. *J Virol* **79**, 12088–12094 (2005).

60. Jolly, C. & Sattentau, Q. J. Retroviral spread by induction of virological synapses. *Traffic* **5**, 643–650 (2004).

61. Boer, M., Duchnik, E., Maleszka, R. & Marchlewicz, M. Structural and biophysical characteristics of human skin in maintaining proper epidermal barrier function. *Postepy Dermatol Alergol* **33**, 1–5 (2016).

62. Zaidi, Z. & Lanigan, S. W. Skin: Structure and Function. in *Dermatology in Clinical Practice* (eds. Lanigan, S. W. & Zaidi, Z.) 1–15 (Springer, 2010). doi:10.1007/978-1-84882-862-9_1.

63. Menon, G. K., Cleary, G. W. & Lane, M. E. The structure and function of the stratum corneum. *Int J Pharm* **435**, 3–9 (2012).

64. Wickett, R. R. & Visscher, M. O. Structure and function of the epidermal barrier. *American Journal of Infection Control* **34**, S98–S110 (2006).

65. Abdo, J. M., Sopko, N. A. & Milner, S. M. The applied anatomy of human skin: A model for regeneration. *Wound Medicine* **28**, 100179 (2020).

66. Nguyen, A. V. & Soulika, A. M. The Dynamics of the Skin's Immune System. *Int J Mol Sci* **20**, (2019).

67. Wong, R., Geyer, S., Weninger, W., Guimberteau, J.-C. & Wong, J. K. The dynamic anatomy and patterning of skin. *Experimental Dermatology* **25**, 92–98 (2016).

68. Ramadon, D., McCrudden, M. T. C., Courtenay, A. J. & Donnelly, R. F. Enhancement strategies for transdermal drug delivery systems: current trends and applications. *Drug Deliv. and Transl. Res.* (2021) doi:10.1007/s13346-021-00909-6.

69. Koguchi-Yoshioka, H. *et al.* Skin T cells maintain their diversity and functionality in the elderly. *Communications Biology* **4**, 1–8 (2021).

70. Mueller, S. N., Zaid, A. & Carbone, F. R. Tissue-Resident T Cells: Dynamic Players in Skin Immunity. *Front Immunol* **5**, (2014).

71. Westercamp, N., Mehta, S. D., Jaoko, W., Okeyo, T. A. & Bailey, R. C. Penile coital injuries in men decline after circumcision: Results from a prospective study of recently circumcised and uncircumcised men in western Kenya. *PLoS One* **12**, (2017).

72. Carias, A. M. *et al.* Defining the Interaction of HIV-1 with the Mucosal Barriers of the Female Reproductive Tract. *J Virol* **87**, 11388–11400 (2013).

73. Dinh, M. H. *et al.* Visualization of HIV-1 interactions with penile and foreskin epithelia: clues for female-to-male HIV transmission. *PLoS Pathog.* **11**, e1004729 (2015).

74. Dinh, M. H. *et al.* No difference in keratin thickness between inner and outer foreskins from elective male circumcisions in Rakai, Uganda. *PLoS ONE* **7**, e41271 (2012).

75. Tobian, A. A. R., Kacker, S. & Quinn, T. C. Male Circumcision: A Globally Relevant but Under-Utilized Method for the Prevention of HIV and Other Sexually Transmitted Infections. *Annu Rev Med* **65**, 293–306 (2014).

76. Siegfried, N. *et al.* Male circumcision for prevention of heterosexual acquisition of HIV in men. *Cochrane Database Syst Rev* CD003362 (2003) doi:10.1002/14651858.CD003362.

77. Weiss, H. A., Quigley, M. A. & Hayes, R. J. Male circumcision and risk of HIV infection in sub-Saharan Africa: a systematic review and meta-analysis. *AIDS* **14**, 2361–2370 (2000).

78. Siegfried, N., Muller, M., Deeks, J. J. & Volmink, J. Male circumcision for prevention of heterosexual acquisition of HIV in men. *Cochrane Database Syst Rev* CD003362 (2009) doi:10.1002/14651858.CD003362.pub2.

79. Gray, R. *et al.* The effectiveness of male circumcision for HIV prevention and effects on risk behaviors in a posttrial follow-up study. *AIDS* **26**, 609–615 (2012).

80. Auvert, B. *et al.* Effect of male circumcision on the prevalence of high-risk human papillomavirus in young men: results of a randomized controlled trial conducted in Orange Farm, South Africa. *J Infect Dis* **199**, 14–19 (2009).

81. Tobian, A. A. R. *et al.* Male Circumcision for the Prevention of HSV-2 and HPV Infections and Syphilis. *New England Journal of Medicine* **360**, 1298–1309 (2009).

82. Tobian, A. A. R. *et al.* Factors Associated with the Prevalence and Incidence of Herpes Simplex Virus Type 2 Infection among Men in Rakai, Uganda. *J Infect Dis* **199**, 945–949 (2009).

83. Mehta, S. D. *et al.* Circumcision status and incident herpes simplex virus type 2 infection, genital ulcer disease, and HIV infection. *AIDS* **26**, 1141–1149 (2012).

84. Wawer, M. J. *et al.* Effect of circumcision of HIV-negative men on transmission of human papillomavirus to HIV-negative women: a randomised trial in Rakai, Uganda. *The Lancet* **377**, 209–218 (2011).

85. Gray, R. H. *et al.* The effects of male circumcision on female partners' genital tract symptoms and vaginal infections in a randomized trial in Rakai, Uganda. *Am J Obstet Gynecol* **200**, 42.e1–7 (2009).

86. Mehta, S. D. *et al.* Microbial Diversity of Genital Ulcer Disease in Men Enrolled in a Randomized Trial of Male Circumcision in Kisumu, Kenya. *PLoS One* **7**, (2012).

87. Prodger, J. L. *et al.* Foreskin T cell subsets differ substantially from blood with respect to HIV co-receptor expression, inflammatory profile and memory status. *Mucosal Immunol* **5**, 121–128 (2012).

88. Hirbod, T. *et al.* Abundant Expression of HIV Target Cells and C-Type Lectin Receptors in the Foreskin Tissue of Young Kenyan Men. *Am J Pathol* **176**, 2798–2805 (2010).

89. Candi, E., Schmidt, R. & Melino, G. The cornified envelope: a model of cell death in the skin. *Nature Reviews Molecular Cell Biology* **6**, 328–340 (2005).

90. McCoombe, S. G. & Short, R. V. Potential HIV-1 target cells in the human penis. *AIDS* **20**, 1491–1495 (2006).

91. Ganor, Y. *et al.* Within 1 h, HIV-1 uses viral synapses to enter efficiently the inner, but not outer, foreskin mucosa and engages Langerhans-T cell conjugates. *Mucosal Immunol* **3**, 506–522 (2010).

92. Patterson, B. K. *et al.* Susceptibility to human immunodeficiency virus-1 infection of human foreskin and cervical tissue grown in explant culture. *Am J Pathol* **161**, 867–873 (2002).

93. Gray, C. M. *et al.* Impact of chemokine C-C ligand 27, foreskin anatomy and sexually transmitted infections on HIV-1 target cell availability in adolescent South African males. *Mucosal Immunol* **13**, 118–127 (2020).

94. Qin, Q. *et al.* Langerhans' cell density and degree of keratinization in foreskins of Chinese preschool boys and adults. *Int Urol Nephrol* **41**, 747–753 (2009).

95. Dinh, M. H., McRaven, M. D., Kelley, Z., Penugonda, S. & Hope, T. J. Keratinization of the adult male foreskin and implications for male circumcision. *AIDS* **24**, 899–906 (2010).

96. Stieh, D. J. *et al.* Th17 cells are preferentially infected very early after vaginal transmission of SIV in macaques. *Cell Host Microbe* **19**, 529–540 (2016).

97. Fischetti, L., Barry, S. M., Hope, T. J. & Shattock, R. J. HIV-1 infection of human penile explant tissue and protection by candidate microbicides. *AIDS* **23**, 319–328 (2009).

98. Zhou, Z. *et al.* HIV-1 Efficient Entry in Inner Foreskin Is Mediated by Elevated CCL5/RANTES that Recruits T Cells and Fuels Conjugate Formation with Langerhans Cells. *PLOS Pathogens* **7**, e1002100 (2011).

99. Fahrbach, K. M., Barry, S. M., Anderson, M. R. & Hope, T. J. Enhanced cellular responses and environmental sampling within inner foreskin explants: implications for the foreskin's role in HIV transmission. *Mucosal Immunology* **3**, 410–418 (2010).

100. Crawford, A., Angelosanto, J. M., Nadwodny, K. L., Blackburn, S. D. & Wherry, E. J. A Role for the Chemokine RANTES in Regulating CD8 T Cell Responses during Chronic Viral Infection. *PLOS Pathogens* **7**, e1002098 (2011).

101. Arnold, K. B. *et al.* Increased levels of inflammatory cytokines in the female reproductive tract are associated with altered expression of proteases, mucosal barrier proteins, and an influx of HIV-susceptible target cells. *Mucosal Immunol* **9**, 194–205 (2016).

102. Hoang, T. *et al.* The cervicovaginal mucus barrier to HIV-1 is diminished in bacterial vaginosis. *PLOS Pathogens* **16**, e1008236 (2020).

103. Cohen, C. R. *et al.* Bacterial Vaginosis Associated with Increased Risk of Female-to-Male HIV-1 Transmission: A Prospective Cohort Analysis among African Couples. *PLOS Medicine* **9**, e1001251 (2012).

104. Zeeuwen, P. L. J. M., Kleerebezem, M., Timmerman, H. M. & Schalkwijk, J. Microbiome and skin diseases. *Curr Opin Allergy Clin Immunol* **13**, 514–520 (2013).

105. Wang, B., Yao, M., Lv, L., Ling, Z. & Li, L. The Human Microbiota in Health and Disease. *Engineering* **3**, 71–82 (2017).

106. Bäsler, K. *et al.* The role of tight junctions in skin barrier function and dermal absorption. *Journal of Controlled Release* **242**, 105–118 (2016).

107. Haftek, M. Epidermal barrier disorders and corneodesmosome defects. *Cell Tissue Res* **360**, 483–490 (2015).

108. Miller, L. S. Toll-like receptors in skin. *Adv Dermatol* **24**, 71–87 (2008).

109. Fore, F., Indriputri, C., Mamutse, J. & Nugraha, J. TLR10 and Its Unique Anti-Inflammatory Properties and Potential Use as a Target in Therapeutics. *Immune Netw* **20**, (2020).

110. Takeda, K. & Akira, S. Toll-like receptors in innate immunity. *International Immunology* **17**, 1–14 (2005).

111. Matsui, T. & Amagai, M. Dissecting the formation, structure and barrier function of the stratum corneum. *Int Immunol* **27**, 269–280 (2015).

112. Michaels, A. S., Chandrasekaran, S. K. & Shaw, J. E. Drug permeation through human skin: Theory and invitro experimental measurement. *AIChE Journal* **21**, 985–996 (1975).

113. Hitomi, K. Transglutaminases in skin epidermis. *Eur J Dermatol* **15**, 313–319 (2005).

114. van Smeden, J., Janssens, M., Gooris, G. S. & Bouwstra, J. A. The important role of stratum corneum lipids for the cutaneous barrier function. *Biochim Biophys Acta* **1841**, 295–313 (2014).

115. Leclerc, E. A. *et al.* Corneodesmosin gene ablation induces lethal skin-barrier disruption and hair-follicle degeneration related to desmosome dysfunction. *Journal of Cell Science* **122**, 2699–2709 (2009).

116. Matsumoto, M. *et al.* Targeted deletion of the murine corneodesmosin gene delineates its essential role in skin and hair physiology. *PNAS* **105**, 6720–6724 (2008).

117. Samuelov, L. *et al.* Desmoglein 1 deficiency results in severe dermatitis, multiple allergies and metabolic wasting. *Nat Genet* **45**, 1244–1248 (2013).

118. Oji, V. *et al.* Loss of Corneodesmosin Leads to Severe Skin Barrier Defect, Pruritus, and Atopy: Unraveling the Peeling Skin Disease. *Am J Hum Genet* **87**, 274–281 (2010).

119. Israeli, S., Zamir, H., Sarig, O., Bergman, R. & Sprecher, E. Inflammatory peeling skin syndrome caused by a mutation in CDSN encoding corneodesmosin. *J Invest Dermatol* **131**, 779–781 (2011).

120. Mazereeuw-Hautier, J., Leclerc, E. A., Simon, M., Serre, G. & Jonca, N. A novel mutation in CDSN causes peeling skin disease in a patient from Morocco. *Br J Dermatol* **165**, 1152–1155 (2011).

121. Mallet, A. *et al.* Identification of the first nonsense CDSN mutation with expression of a truncated protein causing peeling skin syndrome type B. *Br J Dermatol* **169**, 1322–1325 (2013).

122. Brandner, J. M. *et al.* Organization and formation of the tight junction system in human epidermis and cultured keratinocytes. *Eur J Cell Biol* **81**, 253–263 (2002).

123. Furuse, M. *et al.* Claudin-based tight junctions are crucial for the mammalian epidermal barrier. *J Cell Biol* **156**, 1099–1111 (2002).

124. Kirschner, N., Houdek, P., Fromm, M., Moll, I. & Brandner, J. M. Tight junctions form a barrier in human epidermis. *Eur J Cell Biol* **89**, 839–842 (2010).

125. Yokouchi, M. *et al.* Epidermal tight junction barrier function is altered by skin inflammation, but not by filaggrin-deficient stratum corneum. *J Dermatol Sci* **77**, 28–36 (2015).

126. Hashimoto, K. Intercellular Spaces of the Human Epidermis as Demonstrated with Lanthanum. *Journal of Investigative Dermatology* **57**, 17–31 (1971).

127. Ishida-Yamamoto, A. *et al.* Lamellar granule secretion starts before the establishment of tight junction barrier for paracellular tracers in mammalian epidermis. *PLoS One* **7**, e31641 (2012).

128. Kubo, A., Nagao, K., Yokouchi, M., Sasaki, H. & Amagai, M. External antigen uptake by Langerhans cells with reorganization of epidermal tight junction barriers. *J Exp Med* **206**, 2937–2946 (2009).

129. Kirschner, N. *et al.* Contribution of tight junction proteins to ion, macromolecule, and water barrier in keratinocytes. *J Invest Dermatol* **133**, 1161–1169 (2013).

130. Yuki, T. *et al.* Tight junction proteins in keratinocytes: localization and contribution to barrier function. *Exp Dermatol* **16**, 324–330 (2007).

131. Nakajima, M. *et al.* Claudin-1 Binder Enhances Epidermal Permeability in a Human Keratinocyte Model. *J Pharmacol Exp Ther* **354**, 440–447 (2015).

132. De Benedetto, A. *et al.* Tight junction defects in patients with atopic dermatitis. *J Allergy Clin Immunol* **127**, 773-786.e1–7 (2011).

133. Baek, J. H., Lee, S. E., Choi, K. J., Choi, E. H. & Lee, S. H. Acute Modulations in Stratum Corneum Permeability Barrier Function Affect Claudin Expression and Epidermal Tight Junction Function via Changes of Epidermal Calcium Gradient. *Yonsei Med J* **54**, 523–528 (2013).

134. Deckers, J., Hammad, H. & Hoste, E. Langerhans Cells: Sensing the Environment in Health and Disease. *Front Immunol* **9**, 93 (2018).

135. Hain, T. *et al.* Dermal CD207-Negative Migratory Dendritic Cells Are Fully Competent to Prime Protective, Skin Homing Cytotoxic T-Lymphocyte Responses. *Journal of Investigative Dermatology* **139**, 422–429 (2019).

136. Tomura, M. *et al.* Tracking and quantification of dendritic cell migration and antigen trafficking between the skin and lymph nodes. *Scientific Reports* **4**, 6030 (2014).

137. Naik, S. *et al.* Commensal–dendritic-cell interaction specifies a unique protective skin immune signature. *Nature* **520**, 104–108 (2015).

138. Niyonsaba, F., Kiatsurayanon, C., Chieosilapatham, P. & Ogawa, H. Friends or Foes? Host defense (antimicrobial) peptides and proteins in human skin diseases. *Exp Dermatol* **26**, 989–998 (2017).

139. Niyonsaba, F., Nagaoka, I. & Ogawa, H. Human defensins and cathelicidins in the skin: beyond direct antimicrobial properties. *Crit Rev Immunol* **26**, 545–576 (2006).

140. Pfalzgraff, A., Brandenburg, K. & Weindl, G. Antimicrobial Peptides and Their Therapeutic Potential for Bacterial Skin Infections and Wounds. *Front. Pharmacol.* **9**, (2018).

141. Hemshekhar, M., Anaparti, V. & Mookherjee, N. Functions of Cationic Host Defense Peptides in Immunity. *Pharmaceuticals (Basel)* **9**, (2016).

142. Bernard, J. J. & Gallo, R. L. Protecting the boundary: the sentinel role of host defense peptides in the skin. *Cell Mol Life Sci* **68**, 2189–2199 (2011).

143. Braff, M. H., Nardo, A. D. & Gallo, R. L. Keratinocytes Store the Antimicrobial Peptide Cathelicidin in Lamellar Bodies. *Journal of Investigative Dermatology* **124**, 394–400 (2005).

144. Oren, A., Ganz, T., Liu, L. & Meerloo, T. In human epidermis, beta-defensin 2 is packaged in lamellar bodies. *Exp Mol Pathol* **74**, 180–182 (2003).

145. Miyauchi, E. *et al.* Mechanism of protection of transepithelial barrier function by Lactobacillus salivarius: strain dependence and attenuation by bacteriocin production. *Am J Physiol Gastrointest Liver Physiol* **303**, G1029-1041 (2012).

146. Seth, A., Yan, F., Polk, D. B. & Rao, R. K. Probiotics ameliorate the hydrogen peroxide-induced epithelial barrier disruption by a PKC- and MAP kinase-dependent mechanism. *Am J Physiol Gastrointest Liver Physiol* **294**, G1060-1069 (2008).

147. Sultana, R., McBain, A. J. & O'Neill, C. A. Strain-dependent augmentation of tight-junction barrier function in human primary epidermal keratinocytes by Lactobacillus and Bifidobacterium lysates. *Appl Environ Microbiol* **79**, 4887–4894 (2013).

148. Mogensen, T. H. Pathogen Recognition and Inflammatory Signaling in Innate Immune Defenses. *Clin Microbiol Rev* **22**, 240–273 (2009).

149. Lajoie, J. *et al.* A distinct cytokine and chemokine profile at the genital mucosa is associated with HIV-1 protection among HIV-exposed seronegative commercial sex workers. *Mucosal Immunol* **5**, 277–287 (2012).

150. Lajoie, J. *et al.* Differences in immunoregulatory cytokine expression patterns in the systemic and genital tract compartments of HIV-1-infected commercial sex workers in Benin. *Mucosal Immunol* **1**, 309–316 (2008).

151. Sun, T., Jackson, S., Haycock, J. W. & MacNeil, S. Culture of skin cells in 3D rather than 2D improves their ability to survive exposure to cytotoxic agents. *J. Biotechnol.* **122**, 372–381 (2006).

152. Orazizadeh, M., Hashemitabar, M., Bahramzadeh, S., Dehbashi, F. N. & Saremy, S. Comparison of the enzymatic and explant methods for the culture of keratinocytes isolated from human foreskin. *Biomedical Reports* **3**, 304–308 (2015).

153. Rose, W. A. *et al.* Commensal bacteria modulate innate immune responses of vaginal epithelial cell multilayer cultures. *PLoS ONE* **7**, e32728 (2012).

154. Gangatirkar, P., Paquet-Fifield, S., Li, A., Rossi, R. & Kaur, P. Establishment of 3D organotypic cultures using human neonatal epidermal cells. *Nat Protoc* **2**, 178–186 (2007).

155. Choi, M. *et al.* Establishment of Immortalized Primary Human Foreskin Keratinocytes and Their Application to Toxicity Assessment and Three Dimensional Skin Culture Construction. *Biomol Ther (Seoul)* **25**, 296–307 (2017).

156. Fitzner, N., Clauberg, S., Essmann, F., Liebmann, J. & Kolb-Bachofen, V. Human Skin Endothelial Cells Can Express All 10 TLR Genes and Respond to Respective Ligands. *Clin Vaccine Immunol* **15**, 138–146 (2008).

157. Stupp, R. *et al.* Radiotherapy plus concomitant and adjuvant temozolomide for glioblastoma. *N Engl J Med* **352**, 987–996 (2005).

158. Akizuki, R. *et al.* Decrease in paracellular permeability and chemosensitivity to doxorubicin by claudin-1 in spheroid culture models of human lung adenocarcinoma A549 cells. *Biochim Biophys Acta Mol Cell Res* **1865**, 769–780 (2018).

159. Klag, T. *et al.* β-Defensin 1 Is Prominent in the Liver and Induced During Cholestasis by Bilirubin and Bile Acids via Farnesoid X Receptor and Constitutive Androstane Receptor. *Front. Immunol.* **9**, (2018).

160. Edfeldt, G. *et al.* Regular Use of Depot Medroxyprogesterone Acetate Causes Thinning of the Superficial Lining and Apical Distribution of Human Immunodeficiency Virus Target Cells in the Human Ectocervix. *The Journal of Infectious Diseases* (2020) doi:10.1093/infdis/jiaa514.

161. Lamprecht, M. R., Sabatini, D. M. & Carpenter, A. E. CellProfiler: free, versatile software for automated biological image analysis. *Biotechniques* **42**, 71–75 (2007).

162. Buchanan, L., Shao, Z., Jiang, Y. C., Lai, A. & Prodger, J. L. Quantitative Imaging of Mucosal Tissues. in *Methods in Molecular Biology: Fluorescence Microscopy* (ed. Heit, B.) (Springer Nature).

163. Sayedyahossein, S., Rudkouskaya, A., Leclerc, V. & Dagnino, L. Integrin-Linked Kinase Is Indispensable for Keratinocyte Differentiation and Epidermal Barrier Function. *J. Invest. Dermatol.* **136**, 425–435 (2016).

164. Stenn, K. S., Link, R., Moellmann, G., Madri, J. & Kuklinska, E. Dispase, a neutral protease from Bacillus polymyxa, is a powerful fibronectinase and type IV collagenase. *J. Invest. Dermatol.* **93**, 287–290 (1989).

165. Arcus, V. L. *et al.* On the Temperature Dependence of Enzyme-Catalyzed Rates. *Biochemistry* **55**, 1681–1688 (2016).

166. Cornish-Bowden, A. The origins of enzyme kinetics. *FEBS Letters* **587**, 2725–2730 (2013).

167. Lichti, U., Anders, J. & Yuspa, S. H. Isolation and short term culture of primary keratinocytes, hair follicle populations, and dermal cells from newborn mice and keratinocytes from adult mice, for in vitro analysis and for grafting to immunodeficient mice. *Nat Protoc* **3**, 799–810 (2008).

168. Katkov, I. I. & Mazur, P. Factors affecting yield and survival of cells when suspensions are subjected to centrifugation. *Cell Biochem Biophys* **31**, 231–245 (1999).

169. Kim, I. H., Yang, J. D., Lee, D. G., Chung, H. Y. & Cho, B. C. Evaluation of centrifugation technique and effect of epinephrine on fat cell viability in autologous fat injection. *Aesthet Surg J* **29**, 35–39 (2009).

170. Llames, S., García-Pérez, E., Meana, Á., Larcher, F. & del Río, M. Feeder Layer Cell Actions and Applications. *Tissue Eng Part B Rev* **21**, 345–353 (2015).

171. Liu, S., Kam, W. R., Ding, J., Hatton, M. P. & Sullivan, D. A. Effect of Growth Factors on the Proliferation and Gene Expression of Human Meibomian Gland Epithelial Cells. *Invest Ophthalmol Vis Sci* **54**, 2541–2550 (2013).

172. Creek, K. E., Geslani, G., Batova, A. & Pirisi, L. Progressive loss of sensitivity to growth control by retinoic acid and transforming growth factor-beta at late stages

of human papillomavirus type 16-initiated transformation of human keratinocytes. *Adv Exp Med Biol* **375**, 117–135 (1995).

173. Fatimah, S. S., Tan, G. C., Chua, K. H., Tan, A. E. & Hayati, A. R. Effects of epidermal growth factor on the proliferation and cell cycle regulation of cultured human amnion epithelial cells. *Journal of Bioscience and Bioengineering* **114**, 220–227 (2012).
174. McKeehan, W. L. The effect of temperature during trypsin treatment on viability and multiplication potential of single normal human and chicken fibroblasts. *Cell Biology International Reports* **1**, 335–343 (1977).
175. Castellano-Pellicena, I. & Thornton, M. J. Isolation of Epidermal Keratinocytes from Human Skin: The Scratch-Wound Assay for Assessment of Epidermal Keratinocyte Migration. *Methods Mol Biol* **2154**, 1–12 (2020).
176. Celada, A., Allen, R., Esparza, I., Gray, P. W. & Schreiber, R. D. Demonstration and partial characterization of the interferon-gamma receptor on human mononuclear phagocytes. *J Clin Invest* **76**, 2196–2205 (1985).
177. Borowiec, A.-S., Delcourt, P., Dewailly, E. & Bidaux, G. Optimal Differentiation of In Vitro Keratinocytes Requires Multifactorial External Control. *PLoS One* **8**, (2013).
178. Miller, A. D. pa317 Retrovirus Packaging Cells. *Molecular Therapy* **6**, 572–575 (2002).
179. Halbert, C. L., Demers, G. W. & Galloway, D. A. The E7 gene of human papillomavirus type 16 is sufficient for immortalization of human epithelial cells. *J. Virol.* **65**, 473–478 (1991).

180. Katzenellenbogen, R. Telomerase Induction in HPV Infection and Oncogenesis. *Viruses* **9**, (2017).

181. Ruttkay-Nedecky, B. *et al.* Relevance of infection with human papillomavirus: the role of the p53 tumor suppressor protein and E6/E7 zinc finger proteins (Review). *Int. J. Oncol.* **43**, 1754–1762 (2013).

182. Yenofsky, R. L., Fine, M. & Pellow, J. W. A mutant neomycin phosphotransferase II gene reduces the resistance of transformants to antibiotic selection pressure. *Proc Natl Acad Sci U S A* **87**, 3435–3439 (1990).

183. Eustice, D. C. & Wilhelm, J. M. Mechanisms of action of aminoglycoside antibiotics in eucaryotic protein synthesis. *Antimicrob Agents Chemother* **26**, 53–60 (1984).

184. Bar-Nun, S., Shneyour, Y. & Beckmann, J. S. G-418, an elongation inhibitor of 80 S ribosomes. *Biochimica et Biophysica Acta (BBA) - Gene Structure and Expression* **741**, 123–127 (1983).

185. Allen, D., Winters, E., Kenna, P. F., Humphries, P. & Jane Farrar, G. Reference gene selection for real-time rtPCR in human epidermal keratinocytes. *Journal of Dermatological Science* **49**, 217–225 (2008).

186. Nowrouzi, A., Glimm, H., von Kalle, C. & Schmidt, M. Retroviral Vectors: Post Entry Events and Genomic Alterations. *Viruses* **3**, 429–455 (2011).

187. Uc, P. Y. *et al.* E7 oncoprotein from human papillomavirus 16 alters claudins expression and the sealing of epithelial tight junctions. *Int J Oncol* **57**, 905–924 (2020).

188. Mizumoto, Y. *et al.* Creation of tumorigenic human endometrial epithelial cells with intact chromosomes by introducing defined genetic elements. *Oncogene* **25**, 5673–5682 (2006).

189. Choi, M. & Lee, C. Immortalization of Primary Keratinocytes and Its Application to Skin Research. *Biomol Ther (Seoul)* **23**, 391–399 (2015).

190. Ahmed, N. *et al.* Molecular pathways regulating EGF-induced epithelio-mesenchymal transition in human ovarian surface epithelium. *Am J Physiol Cell Physiol* **290**, C1532-1542 (2006).

191. Chapman, S., Liu, X., Meyers, C., Schlegel, R. & McBride, A. A. Human keratinocytes are efficiently immortalized by a Rho kinase inhibitor. *J Clin Invest* **120**, 2619–2626 (2010).

192. Anderson, E. D. *et al.* Prolonging culture of primary human keratinocytes isolated from suction blisters with the Rho kinase inhibitor Y-27632. *PLoS One* **13**, (2018).

193. Lundberg, A. S., Hahn, W. C., Gupta, P. & Weinberg, R. A. Genes involved in senescence and immortalization. *Curr Opin Cell Biol* **12**, 705–709 (2000).

194. Matsumura, T. *et al.* Establishment of an immortalized human-liver endothelial cell line with SV40T and hTERT. *Transplantation* **77**, 1357–1365 (2004).

195. Yang, G., Rosen, D. G., Colacino, J. A., Mercado-Uribe, I. & Liu, J. Disruption of the retinoblastoma pathway by small interfering RNA and ectopic expression of the catalytic subunit of telomerase lead to immortalization of human ovarian surface epithelial cells. *Oncogene* **26**, 1492–1498 (2007).

196. Yang, G. *et al.* Knockdown of p53 combined with expression of the catalytic subunit of telomerase is sufficient to immortalize primary human ovarian surface epithelial cells. *Carcinogenesis* **28**, 174–182 (2007).

197. Gerardo, H. *et al.* Soft culture substrates favor stem-like cellular phenotype and facilitate reprogramming of human mesenchymal stem/stromal cells (hMSCs) through mechanotransduction. *Sci Rep* **9**, 9086 (2019).

198. Goodpaster, T. *et al.* An Immunohistochemical Method for Identifying Fibroblasts in Formalin-fixed, Paraffin-embedded Tissue. *J Histochem Cytochem* **56**, 347–358 (2008).

199. Chang, H. Y. *et al.* Diversity, topographic differentiation, and positional memory in human fibroblasts. *PNAS* **99**, 12877–12882 (2002).

200. McDonald-Hyman, C. *et al.* The vimentin intermediate filament network restrains regulatory T cell suppression of graft-versus-host disease. *J Clin Invest* **128**, 4604–4621.

201. Parysek, L. M. & Eckert, B. S. Vimentin filaments in spreading, randomly locomoting, and f-met-leu-phe-treated neutrophils. *Cell Tissue Res* **235**, 575–581 (1984).

202. Chistiakov, D. A., Killingsworth, M. C., Myasoedova, V. A., Orekhov, A. N. & Bobryshev, Y. V. CD68/macrosialin: not just a histochemical marker. *Laboratory Investigation* **97**, 4–13 (2017).

203. Collin, M., McGovern, N. & Haniffa, M. Human dendritic cell subsets. *Immunology* **140**, 22–30 (2013).

204. Mizumoto, N. & Takashima, A. CD1a and langerin: acting as more than Langerhans cell markers. *J Clin Invest* **113**, 658–660 (2004).

205. Aniansson Zdolsek, H., Ernerudh, J., Holt, P. G., Nilsson, J. & Björkstén, B. Expression of the T-cell markers CD3, CD4 and CD8 in healthy and atopic children during the first 18 months of life. *Int Arch Allergy Immunol* **119**, 6–12 (1999).

206. Young, P. *et al.* E-cadherin controls adherens junctions in the epidermis and the renewal of hair follicles. *EMBO J* **22**, 5723–5733 (2003).

207. Yap, A. S., Brieher, W. M. & Gumbiner, B. M. Molecular and functional analysis of cadherin-based adherens junctions. *Annu Rev Cell Dev Biol* **13**, 119–146 (1997).

208. Jamora, C. & Fuchs, E. Intercellular adhesion, signalling and the cytoskeleton. *Nat Cell Biol* **4**, E101-108 (2002).

209. Moll, R., Divo, M. & Langbein, L. The human keratins: biology and pathology. *Histochem Cell Biol* **129**, 705–733 (2008).

210. Chen, J.-Q. *et al.* Regulation of involucrin in psoriatic epidermal keratinocytes: the roles of ERK1/2 and GSK-3β. *Cell Biochem Biophys* **66**, 523–528 (2013).

211. Short, A. R. *et al.* Imaging Cell-Matrix Interactions in Three-Dimensional Collagen Hydrogel Culture Systems. *Macromol Biosci* **17**, (2017).

212. Yang, C.-C., Jenkins, L. & Burg, K. J. L. Adapted Cryosectioning Method for Hydrogels Used in Regenerative Medicine. *Journal of Histotechnology* **30**, 185–191 (2007).

213. Gumbiner, B., Stevenson, B. & Grimaldi, A. The role of the cell adhesion molecule uvomorulin in the formation and maintenance of the epithelial junctional complex. *Journal of Cell Biology* **107**, 1575–1587 (1988).

214. Ozawa, M. & Kobayashi, W. Cadherin Cytoplasmic Domains Inhibit the Cell Surface Localization of Endogenous E-Cadherin, Blocking Desmosome and Tight Junction Formation and Inducing Cell Dissociation. *PLoS One* **9**, (2014).

215. Woichansky, I., Beretta, C. A., Berns, N. & Riechmann, V. Three mechanisms control E-cadherin localization to the zonula adherens. *Nature Communications* **7**, 10834 (2016).

216. Gomes, I., Becker, K., Rothschild, M. A. & Schneider, P. M. Validation study of endogenous reference genes for normalization of quantitative real time PCR data in post mortem skin tissue. *Forensic Science International: Genetics Supplement Series* **4**, e156–e157 (2013).

217. gBlocks Gene Fragments. *Integrated DNA Technologies* https://www.idtdna.com/pages/products/genes-and-gene-fragments/double-stranded-dna-fragments/gblocks-gene-fragments.

218. Taylor, S. C. *et al.* The Ultimate qPCR Experiment: Producing Publication Quality, Reproducible Data the First Time. *Trends in Biotechnology* **37**, 761–774 (2019).

219. Brankatschk, R., Bodenhausen, N., Zeyer, J. & Bürgmann, H. Simple Absolute Quantification Method Correcting for Quantitative PCR Efficiency Variations for Microbial Community Samples. *Appl Environ Microbiol* **78**, 4481–4489 (2012).

220. Thomas, M. P. *et al.* Apoptosis Triggers Specific, Rapid, and Global mRNA Decay with 3' Uridylated Intermediates Degraded by DIS3L2. *Cell Rep* **11**, 1079–1089 (2015).

221. El-Domyati, M. *et al.* Expression of Apoptosis Regulatory Markers in the Skin of Advanced Hepatitis-C Virus Liver Patients. *Indian J Dermatol* **57**, 187–193 (2012).

222. Liu, L., Roberts, A. A. & Ganz, T. By IL-1 Signaling, Monocyte-Derived Cells Dramatically Enhance the Epidermal Antimicrobial Response to Lipopolysaccharide. *The Journal of Immunology* **170**, 575–580 (2003).

223. Cho, J.-S. *et al.* Lipopolysaccharide Induces Pro-Inflammatory Cytokines and MMP Production via TLR4 in Nasal Polyp-Derived Fibroblast and Organ Culture. *PLOS ONE* **9**, e90683 (2014).

224. Brown, J. L. *et al.* Biofilm-stimulated epithelium modulates the inflammatory responses in co-cultured immune cells. *Scientific Reports* **9**, 15779 (2019).

225. Yuki, T. *et al.* Activation of TLR2 enhances tight junction barrier in epidermal keratinocytes. *J Immunol* **187**, 3230–3237 (2011).

226. Frost, T. S., Jiang, L., Lynch, R. M. & Zohar, Y. Permeability of Epithelial/Endothelial Barriers in Transwells and Microfluidic Bilayer Devices. *Micromachines (Basel)* **10**, (2019).

227. Kippenberger, S. *et al.* Signaling of Mechanical Stretch in Human Keratinocytes via MAP Kinases. *Journal of Investigative Dermatology* **114**, 408–412 (2000).

228. Sriram, G. *et al.* Full-thickness human skin-on-chip with enhanced epidermal morphogenesis and barrier function. *Materials Today* **21**, 326–340 (2018).

229. Takei, T. *et al.* Effect of strain on human keratinocytes in vitro. *Journal of Cellular Physiology* **173**, 64–72 (1997).

230. Takei, T. *et al.* Cyclic strain stimulates isoform-specific PKC activation and translocation in cultured human keratinocytes. *Journal of Cellular Biochemistry* **67**, 327–337 (1997).

231. Agarwal, T., Narayana, G. H. & Banerjee, I. Keratinocytes are mechanoresponsive to the microflow-induced shear stress. *Cytoskeleton* **76**, 209–218 (2019).

232. De Pascalis, C. & Etienne-Manneville, S. Single and collective cell migration: the mechanics of adhesions. *MBoC* **28**, 1833–1846 (2017).

233. Strüver, K., Friess, W. & Hedtrich, S. Development of a Perfusion Platform for Dynamic Cultivation of in vitro Skin Models. *SPP* **30**, 180–189 (2017).

234. Sugihara, H., Toda, S., Miyabara, S., Kusaba, Y. & Minami, Y. Reconstruction of the skin in three-dimensional collagen gel matrix culture. *In Vitro Cell Dev Biol - Animal* **27**, 142–146 (1991).

Appendices

Appendix A: Statements of Approval for the Use of Human Tissues in Experimental Research.

All experimentation using human subjects was performed in compliance with protocol 111054 and 113008 (below) held by Drs. Eric Arts and Jessica Prodger, principal investigators at the University of Western Ontario Schulich School of Medicine and Dentistry, Department of Microbiology and Immunology, London, Ontario, Canada.

Western Research

Date: 11 February 2019

To: Dr. Eric Arts

Project ID: 111054

Study Title: Human Mucosal Tissue for the Study of HIV-1 Transmission

Application Type: Continuing Ethics Review (CER) Form

Review Type: Delegated

REB Meeting Date: 26/Feb/2019

Date Approval Issued: 11/Feb/2019

REB Approval Expiry Date: 09/Feb/2020

Lapse in Approval: February 10, 2019 to February 11, 2019

Dear Dr. Eric Arts,

The Western University Research Ethics Board has reviewed the application. This study, including all currently approved documents, has been re-approved until the expiry date noted above.

REB members involved in the research project do not participate in the review, discussion or decision.

Western University REB operates in compliance with, and is constituted in accordance with, the requirements of the TriCouncil Policy Statement: Ethical Conduct for Research Involving Humans (TCPS 2); the International Conference on Harmonisation Good Clinical Practice Consolidated Guideline (ICH GCP); Part C, Division 5 of the Food and Drug Regulations; Part 4 of the Natural Health Products Regulations; Part 3 of the Medical Devices Regulations and the provisions of the Ontario Personal Health Information Protection Act (PHIPA 2004) and its applicable regulations. The REB is registered with the U.S. Department of Health & Human Services under the IRB registration number IRB 00000940.

Please do not hesitate to contact us if you have any questions.

Sincerely,

Daniel Wyzynski, Research Ethics Coordinator, on behalf of Dr. Joseph Gilbert, HSREB Chair

Note: This correspondence includes an electronic signature (validation and approval via an online system that is compliant with all regulations).

Western Research

Date: 16 June 2020

To: Dr Jessica Prodger

Project ID: 113008

Study Title: Impact of the foreskin microbiome on health and disease

Application Type: Continuing Ethics Review (CER) Form

Review Type: Full Board

REB Meeting Date: 16/Jun/2020

Date Approval Issued: 16/Jun/2020

REB Approval Expiry Date: 04/Jul/2021

Dear Dr Jessica Prodger,

The Western University Research Ethics Board has reviewed the application. This study, including all currently approved documents, has been re-approved until the expiry date noted above.

REB members involved in the research project do not participate in the review, discussion or decision.

Western University REB operates in compliance with, and is constituted in accordance with, the requirements of the TriCouncil Policy Statement: Ethical Conduct for Research Involving Humans (TCPS 2); the International Conference on Harmonisation Good Clinical Practice Consolidated Guideline (ICH GCP); Part C, Division 5 of the Food and Drug Regulations; Part 4 of the Natural Health Products Regulations; Part 3 of the Medical Devices Regulations and the provisions of the Ontario Personal Health Information Protection Act (PHIPA 2004) and its applicable regulations. The REB is registered with the U.S. Department of Health & Human Services under the IRB registration number IRB 00000940.

Please do not hesitate to contact us if you have any questions.

Sincerely,

Daniel Wyzynski, Research Ethics Coordinator, on behalf of Dr. Joseph Gilbert, HSREB Chair

Note: This correspondence includes an electronic signature (validation and approval via an online system that is compliant with all regulations).

Curriculum Vitae

Name: Geoffrey J. Rempel

Post-secondary Education and Degrees:

University of Windsor
Windsor, Ontario, Canada
2015 – 2019 B.Sc.

The University of Western Ontario
London, Ontario, Canada
2019 – 2021 M.Sc.

Honours and Awards:

Frederick Banting and Charles Best Canada Graduate Scholarship - Master's Program **(**CGS M)
2020 – 2021

Dr. Frederick Winnett Luney Graduate Travel Award
2021

Conference Meetings – Poster Presentations:

Rempel, G., Palazzolo. R, Nakhoul, R., Ristoski, P., D'Agnillo, M., Smoczer, C., Hooker, L., Hudson, J. & Crawford, M. (2019). Does pitx3 Regulate *X. laevis crybb1* During Lens Development? *Annual Meeting of The Canadian Society of Zoologists*, Windsor, Ontario, Canada.

Rempel, G., Madden. K, Liu, C. M. & Prodger, J. L. (2019). Generation and Characterization of an *in vitro* Model of Foreskin Epithelium in Relation to the Penile Microbiome. *14th Annual Infection and Immunity Research Forum,* London, Ontario, Canada.

Rempel, G., Zuanazzi, D. M., Madden. K, Buchanan, L. B., Shao, E., Liu, C. M. & Prodger, J. L. (2020). Generation and Characterization of an *in vitro* Organotypic Foreskin Model to Study the Penile Microbiome. *15th Annual Infection and Immunity Research Forum* (Virtual).

Rempel, G., Zuanazzi, D. M., Madden. K, Buchanan, L. B., Shao, E., Liu, C. M. & Prodger, J. L. (2021). Generation and Characterization of an *in vitro* Organotypic Foreskin Model to Study HIV-1 Susceptibility. *30th Canadian Conference on HIV/AIDS Research* (Virtual).